THE HUB BOUNDARY LAYER OF AN
AXIAL FLOW COMPRESSOR

BY

B.A. RUSSELL, B.E. (HONS)

Resubmitted in partial fulfilment of the requirements
for the degree of
Master of Engineering Science

University of Tasmania
Hobart

December, 1969

I hereby declare that, except as stated herin, this thesis contains no material which has been accepted for the award of any other degree or diploma in any University, and that, to the best of my knowledge or belief this thesis contains no copy or paraphrase of material previously published or written by another person, except when due reference is made in the text of this thesis.

Bruce A Burnell

ACKNOWLEDGEMENTS

This work was carried out in the Civil Engineering Department of the University of Tasmania. The author wishes to thank members of the staff of the University. In particular the author wishes to thank Professor A.R. Oliver, Professor of Civil Engineering and supervisor of this research for his help and encouragement, and Mr. A. Robinson for his assistance with the experimental work.

The author also wishes to thank Mr. R.A. Wallis and Dr. D.C. Gibson of the C.S.I.R.O. Division of Mechanical Engineering for their valuable suggestions and discussions.

CONTENTS

PAGE

1. INTRODUCTION 1

2. A REVIEW OF SECONDARY FLOW AND LOSSES IN AXIAL FLOW COMPRESSORS 4

3. EQUIPMENT AND INSTRUMENTATION 29

  3.1. Vortex Wind Tunnel 29

  3.2. Hot Wire Anemometer 31

  3.3. Cobra Yaw Meter 33

  3.4. Factors Affecting Pressure Probes 36

4. THE HUB BOUNDARY LAYER THROUGH THE STATOR 39

  4.1. Experimental Procedure 39

  4.2. Experimental Results

    4.2.1. Total Pressure 39

    4.2.2. Velocity 40

    4.2.3. Flow Angle 40

  4.3. Vorticity 41

  4.4. Discussion 41

5. THE HUB BOUNDARY LAYER BETWEEN THE ROTOR AND STATOR

  5.1. Experimental Procedure 44

  5.2. Experimental Results

    5.2.1. Velocity 44

    5.2.2. Flow Direction 46

    5.2.3. Turbulence Components 46

  5.3. Vorticity 48

  5.4. Discussion 50

PAGE

6. TURBULENCE STRUCTURE OF BOUNDARY LAYER

6.1. Determination of Turbulence Components

6.1.1. Solution of Reynolds Equations 53

6.1.2. Discussion of Results 54

6.2. Component of Turbulence Resulting from Blade Wakes 55

6.2.1. "Turbulence Components" Downstream of Stator 55

6.3. Boundary Layer Equations 57

7. CONCLUSION 59

APPENDIX 60

NOTATION 72

REFERENCES 74

FIGURES

1. INTRODUCTION

In this thesis an investigation of flow in the hub region of a single stage axial flow compressor has been made. This study represents the initial portion of a program being undertaken at the University of Tasmania, aimed at improving the understanding of the flow mechanism and reducing the losses resulting from this region.

The viscous effects resulting from blade passage end wall boundary layer growth are taken into account in axial flow compressor design by the use of empirical factors applied to inviscid flow theory. Servoy (Ref. 1) in a review of recent progress in the field states "that most designers in the United States extropolate main passage velocity profiles to the inner and outer walls as if no boundary layers were present, changes due to the presence of the boundary layers are accounted for by a blockage factor the value of which is poorly defined". British designers use a similar system introducing a work done factor (Howell (Ref. 2) and Horlock (Ref. 3)), to estimate the decrease in temperature rise per stage due to wall effects.

In addition to causing deformation of the mainstream and hence making the factors discussed above necessary, the hub and tip regions account for the major portion of the losses occurring in a machine. An example of the importance of these regions is given by Howell (Ref. 2) shown in Fig. 1. At the design point the losses occurring in the end wall region, i.e. the annulus and the major portion of the secondary flow losses, account for 60% of the total loss. If a significant reduction in the losses in turbomachinery is to be made a reduction in this major component will be necessary.

A better understanding of the mechanism of the flow in the wall boundary layers is necessary to permit the development of a model of the flow which will allow the influence of these regions to be accounted for in design, and to determine the main sources of loss and the factors controlling these sources.

The flow in the end regions of a blade passage is complex. The main features contributing to this complexity are the blade passage secondary flow, tip clearance flows, effects due to relative motion between moving blade rows and the stationary walls, flows resulting from radial pressure gradients and the influence of flow separation which occurs at the junction of blade suction surface and the end wall. These various influences are illustrated in Fig. 2; a detailed discussion of each will be found in Chapter 2.

Qualitative and limited quantitative information is available on passage secondary flows and tip leakage effects but the flow separation originating in the corner bounded by the end wall and the suction surface of a blade appears to be the major cause of loss. Data on this phenomenom are limited. In this thesis a detailed study of the boundary layer on the hub wall downstream of the rotor and through the stator row of a single stage axial flow compressor is reported.

The flow in the stator hub region is dominated by a separation region in the suction surface/hub corner which sheds low energy air in the form of a streamwise vortex. The boundary layer downstream of the rotor has been found to consist of three distinct regions.

Next to the wall there is a region controlled by the wall in which the flow angle remains constant and the velocity profile can be described by a logarithmic distribution. Further from the wall the flow is dominated by vorticity generated by the turning of the end wall boundary layer and undergoes considerable over turning. On the outer edge of the boundary layer a third region dominated by a second vortex rotating in the opposite direction to the passage vortex exists. This vortex appears to originate from a separation region similar to that found in the stator row and it contains a major portion of the losses occurring in the hub region.

Measurement of the distribution of turbulence components downstream of the rotor indicate distinct directional properties, which appear to be due to the rotor wakes. As a result a model of the hub boundary layer as a quasi turbulent layer has been developed.

2. A REVIEW OF SECONDARY FLOWS AND LOSSES IN AXIAL FLOW COMPRESSORS

The main features controlling the flow in the hub and tip regions of a compressor are

(i) Secondary flows set up by turning of the wall boundary layer.

(ii) The effect of separation of the wall boundary layers.

(iii) Tip clearance leakage flows.

(iv) Effect of relative motion between the end walls and rotating rows.

(v) Flow due to radial pressure gradients.

In this chapter these flows will be discussed and various estimates of the component losses will be reviewed.

2.1. Estimation of Losses

In an actual machine it is difficult to separate the effects and resulting losses due to each of the flows mentioned above. The system in general use is that suggested by Howell (Ref. 5). Howell divides the total losses occurring in a machine into three components. The drag coefficient C_D can then be expressed as

$$C_D = C_{DP} + C_{DA} + C_{DS} \qquad - \quad (1)$$

The profile drag (C_{DP}) accounting for losses in the two dimensional flow over the blade, annulus drag (C_{DA}) due to the friction on the hub and casing walls and secondary drag (C_{DS}) arising from secondary flows in the hub and tip regions, and vorticies shed into the mainstream due to variation in circulation along the blade.

Howell has allowed for the annulus drag by using the relation

$$C_{DA} = 0.02\ s/h \qquad - \quad (2)$$

This estimate is obtained by assuming a wall friction coefficient of 0.010 which is approximately twice that normally encountered in pipe flow. It is stated by Carter (Ref. 6) that the high value is used to allow for adverse pressure gradients found in a compressor stage. However, as noted by Wallis (Ref. 7) in regions with adverse pressure gradients the skin friction should be reduced. The reason for Howell's selection of this large value can be found in Reference (5), which states in reference to cascades, that the secondary losses are negligible and the total loss in a cascade can be accounted for by the profile loss and wall friction loss (Equation 2). This statement has been proved incorrect by subsequent research (Ref. 8) and it is apparent that the annulus drag expressed by Equation (2) not only accounts for the wall friction losses but also for the considerable losses due to secondary flows and flow separation which occur in cascades.

In an actual compressor Howell states that the profile and skin friction losses remain as for a cascade and introduces a secondary drag coefficient, C_{DS} to account for the secondary flow losses which are no longer considered negligible.

$$C_{DS} = a\ C_L^{\,2} \qquad - \quad (3)$$

This relationship was obtained as the best fit to the available data. The constant a was found to be a function of Reynolds number only, varying from 0.019 at $Re = 1 \times 10^5$ to 0.015 at $Re = 5 \times 10^5$. The commonly used value is 0.018.

These two drag coefficients give a reasonable estimate of the losses occurring in the hub and tip regions of a compressor. However, the simple approach cannot be expected to be accurate under all conditions particularly for off-design operation, as these relationships are a function of blade loading only, while the total losses are dependent on a large number of parameters (Ref. 4)

$$C_{DS} = f(Re,\ s/c,\ h/c,\ t/c,\ \delta/c,\ M,\ \phi,\ C_L,\ R) \qquad - (4)$$

2.2. Secondary Flow Due to Turning of the End Wall Boundary Layer

One of the most important sources of secondary flow in the end wall region of a blade passage results from the turning of the wall boundary layer. Assuming that the static pressure is constant through the hub and casing boundary layers, in the radial direction, when this low velocity air is deflected through an angle equal to that of the main stream, the centrifugal forces developed are not sufficient to balance the pressure gradients imposed by the mainstream. Hence to maintain equilibrium the boundary layer is deflected through a greater angle giving rise to a cross flow and a resulting streamwise vorticity. This vortex will hereafter be referred to as the passage vortex.

The presence of this vorticity has been demonstrated by the flow visualization studies in cascades carried out by Herzig and Hansen (Ref. 9). Smoke filaments showed a strong cross flow in the end wall boundary layer toward the suction surface where all filaments rolled up into a vortex. The size and strength of this vortex increased with mainstream turning. Once formed this vortex "resisted" turning in subsequent cascades causing separation at the point of impact. The formation of the vortex was observed in both accelerating and decelerating blade rows.

An analytical method of prediction of this flow has been developed by Squire and Winter (Ref. 10). For an incompressible inviscid fluid with a small component of vorticity normal to the flow the secondary vorticity W_s generated by turning the flow through a small angle ϵ can be expressed by

$$W_{s2} - W_{s1} = -2 \frac{dU_1}{dy} \epsilon \qquad - (5)$$

Hawthorne (Ref. 11) using a more general theory has shown that

$$\frac{W_{s2}}{U_2} - \frac{W_{s1}}{U_1} = 2 \int_1^2 \frac{dP_0 \sin \gamma}{\rho U^2} d\epsilon \qquad - (6)$$

where P_0 is the total pressure and γ the angle between the principle normal to the streamline and the surface of constant total pressure or Bernoulli surface.

An alternative derivation of the above expression is given by Preston (Ref. 12) ; the theory has been further developed by Smith (Ref. 13) and Marris (Ref. 14)

Various investigators have attempted to simplify Equation (6) by assuming $\gamma = \pi/2$ and $W_{s1} = 0$ but at low turning angles the difference between the results given by these more complex relationships and the simple expression of Squire and Winter, Equation (5), is small.

The velocity components induced by this secondary vortex ψ_s can be obtained by introducing a secondary stream function such that the induced velocities downstream of the cascades are

$$u_2 = \frac{\partial \psi_s}{\partial y}$$

$$u_3 = -\frac{\partial \psi_s}{\partial z} \qquad - (7)$$

The secondary stream function then satisfies the Equation

$$\nabla^2 \psi_s = W_{s2} \qquad - (8)$$

Hawthorne has shown that by assuming $W_{s1} = 0$ and using Equation (5) that the change in average outlet angle through a cascade, $\Delta\alpha_2$ is given by the Equation

$$\Delta\alpha_2 = \frac{\bar{U}}{U_2} = \frac{-2\cos\alpha_2}{\pi U_1 \cos\alpha_1} \sum \frac{\psi_n'}{n} \qquad - (9)$$

where $\bar{u}$ is average secondary velocity in the x direction and

$$\psi_n' = \frac{8\epsilon}{n\pi}\left[\frac{\cosh\frac{n\pi z}{s\cos\alpha_2}}{\sinh\frac{n\pi\ell}{s\cos\alpha_2}}\int_z^\delta \frac{dU_1}{d\lambda}\sinh\frac{n\pi}{s\cos\alpha_2}(\ell-\lambda)\,d\lambda - \frac{\cosh\frac{n\pi(\ell-z)}{s\cos\alpha_2}}{\sinh\frac{n\pi\ell}{s\cos\alpha_2}}\int_0^z \frac{dU_1}{d\lambda}\sinh\frac{n\pi\lambda}{s\cos\alpha_2}\,d\lambda\right] \qquad - (10)$$

where $U_1(\lambda)$ is the boundary layer profile .

The basis of Equation (9) is that it is assumed that there is no rotation of the Bernoulli surface. However, measurement in cascades have shown that rotations of the order of 30° to 40° can occur. Because of this significant rotation, Hawthorne's inviscid model overestimates the secondary vorticity.

Lakshminarayana and Horlock (Ref. 15) have developed a theory taking into account the rotation of the Bernoulli surface and in addition allow for the effect of viscosity and spanwise displacement of the flow. With these modifications the model is in good agreement with experimentally obtained outlet angles for secondary flow removed from wall effects. Such a flow can be obtained by turning a wake through a cascade. However, attempts to predict the result of secondary flow in the end boundary layer of a cascade using the above theory have proved unsuccesful.

Horlock et al (Ref. 16) report that the outlet angle distribution found near the wall downstream of a cascade showed overturning near the wall and underturning in the mainstream but the position of maximum underturning occurred at a distance of twice the inlet boundary layer thickness from the wall. The theory predicts it to occur at a distance equal to the inlet boundary layer thickness.

The failure of the theory outlined in this section to predict the flow is due to the presence of flow separation occurring in the suction surface end wall corner of the cascade.

2.3. End Wall Boundary Layer Separation

The available data (Ref. 16 and 17) indicate that this separation is due to the presence of the wall and is not a direct result of the secondary flow, although the secondary flow may be a major factor affecting the condition of the wall layer.

Louis (Ref. 17) has carried out a number of experiments on the secondary flow in cascades, with and without the presence of a wall. To study the phenomena without wall effect a plate was placed upstream of the cascade and the wake used to supply the required spanwise velocity distribution. Under these conditions no evidence of separation was observed. To investigate the effect of a wall without secondary flow a thin wall was placed in the cascade at mid span with its leading edge in the plane of the cascade inlet. With this arrangement the boundary layer growth on the plate is small and as a result the secondary flow generated through the cascade is minimised. Separation was found to occur. Combining both effects, by extending the wall, produced a separated region similar to that obtained with the wall efect alone.

The argument that the flow separation occurs as a result of high local lift coefficients has been disproved in the tests described above. With no wall present, tests with a local $C_L = 1.015$ at the spanwise position corresponding to the centre of the wake showed no sign of separation but with a wall present separation occurred with a local $C_L = 0.653$.

A portion of the losses which appear in the region of separation are created at other positions in the blade passage. The passage vortex carries low energy air from the wall boundary layer into the suction surface end wall corner and in the stator row of a machine radial pressure gradients feed low energy air from the blade boundary layers and outer casing wall into the corner. This is illustrated in Figure (3).

The spearation does not appear to occur abruptly but grows slowly, increasing with mainstream turning. Hanley (Ref. 18) found that the separation was primarily a function of the inlet boundary layer thickness and pressure rise through the blade row, and states that severe separation will occur if

$$\left(\frac{\delta_1^*}{c} + 0.0285 \right) \frac{\Delta P}{\frac{1}{2}\rho U_1^2} > 0.0185 \qquad - (11)$$

Horlock (Ref. 16) correlates severe wall separation with passage blockage and on the information of Haller states that serious separation will occur in cascades if

$$\frac{\cos \alpha_1}{\cos \alpha_2} < 0.72 \qquad - (12)$$

In actual machines the axial velocity increase does not appear to be as great (Ref. 19) and machines with $\frac{\cos \alpha_1}{\cos \alpha_2}$ as low as 0.65 (Ref. 20) have operated without serious flow separation.

The geometry of the blade passage plays an important part in the growth of secondary flows. Blade aspect ratio (A = span/chord) not only controls the relative magnitude of the effects which end wall disturbances have on the mainstream but studies by Shallaan reported in Reference (34) indicate that it also has a major influence on the form of the secondary flows.

Shallaan found that in low aspect ratio cascades (A = 2) the flow appears to rotate more and separation occurs further out along the blade than in higher aspect ratio (A = 5) cascades where the separation occurs equally on the end wall and blade surface. The separation in low aspect ratio cascades was found to be more severe.

2.4. Passage Vortex and End Wall Separation Losses

Secondary flows resulting from the passage vortex and disturbances due to flow separation in the suction surface/end wall junction are the two features controlling the flow in the end wall region of a cascade. As a result the information on these two losses, which is purely empirical, combines the losses resulting from these two factors.

Louis (Ref. 17), carried out loss measurements in cascades in conjunction with the investigation described in the previous section. The measurements indicate that the losses in a region of secondary flow removed from a wall are of the same magnitude as the losses in the two dimensional flow over the blade. When the wall was introduced a high loss core was found in the corner between the end wall and suction surface and this core appeared to be independent of the intensity of the secondary flow. These measurements were of the total pressure losses through the cascade, the kinetic energy of the secondary flow, was not considered as a loss. The work of Eischenberger and Van le Nguyen reported in Reference (4), shows that for a flow in two bends of 24° and

90° the loss due to complete dissipation of the kinetic energy of the secondary flow would be 0.2% and 1% of the inlet kinetic energy compared with total losses through the bend of 5% and 25% respectively. This evidence that the kinetic energy of the secondary flows generated when a boundary layer region is turned is negligible compared with the magnitude of other losses occurring is supported by Mellor and Dean in the discussion of Reference (13).

From the data reviewed above, it is evident that the losses due to the secondary flow are negligible compared with those resulting from the end wall separation. Hence any expression derived to account for the losses must consider the parameters controlling the wall boundary layer, it must not be based on parameters describing the secondary flow resulting from the passage vortex.

Meldahl (Ref. 21) has proposed the following drag coefficient to account for these losses.

$$C_{DSP} = 0.055 \frac{C_L^2}{A} \qquad - (13)$$

Vavra (Ref. 31) on the basis of a comparison of the expression presented by Meldahl with that given by Howell for secondary flow losses (Equation 3) claims that the coefficient is too large and suggests the modified form

$$C_{DSP} = 0.04 \frac{C_L^2}{A} \qquad - (14)$$

As stated in Section 2.2 the expression given by Howell for the secondary flow losses only accounts for a portion of the flow losses because the annulus drag coefficient, Equation (2), also contains a component of the secondary drag losses. Vavra reasons that the coefficient should be reduced since part of the secondary flow loss is recovered. This appears to be based on the assumption that the losses are manifest as kinetic energy of the passage vortex which may be recoverable and not as a result of the flow separation which constitutes the major source of the losses. There appears to be no sound reason for the reduction in the coeffecient as suggested by Vavra.

Ehrich and Detra (Ref. 22) have obtained the following empirical relationship for the loss coefficient allowing for the transport, toward the blade suction surface, of the wall boundary layer by the passage secondary flow

$$C_{DSP} = \frac{0.1178\,\epsilon^{2}}{h/s\,(1 - 0.2\,s/h)^{2}} \qquad - \quad (15)$$

Fujie (Ref. 23) suggests the expression

$$C_{DSP} = 0.0275\,C_L^{2}\left(1 + 2.9\,\frac{i - id}{\epsilon\,d}\right)^{\frac{1}{2}} \qquad - \quad (16)$$

where i_d and ϵ_d are the design incidence and flow deflection respectively.

A comparison of the drag coefficients given in Equations (13) to (16) is made in Figure (4), for a representative set of compressor parameters.

Hanley (Ref. 18) assumed that the losses due to the passage vorticity were negligible and that the major component is due to the loss in kinetic energy of the streamwise velocity component of the flow through the cascade as a result of corner separation. This loss was found to be independent of gap/chord ratio , camber, stagger, incidence and aerofoil shape but dependent on the inlet boundary layer thickness and the pressure rise through the cascade. By assuming that the boundary layer retained its two dimensional characteristics, correlations of the outlet boundary layer thickness and a profile defining parameter were obtained. These allow a reasonable estimate of the losses to be made, for the range of cascade geometries investigated, provided the inlet boundary layer thickness and mainstream turning angle are known.

2.5. Reduction of Effects of Passage Secondary Flow and Separation

Ehrich (Ref. 24) suggests that a reduction in the passage secondary flow through a cascade can be obtained by increasing the turning angle in the wall boundary layers. For flow in a cascade of twisted blades the total streamwise vorticity at outlet is given by

$$\nabla^2 \psi_s = 2\epsilon \frac{\partial U_1}{\partial y} + U \frac{\partial \epsilon}{\partial y} \qquad - \ (17)$$

The first term on the right hand side is the secondary vorticity due to turning of the wall boundary layer and the second is that due to the variation in deflection along the cascades. For complete elimination of the streamwise vorticity the following equation must be satisfied.

$$\epsilon U^2 = \text{constant} \qquad - \ (18)$$

The expression requires an increase in the turning angle as the velocity decreases.

It has been indicated earlier in this section that the losses due to the kinetic energy of the secondary flow are negligible compared with the losses resulting from flow separation. Increasing the turning angle will reduce the former but will certainly increase the likelihood of separation.

Martin (Ref. 25) has attempted to reduce the disturbance in the end wall region of a cascade by reducing the camber at the blade tip and hence the turning angle. The results of this investigation were not conclusive. No marked reduction in losses were reported but the wall separation appeared to be reduced considerably.

These two possible solutions are conflicting. However, the prevention of separation appears to be the main requirement for reducing losses. As a result the technique suggested by Martin would appear to be more promising.

Louis (Ref. 17) suggests the use of fillets between the blade and end wall as a method of reducing separation in machines with light blade loading ($\frac{\cos \alpha_1}{\cos \alpha_2} \geqslant 0.7$) and high stagger blading. At higher loadings their use does not appear to have any advantage.

2.6. Mainstream Secondary Flows

When a variation in circulation, in the spanwise direction, occurs along a blade, vorticity is shed into the mainstream from the trailing edge. In a typical compressor the magnitude of the resulting loss is small.

By assuming a linear lift distribution along the blade Tsien (Ref. 26) has obtained the following expression for the induced drag.

$$C_{DST} = \frac{(C_{Li} - C_{Lo})^2}{\pi^3} \left(\frac{s}{2h}\right) \left(1.0518 + \sum_{n=1,3,5} \frac{\coth n\pi s \cos g/4h - 1}{n^2}\right) \quad (19)$$

where o and i refer to the tip and hub conditions.

Van Karman (Ref. 27) also assumes a linear lift distribution, but neglects the interference effect of adjacent blades, and obtains the relationship

$$C_{DST} = 0.0423 \left(1 - \frac{C_{Lo}}{C_{Li}}\right)^2 \frac{C_{Li}{}^2}{A} \qquad - \quad (20)$$

For the range of parameters normally found in compressors Lakshminarayana and Horlock (Ref. 4) have found that Equations (19)and (20) give almost identical results.

Vortices will also be shed into the main stream when large tip clearances exist resulting in leakage flows which reduce the lift at other spanwise positions. However in Reference 29, it has been found that no lift reduction occurs at the blade tip until the clearance/chord ratio exceeds 0.06. For the range of clearance/chord ratio normally found in turbomachinery (0.02 to 0.04) there will be no increase in the vorticity shed.

2.7. End Clearance Flows

Due to the pressure difference between the two surfaces of a blade the presence of end clearance will give rise to a leakage flow. This flow sets up a vortex which rotates on the opposite sense to the vortex set up as a result of the flow induced by turning the end wall boundary layer.

The flow due to tip clearance with other influences removed has been studied by Lakshminarayana and Horlock (Refs. 29 and 30) by using single aerofoil with clearance gap at mid span. The presence of a thin wall in the centre of the gap did not appreciably alter the lift and drag measurements, indicating that the split blade is a valid model for studying clearance flow.

At low clearance/chord ratios the clearance flow first resulted in a vortex sheet parallel to the tip which rolled up into a single vortex some distance away from the blade suction surface, and at an angle to the main flow. As the clearance/chord ratio was increased, the distance from the suction surface at which the vortex formed, and the angle between the vortex and the main flow both decreased, the leakage flow eventually rolling up into a vortex as soon as the flow reached the suction surface. This behaviour can be explained by the fact that at low clearance/chord ratios only leakage flow occurs but as it is increased a portion of the main flow also passes through the gap and the resulting mixing reduces the leakage flow velocity and angle of the leakage vortex relative to the blade chord. Leakage results in underturning of the flow near the tip and slight overturning at a greater distance from it. As a result of the leakage vortex, spanwise flow is induced along the suction surface toward the tip.

It was found in Reference (29) that for the range of clearance/chord ratio normally found in turbomachinery (0.02 - 0.04), no reduction in lift occurred due to leakage flow. In this range of clearances, viscous effects have a restraining influence and only a portion of the bound vorticity of the blade is shed at the tip. At larger clearances (> 0.06) the vorticity retained at the tip drops to zero and vorticity is also shed at other spanwise positions resulting in a rapid decrease in lift.

Theoretical analysis of the losses due to tip clearance flows have been based on two methods : leakage flow concepts and shed vortex theory.

The former considers the flow to result from the pressure difference across the gap and calculates the losses by assuming complete dissipation of the leakage flow kinetic energy.

This approach has been used by Rains (Ref. 32) whose analysis has been modified by Vavra (Ref. 31) for the case of a stationary blade with a triangular pressure distribution, to obtain a drag coefficient given by

$$C_{DSC} = \frac{4\sqrt{2}}{5} \; C_c \, C_R^3 \left(\frac{t}{h}\right) C_L^{3/2} \qquad - (21)$$

where C_R is a gap resistance coefficient,

C_c a contraction coefficient

suitable values are $C_R = 0.8$ and $C_c = 0.5$ resulting in

$$C_{DSC} = 0.29 \left(\frac{t}{h}\right) C_L^{3/2} \qquad - (22)$$

Shed vortex theory assumes the leakage is induced by the vortices shed at the tip and uses lifting line concepts to calculate the losses. Early investigators such as Betz (Ref. 35) assumed the lift dropped to zero in the gap, however, Lakshminarayana and Horlock in the studies described earlier in this section have found that due to real fluid effects some lift is retained at the tip for small clearances (clearance/chord ratios < 0.06).

For the aerofoil with mid span gap Lakshminarayana has devised the following expression which shows good agreement with experimental drag coefficients.

$$\frac{C_{DSC}}{C_L^2(1-K)} = \frac{1}{8\pi A} \ln \frac{(e^{2\pi \ell/s}-1)(2{\cdot}17 + 0{\cdot}17 \coth 2\pi t/s)}{0{\cdot}17\left[(1-\coth 2\pi t/s)+(1+\coth 2\pi t/s)\, e^{2\pi \ell/s}\right]} \qquad - (23)$$

Where K is the fraction of the two-dimensional lift retained at the tip. K will depend on a number of factors making theoretical prediction difficult. The values obtained experimentally in Reference 29 are shown in Figure 5.

For small clearance/chord ratios of the order of those found in turbomachinery (0.02 - 0.04) Equation (23) can be approximated by the linear relationship

$$C_{DSC} = \frac{1{\cdot}4\,(1 - K)\,C_L{}^2}{A} \left(\frac{t}{s}\right) \qquad - (24)$$

and assuming K = 0.5 in this range

$$C_{DSC} = 0.7\,\frac{C_L{}^2}{A} \left(\frac{t}{s}\right) \qquad - (25)$$

Meldahl (Ref. 21) suggests the empirical relationship for the losses due to leakage

$$C_{DSC} = 0.25 \left(\frac{t}{c}\right) \left(\frac{1}{\cos \alpha_2}\right) \frac{C_L{}^2}{A} \qquad - (26)$$

The expression given by Rains - Vavra, Meldahl and Equation (25) are compared for a typical cascade in Figure 6. The first two predict a considerably lower value of drag than the latter.

Shrouding of the blades has been suggested as a means of reducing the effect of tip clearance. There is little information on this aspect, but as is pointed out by Carter (Ref. 6) shrouding a blade row replaces circumferential leakage between blade passages with an axial leakage. As a result there is little to be gained.

2.8. Interaction of Leakage and Passage Secondary Flows

The discussion in the previous section only considered clearance flow isolated from other influences. In this section the interaction of leakage flow with other secondary flows is discussed.

Herzig and Hansen (Ref. 9) report that flow visualisation studies show the clearance vortex displacing the passage vortex and the two vortices rotating side by side in opposite directions with little apparent mixing. This results in a large disturbed region.

Lakshminarayana and Horlock (Ref. 29) investigated the losses resulting from leakage and cross passage flows in cascades and discovered that a controlled amount of leakage flow had a beneficial effect ; by reducing the severity of the separation occurring in the corner between the suction surface and the end wall the total losses are considerably reduced. For the cascade investigated the optimum clearance/chord ratio was found to be 0.04.

This behaviour is shown diagrammatically in Figure (7) based on the flow visualisation studies of Reference (29). With no clearance (a) there is a severe separation zone in the corner between the suction surface and the end wall. With a clearance gap (b) the leakage flow tends to lift the separated region off the end wall. As the clearance is increased to that corresponding to the minimum loss (c) the clearance flow tends to sweep the separated region off the end wall and moves along the suction surface before rolling up into the leakage vortex, the spanwise flows induced by this vortex also tend to remove the separated region from the suction surface. When the clearance is further increased (d) the leakage flow rolls up as soon as it reaches the suction surface ; the degree of interaction with the separated region is reduced, resulting in increased losses.

It was noted during these studies that a small separated region occurred on the suction surface at the blade tip. This has been referred to as a leakage separation and occurs when the leakage flow is high.

The mechanism described above for the reduction in losses when leakage and passage secondary flows interact is controlled by the relative magnitude of the two flows. It appears in the investigation reported in Reference 29 that the leakage flow was the dominant flow and the secondary flow relatively weak at all times.

The presence of a finite value of tip clearance at which total losses are a minimum has been reported by Dean and Hubert though this minimum is not necessarily less than the loss value at zero clearance. The information from these sources is reproduced in Figure (8) which is taken from Reference (29).

It is evident that if the reduction in losses resulting from the mixing of the flows in cascades described above occurs in machines, then extremely small clearances are not necessary and a finite value will give a better performance. Horlock (Ref. 34) states that, in machines, the effect of blade rotation may reduce the optimum value of the clearance/chord ratio below that found in cascades though no detailed measurements in machines are available.

The drag coefficients given in Equations (22) and (25) can be used to give a reasonable estimate of the losses occurring in isolated leakage flow but when there is interation between leakage and other secondary flows, as described in this section, there is no satisfactory method of estimating the combined drag.

2.9. Relative Motion Between Blades and Wall

Leakage flows occurring at the tip of a rotor are further complicated by the relative motion between the blade and wall which generates a "scraping" vortex. In the case of a compressor where the pressure surface leads, this results in a deflection of some of the air which would have passed through the tip gap, with a resulting reduction in clearance flow. On the suction surface spanwise flows are induced toward the wall. These flows are shown in Figure 9. The relative motion appears to increase the loading at the tip.

Howell (Ref. 2) reports that clearances up to 1% - 2% of blade height appear to have little effect on losses in actual machines but at greater clearances the efficiency falls by approximately 3% for each 1% increase in clearance. This insensitivity at low clearances may possibly be the result of the effect of the scraping vortex discussed above or the effect of the interaction of leakage and passage secondary flow discussed in the previous section.

2.10. Radial Flows

For radial equilibrium in turbomachinery radial static pressure gradients must exist to balance centrifugal forces. These must satisfy the equation

$$\frac{\partial P}{\partial r} = \rho \frac{V_u^2}{r} \qquad - (27)$$

where V_u is the tangential velocity component of the air.

This results in a radial pressure gradient toward the hub. In a stator row, assuming static pressure is constant across the blade boundary layer normal to the blade, this pressure gradient will be imposed on regions in which the air has a low tangential velocity component and hence a low centrifugal force acting on it. The resulting unbalanced force will cause this air to flow toward the hub.

In a rotor the absolute tangential velocity of the air is considerably less than the blade velocity. As a result, stagnent air relative to the rotor will have a tangential velocity component greater than that of the mainstream air and the resulting higher centrifugal force causes this air to flow toward the tip.

Regions of stagnent air which may be transported by these radial pressure gradients exist in the blade suction surface boundary layer, particularly in areas such as separation bubbles and in the wake.

Flow visualization studies (Ref. 35) have shown that the radial flow on the suction surface of a stator blade forms a vortex in the end wall/suction surface corner of the blade passage which rotates in the opposite direction to the passage vortex. This is illustrated in Figure 10. Radial flow between the tip and hub regions explains the improved conditions and in some instances the absence of secondary vortices at the tip of stator rows (Ref. 35). If the flow disturbances near the tip are small and a suitable radial flow path is present the low energy air will be fed into the hub region rather than forming a vortex near the tip. In a rotor the direction of the radial flow is reversed and an improvement in hub conditions can be expected.

In multi stage machines radial flows of low energy air between tip and hub regions result in a certain amount of mixing with the mainstream. In Reference (36) Hansen and Herzig state that this mixing prevents continuous growth of the hub and casing boundary layers and generates a more uniform radial distribution of axial velocity.

It has been suggested that fences at mid span be used to prevent the flow of low energy air along the blade into already critical regions. These reduce the radial flows (Ref. 35), feeding the low energy air into the mainstream but the increase in viscous losses resulting from their introduction makes any nett improvement a debatable issue.

As the radial pressure gradient is fixed for a given design the most effective method of reducing radial flow appears to be by improved blade design this will reduce the amount of low energy air available for transport, and by reducing blade boundary layers and wake thickness, reduce the size of the radial flow paths.

2.11 Annulus Drag

The annulus drag is equally as important as the secondary drag in the estimation of the losses in the hub and tip regions of a cascade. The annulus drag coefficient was introduced by Howell (Ref. 2) to allow for the friction losses in the end walls of a blade passage. Howell suggested the relationship

$$C_{DA} = 0.02\ s/h \qquad - (2)$$

This is obtained by assuming a skin friction coefficient of 0.01 which is approximately twice that normally encountered. The reason for this high value has been discussed in Section 2.1. A more realistic expression is obtained by taking a skin friction coefficient of 0.005 which results in

$$C_{DA} = 0.01\ s/c \qquad - (28)$$

Vavra (Ref. 31) recommends the expression

$$C_{DA} = 0.018\ c/h \qquad - (29)$$

The coefficient in Equation (29) was obtained by comparison with Equation (2). As a result this expression also includes the portion of the secondary drag included in the Howell relationship. The form of the expression does not appear to have advantages over the simple relationship obtained using the Howell principle of considering a friction force acting on an area equal to that of the end walls of the blade passage.

2.12 Total Secondary Flow Losses in an Axial Flow Compressor

In Section 2.11 it was argued that a more realistic value for the annulus drag would be half that indicated by Howell, Equation (2), and that the remainder of the annulus drag as calculated by Howell was due to secondary flow losses. As a result the total secondary losses using the Howell expressions will be given by

$$C_{DS} = 0.018\ C_L^2 + 0.01\ s/h \qquad - (30)$$

Meldahl (Ref. 21) suggests a secondary drag coefficient given by

$$C_{DS} = 0.055\ \frac{C_L^2}{A} + 0.25\left(\frac{t}{c}\right)\left(\frac{1}{\cos\alpha_2}\right)\frac{C_L^2}{A} \qquad - (31)$$

where the first term (Equation 13) allows for the losses due to secondary flows and separation in the blade passage, and the second (Equation 26) is related to clearance flows.

In this section the various sources of secondary flow loss in a compressor have been discussed and various expressions for the resulting drag have been presented. These can be combined in the manner suggested in Reference (4), to give a total secondary drag coefficient given by

$$C_{DS} = C_{DSP} + C_{DSC} + C_{DST} \quad - (32)$$

suitable values for the components are

$$C_{DSP} = 0.055 \frac{C_L^2}{A}$$ Meldahl (Ref. 21).

$$C_{DSC} = 0.7 \frac{C_L^2}{A} \left(\frac{t}{c}\right)$$ Lakshminarayana & Horlock (Ref.29)

$$C_{DST} = 0.0423 \left(1 - \frac{C_{Lo}}{C_{Li}}\right)^2 \frac{C_{Li}^2}{A}$$ Von Karman (Ref. 28)

Equation (32) does not take account of the effect of radial flows and blade rotational influences such as scraping vortices and flows induced by centrifugal effects but these omissions are balanced by the fact that no allowance has been made for the reduction in total losses due to beneficial interaction between the component flows as discussed in Section 2.8.

The drag coefficients predicted by Equations (30), (31) and (32) are shown in Figure 11 for a representative compressor geometry. It is evident from Figure 11 that, for a typical compressor, the three expressions give similar values. As a result there is little value in using the more complex expressions except at small aspect ratios and large tip clearances.

2.13. Concluding Remarks

The information which has been presented in this section has been obtained almost entirely from studies of two dimensional cascades and isolated aerofoils. The data on losses has been obtained from detail measurements in cascades and from losses inferred from efficiency calculations on machine tests. No detailed measurements have been made in machines with the aim of describing the mechanism of the flow directly rather than inferring what might be from other evidence.

From the work which has been carried out on two dimensional cascades, models exist for secondary flow originating from the passage vortex when removed from end wall effects (Ref. 15) and for tip clearance flow when removed from other influences (Ref. 29). However a study of the components of the secondary drag coefficient given by Equation (32), shown in Figure 12, indicates that the major portion is due to C_{DSP}, the greater part of which results from flow separation in the suction surface/end wall corner of the blade passage. The information available on the mechanism of this latter phenomenom is small, though the extent of the separation does appear to be influenced by the history of the wall boundary layer and by the load on the blade row (Ref. 18).

A second factor of importance in a machine is the effect of interaction of the various secondary flows. It appears that the nett loss in a machine may be less than the sum of the losses due to individual flows (Ref. 29), but at present no measurements have been made in machines to investigate this point.

Research into the flow in the tip and hub regions of turbomachinery is at present necessary (i) to obtain a suitable model of the flow in these areas which will enable improved design methods to be devised and (ii) to reduce the losses arising from these regions. If these two objectives are to be reached it is apparent that an understanding of the mechanism of the flow separation ocurring in the hub and tip regions must be obtained. Initial studies in this direction were the objects of the work described in this thesis.

3. EQUIPMENT AND INSTRUMENTATION

3.1. Vortex Wind Tunnel

The work described here was carried out on the Vortex Wind Tunnel at the University of Tasmania. The experimental rig shown in Figure 13 is a single stage axial flow compressor containing three blade rows, namely, inlet guide vanes, rotor and stator. A brief description of the rig is given below. A more detailed description, together with a summary of previous work carried out is given by Oliver (Ref. 9). The major dimensions of the machine are listed in Appendix A.

Air enters the tunnel radially and is turned through 90° with a contraction of 7 to 1 into a 45 inch diameter aluminium section one diameter in length containing the three blade rows. This is followed by a 13 feet, 7° included angle diffuser with a cylindrical core which is flared out to give a radial exit. The exit opening is controlled by a cylindrical throttle giving an opening from zero to 30 inches.

The blades are 9 inches long and have a 3 inch chord giving an aspect ratio of 3. The hub/tip ratio is 0.6. There are 38 blades in the two stationary rows and 37 in the rotor giving mid blade height space/chord ration of 0.99 and 1.02 respectively. The blade row centres have an axial spacing of two chord lengths.

The blading has a circular arc camber line clothed with a C.4 profile with a thickness/chord ratio of 10%. The blades are twisted about a radial straight line through the middle of the camber lines of all sections. They are designed on the basis of the Howell data to give nominally free vortex conditions at the design duty ($\phi = 0.8$) with 50% reaction at mid blade height and uniform work output along the blade.

The tunnel may be split at flanges on the centre line and between each blade row allowing the inlet and required portion of the outer casing to be rolled back to provide access to the blades. The stationary blade rows are mounted on rings, which can be rotated through a circumferential distance of two blade spaces thus allowing the blades to be traversed past a stationary measuring probe. Blade clearance at the hub is approximately 0.04 inches i.e. 0.5% of the blade height.

The rotor is driven by a 40 horse power electric motor controlled by a Ward Leonard set, maximum speed is 750 R.P.M. which corresponds to a blade chord Reynolds number of 2×10^5, based on blade speed at mid span.

The rotor speed is set by a stroboscope triggered by a 100 cycle signal from a crystal clock and is monitored by use of a photo electric cell arranged to give one pulse per revelution with counting on a decade counter over a period of one minute. The result is then displayed for one minute and the cycle repeated ; the minute intervals are also timed by the crystal clock. This method enables the speed to be maintained within ± 1 R.P.M. i.e. ± 0.2%.

Instrument slots are fitted on the horizontal diameter between the blade rows. Probes are mounted in a chuck fitted to the tunnel side allowing movement in the axial and radial directions and rotation of the instrument on its horizontal axis. The axial position can be set using a vernier scale to an accuracy of 0.01 inch. The radial position is controlled by a micrometer screw, when working near the wall (particularly when using hot wire probes) a dial gauge (0.0001 inch/division) was used. The angular position of the probe is controlled by a micrometer drive, which permits the yaw angle to be set at 0.02°.

Pressure measurements were made on a multitube manometer inclined at a slope of one in four. The working fluid was methyl alchol the specific gravity of which was taken as 0.80 and constant. A "Betz" projection manometer was used during calibration of the various probes.

3.2. Hot Wire Anemometer

Hot wire measurements were made using a "Disa" 55 A01 constant temperature anemometer in conjunction with probes constructed at the University of Tasmania. These consisted of 0.0003 inch diameter tungsten wire approximately 0.1 inch long welded to nickel prongs 0.03 inches in diameter and $\frac{3}{4}$ inch in length. It was suspected that this long length of prong could have introduced a vibration problem. The effect of vibration of the probe and supports is always an unknown factor but normally this produces peaks in the turbulance components where the exciting frequency corresponds to the natural frequencies of the wire and its supports, no such peaks were discerned in the readings obtained during this investigation.

The wires were calibrated in an open circuit wind tunnel where velocity was measured using a pitot static tube connected to a "Betz" micro-manometer. The turbulance level in the tunnel was approximately 2%.

The hot wires were used to measure mean velocity, turbulance components and flow direction. The turbulance components were obtained using the method presented by Hinze (Ref. 37). Details of the technique can be found in Appendix B.

The directional sensitivity of the wire to flow direction was used when measuring flow angle. The D.C. voltage changes with angle in the manner shown below.

$$V \approx V_{\theta=0} \cos\theta \qquad - (35)$$

When the wire is nearly normal to the flow the variation with angle is small but at ± 45° the sensitivity is sufficient to set angle for a given voltage repeatedly to better than 0.25°. The method used to obtain flow direction was to select a voltage at approximately 45° to the direction of the flow, find the two angles corresponding to it and bisect them to give the flow direction.

Although this method of measuring angle was rather tedious there seemed to be no alternative in the presence of blade wakes from the rotor row which were known to give misleading readings on pressure probes. The non linear effects of the high turbulance levels within the blade wakes probably also upset the hot wire readings but this source of error is thought to be small.

The datum for angle measurement was obtained by attaching a cross bar to the probe holder and measuring the angle between the bar and wire with the equipment shown in Figure 14. The horizontal position of the bar was recorded and the probe rotated until the wire was horizontal. This was determined by the cross hair of the level, or rather by traversing one end of the cross hair along the wire. The angle between the wire and bar could be found to within 0.1°. Measurements of angle in the tunnel could be repeated with different wires to within 0.5°.

To allow for changes in ambient temperature a correction of the form

$$dE = -\tfrac{1}{2}E\,\alpha\,R_a dt/(R_w - R_a) \qquad - (36)$$

where α is the thermal coefficient of resistivity.

E the measured voltage

R_a wire resistance at ambient temperature

R_w operating wire resistance

was applied to all voltages measured.

When operating a hot wire close to a wall the heat loss to the boundary introduces errors as also does the change in flow pattern around the wire due to the proximity of the wall. Little information is available on this problem, the most recent is that of Wills (Ref. 38) whose method has been used in this investigation.

Wills applies his correction by subtracting a number K_w from the value of $R_{ew}^{0.45}$ where R_{ew} is the wire Reynolds number based on the wire diameter. The value of K_w depends on the distance from the wall as shown in Figure 15. The correction factor was obtained for laminar flow. For turbulent flow a value of approximately half this is suggested by Wills and this recommendation, in absence of better data has been used in this thesis.

3.3. Cobra Yaw Meter

The cobra yaw meters shown in Figure 16 were used for measuring total pressure, velocity and flow direction through and downstream of the stator. They consist of three one millimeter tubes arranged in the form of an arrow head, the two side tubes being cut off at an angle of 35° to the probe centre line and the centre one being square to measure total head.

Instead of the usual method of nulling the two side hole readings to obtain direction and using a factor on the difference between side and centre readings to give velocity, the probes were calibrated for use in the yawed position. This reduces the time required to obtain data and enables the probe to be placed in positions not otherwise possible. The amount of work required in calculation of results is increased considerably but with the use of computor this is not a major consequence.

The derivation of the relationships given below, used to calibrate the probes, can be found in Appendix C.

The angle from null, α, can be determined from the pressures in the three tubes by the relationship

$$\frac{h_A - h_c}{h_B - h_c} = F(\alpha) \qquad - (37)$$

the velocity from either of the two relationships

$$\begin{aligned} U &= \left| 2g(h_A - h_c) \right|^{\frac{1}{2}} G_1(\alpha) \\ &= \left| 2g(h_B - h_c) \right|^{\frac{1}{2}} G_2(\alpha) \qquad - (38) \end{aligned}$$

and the difference between true total head and the centre tube reading by

$$h_o - h_c = \frac{U^2}{2g} H(\alpha) \qquad - (39)$$

Where F, G_1, G_2 and H are functions of α, the angle from the null position.

Probe number 1, Figure 16, was used for measurement downstream of the stator. It was calibrated for use in the range ± 10° from null but in operation the wire was kept within ± 5°.

The design of the wind tunnel made probe number 2 necessary for measurement through the stator. Becasue of the shape of the blade passage and high cross flows in regions of flow separation the probe was at times operating at large angles from the null position. For this reason the probe was calibrated through a large range, ± 100°. In the ordered regions of flow (away from the blade walls), the probe was kept as close to null as possible but due to the fact that rotation of the probe changed the axial position of the measuring station it was not usually operated as close to null as was probe 1. The accuracy outside the range ± 15° is doubtful but the probe measurements enable an order of magnitude to be obtained where as no information would otherwise have been available.

The calibration of meter No. 2 against yaw, shown in Figure 17, was carried out at velocities varying between 20 and 100 f.p.s. but no variation with Reynolds number was detected.

For the velocity calibration $U/|\Delta h|^{1/2}$ against α, Figure 18, where Δh is the difference between the centre and one side hole, the difference between the same pair of holes could have been used throughout but Δh was taken as the largest of the two head differences to avoid errors in using small differences of large numbers.

The total head correction is shown in Figure 19. For ± 4° from null the centre hole reads true total pressure within the accuracy of this work (± 3% of dynamic head).

3.4. Factors affecting Pressure Probes

When a pressure probe is used in a boundary layer allowance must be made for the effect of

(1) proximity of the wall

(2) the transverse velocity gradient

(3) turbulence

and if the probe is used in a turbo-machine

(4) the influence of the wakes of upstream blade rows.

Macmillan (Ref. 39) states that the wall has an influence when the probe is closer than two diameters from it and suggests that this can be accounted for by adding an increment to the velocity measured varying exponentially from 1.5% when the probe is on the wall to zero when the probe centre line is two diameters away.

The effect of the transverse velocity gradient can be expressed as a displacement of the effective centre of the tube toward the region of higher velocity. The apparent increase in velocity is roughly proportional to the velocity gradient with the result that the displacement is approximately constant. Young and Maas (Ref. 40) have suggested for square cut tubes the relationship

$$\frac{\Delta y}{D} = 0.13 + 0.08 \frac{d}{D} \qquad - \quad (40)$$

where Δy is the effective displacement, D the probe outer diameter and d the probe inner diameter. However, later work by Macmillan (Ref 39) suggests that the above relationship overestimates the displacement and a more accurate result is given by

$$\frac{\Delta y}{D} = 0.15 \qquad - \quad (41)$$

This would decrease the velocity indicated by the cobra probes when touching the wall by approximately 2% and by 0.8% when 0.05 inches from it.

The correction for wall proximity and that due to shear act in opposite directions. Combining the two the nett result is small, less than 1%. As the information given above is for pitot tubes i.e. a single tube probe, and that the effects on multitube probes have not been investigated, it was considered that no improvement in accuracy would be obtained by applying corrections for these influences.

The effect of turbulence is to increase the pressure indicated by the probe by $\frac{1}{2}\rho \overline{u_1^2}$ where u_1 is the fluctuating component of the velocity in the direction of the probe. No hot wire measurements were taken through and donwstream of the stator. However, at $\frac{1}{2}$ inch upstream of the stator leading edge the maximum value of $\frac{1}{2}\rho \overline{u_1^2}$ in the boundary layer was 1.4% of the local dynamic head.

Measurements in turbo machines downstream of rotors have shown effects of a greater magnitude than those indicated by the classical corrections mentioned above.

In Fig. 20, total pressure measurements in the flow downstream of rotor in the Vortex Wind Tunnel, reported in (Ref. 41) are shown. The total pressure $\frac{1}{2}$ inch from the rotor trailing edge is approximately 50% greater than that measured at $1\frac{1}{2}$ inches. The difference is approximately constant across the annulus and can not be explained as a boundary layer effect. In Fig. 21, the measured mid span total pressure is plotted as a function of distance from the rotor. The pressure drops rapidly within the first half chord length after which the decline is small.

A similar occurrence has been noted by Wallis (Ref. 7) who reported that measurements near the trailing edge of the rotor in an axial flow fan gave total head rises which when used to calculate efficiencies gave unreasonably high values. Wallis also found the excess in total pressure to be approximately constant across the fan annulus. Neustein (Ref. 42) also reports high values close to the trailing edge of a rotor.

The cause of these errors cannot be accounted for by the effects mentioned earlier in this section and appear to be due to the rotor blade wakes. No satisfactory explanation of this phenominom is available.

In this investigation pressure probes were not used in the region adjacent to the rotor but were employed through and downstream of the stator. Efficiencies calculated from pressure measurements $1\frac{1}{2}$ inches from the rotor trailing edge appear to be no more than 1% high. Allowing for a further decrease between this station and the stator the effect of this phenominom on the measurements in the investigation should be less than the accuracy of the measurements (± 3%).

4. THE HUB BOUNDARY LAYER THROUGH THE STATOR

4.1. Experimental Procedures

The boundary layer on the hub through and downstream of the stator row was studied using the cobra yaw meters described in Section 3.3. The distributions of velocity, total pressure and flow angle were measured at 0.5 inch (0.167 chord lengths) intervals through the blade passage and at 0.5 and 1.5 inches (0.167 and 0.50 chord lengths) downstream of the trailing edge.

These measurements were carried out at a duty specified by a flow coefficient $\phi = 0.75$ and pressure coefficient $\psi = 0.70$ corresponding to a rotor speed of 500 R.P.M. and 8 inch throttle setting. This is close to the blading design point ($\phi = 0.80$ and $\psi = 0.64$).

Measurements were taken at radial spacings varying between 0.025 inches near the wall to 0.5 inches in the mainstream. The probes were placed at the required radial distance from the wall and the blade row rotated past the stationary probe. The distance between readings in the circumferential direction varied between 0.1 and 0.3 inches.

4.2. Experimental Results

4.2.1 Total Pressure

Total pressure contours at the various axial stations are presented in Figs. 22 to 28. The reference level for total pressure was taken as the mean total pressure upstream of the inlet guide vanes, all data are non-dimensionalized by dividing by $\frac{1}{2}\rho U_m^2$ where U_m is the peripheral velocity of the rotor at mid blade height.

The feature of these plots is the growth of the region of separation in the suction surface/hub wall corner. A region of separation is already present at 0.167 chord lengths from the leading edge (Fig. 22). The region grows as it passes through the row and the contours suggest a radial movement of the low energy core from the hub surface to the blade surface. Downstream of the trailing edge the low energy core appears to diffuse and move away from the wall, and relative to the blade wake in the mainstream is displaced away from the side of the wake originating on the suction surface of the blade.

4.2.2. Velocity

Representative velocity distributions are presented in Figs. 29 to 31. These show the same basic feature of a low energy region forming and being displaced from the hub described in the previous section. The distribution at 0.5 chord lengths downstream from the trailing edge (Fig. 28) indicates that the flow in the low energy core strengthens rapidly.

4.2.3. Flow Angle

Flow angle distributions at and downstream of the trailing edge of the blade row are shown in Figs. 32 to 34.

Two important regions are shown in these distributions. Close to the wall the flow undergoes severe under turning and at some distance from the wall there is a zone in which the flow is over-turned relative to the mainstream direction.

4.3. Vorticity

Vorticity components in the radial, streamwise and normal to streamwise directions were calculated using the relationships given in Appendix D. These are shown in Figures 35 to 37.

These components are relative to a local mean flow direction at each point.

The distribution of vorticity normal to the streamline indicates two main regions of vorticity of opposite sign, one near the wall and the second some distance out. The streamwise component indicates one dominant vortex with a centre approximately 0.2 inches from the wall. The radial vorticity component, Figure 36, shows a vortex sheet associated with the blade wake. The radial vorticity generated as a result of the flow separation is smaller than that generated by the blade wake.

4.4. Discussion

The dominant feature of the boundary layer in the stator row is the separation region which occurs in the suction surface/hub corner of the blade passage.

Leakage flow transports the low energy air from the corner in the manner discussed in Section 2.8. Initially, growth of the separation region is confined to hub wall but at the trailing edge the vortex has moved to pass over the suction surface of the blade. The rolling up of leakage flow would account for this movement.

When the total pressure and flow angle distributions at 0.167 chord lengths from the trailing edge are superimposed (Figure 38) it can be seen that the region of overturning corresponds with the upper side of the low energy zone and the region of highly underturned air, which results from the tip clearance flow, corresponds to the lower portion of this zone. It would appear that the leakage flow influences the rotation of the low energy region creating a streamwise vortex. The centre of the dominant streamwise vortex shown in the vorticity plots coincides with the centre of the low energy core.

The vortex described above rotates in the opposite direction to that which would be set up by the secondary flow resulting from the turning of the boundary layer through the blade row. Downstream of the trailing edge there is a region of streamwise vorticity (Figure 37) of the opposite sign to that of the main vortex near the wall and another on the outer edge of the main vortex. These are possibly induced by the vortex resulting from the interaction of the separation and leakage flow. There is no evidence in either the angle or vorticity distributions of the formation of a major passage vortex resulting from the turning of the hub boundary layer. This could result from the fact that the flow at inlet to the stator has a high streamwise vorticity component resulting from the passage vortices in the inlet guide vanes and rotor ; turning the flow through the stator will generate streamwise vorticity in the opposite direction to that in the incoming air and the two will tend to cancel.

In the stator row studied the direction of the separation vortex is controlled by the direction of the leakage flow. In general the direction of rotation of the vortex generated in this region will depend on the interation of a number of forces. In the case of a blade row with no clearance flow and a high passage cross flow resulting from turning the wall boundary layer it would be expected that the vortex would rotate in the opposite direction to that reported above.

The two regions of normal vorticity of opposite sign result from the form of the boundary layer. Due to the leakage flow the boundary layer in the region of the separation core takes the form shown in Fig. 39 with a velocity peak near the wall decreasing through the low energy core and then increasing to the mainstream value. This is indicative of two regions with vortices with axes normal to the flow but rotating in opposite directions as shown in Fig. 39.

5. THE HUB BOUNDARY LAYER BETWEEN THE ROTOR AND STATOR

5.1. Experimental Procedure

Detailed measurements of the hub boundary layer between the rotor and stator rows were made using the hot wire anemometer described in Section 3.3. The mean velocity, flow direction, the root mean square value of the velocity fluctuation along and normal to the flow direction and the turbulence cross product in the axial-tangential plane were measured. The measurements were carried out at the same loading as for measurements through the stator reported in Section 4.

Five radial traverses were made at half inch axial intervals i.e. 0.167, 0.333, 0.50, 0.667 and 0.833 chord lengths, from the rotor trailing edge. The radial spacing between measurements was varied according to the rate of change of the parameters, varying from 0.001 inch near the wall to 0.5 inch outside the boundary layer. The wall position was determined by connecting an avometer between the tunnel wall and the probe and moving the probe in until contact was just made. Using a dial gauge the wall position could be determined to approximately 0.0005 inches. To detect any errors in calibration resulting from touching the wire on the wall, the wire was recalibrated after each set of measurements.

5.2. Experimental Results.

5.2.1. Velocity

The mean velocity distributions are shown in Figure 40. The velocity profiles are orderly to a distance of approximately 0.3 inches from the wall. (Blade chord = 3 inches, blade spacing = 2.25 inches at the hub). In the outer portion of the boundary layer the profiles become less regular until the main stream conditions dominate at a distance of approximately

1.25 inches from the wall. The outer limit of the boundary layer is difficult to define in a manner similar to that used for two dimensional boundary layers due to the mainstream velocity variations resulting from spanwise blade loading effects.

A logarithmic plot of velocity, Figure 41, indicates that from approximately 0.01 inches to 0.1 inches from the wall the distribution can be described by a relationship of the form

$$\frac{U}{U^*} = \frac{1}{K} \log \frac{yU^*}{\nu} + B \qquad - \quad (42)$$

where B and K are constants.

$$U^* = \left(\frac{\tau_0}{\rho}\right)^{1/2}$$

and τ_0 is the wall shear stress.

The shear gradients near the wall are large. It was not possible to obtain sufficient points close to the wall to define the wall shear stress. Differentiation of Equation (42) with respect to y gives the following relationship.

$$\frac{U^*}{K} = y \frac{\partial U}{\partial y} \qquad - \quad (43)$$

From the measurements the value of $y\frac{\partial U}{\partial y}$ was found to be a constant for all axial stations, with a value of approximately 9.5, indicating that if K is a constant the wall shear stress is constant in this region.

The outer limit of the logarithmic region grows almost linearly with distance from the rotor trailing edge as is shown in Figure 42.

5.2.2. Flow Direction

The variation in flow direction through the boundary layer is shown in Figure 44. The dominant feature is the conventional overturning near the wall and associated underturned region a further distance out. There are however, two other regions of importance. Extending to approximately 0.1 inches from the wall i.e. in the region in which the velocity distribution is logarithmic, there exists a region in which the flow angle remains constant. This region extends to the wall near the rotor but as the stator is approached there is evidence of a reduction in the angle close to the wall. The flow angle in this region decreases, as shown in Figure 43, with axial distance from the rotor. The second region lies between 0.4 and 1.2 inches from the wall where the flow is again overturned.

5.2.3. Turbulence Components

Axial - Tangential Cross Product

The distribution of the turbulence cross product in the axial tangential plane is shown in Figure 45.

Near the rotor trailing edge there are two distinct regions of high shear stress, one with a maximum value occurring at approximately 0.1 inches from the wall and a second region with a peak at 0.5 inches from the wall. Between these two peaks the shear stress falls to almost zero.

The shear stress increases almost linearly through the logarithmic velocity region from a wall value close to zero reaching a maximum at the outer limit of the log region. The distance of this maximum from the wall increases with distance from the rotor, varying from 0.085 inches 0.16 chord lengths, from the rotor trailing edge to 0.120 inches near the stator leading edge. The peak value reduces rapidly with distance from the rotor, the maximum value near the stator leading edge being only 30% of the value near the rotor.

In the region of high shear stress further from the wall the reduction is more rapid, clear definition of the peak disappearing within half a chord length from the rotor trailing edge.

R.M.S. Velocities

The root mean square value of the turbulence fluctuations in the streamwise direction is plotted in Figure 46.

The distribution is similar to that of the cross product discussed above. There are two regions of high turbulence, one near the wall and the other at approximately 0.6 inches from the wall, though the demarcation between the two zones is not marked as in Figure 45.

The value near the wall is high, reaching 50% of the maximum value at a point 0.002 inches from the wall. The position of the peak moves away from the wall with distance from the rotor, varying from 0.05 to 0.10 inches.

Decay is rapid. The region of high turbulence at approximately 0.5 inches from the wall has disappeared in a distance of one half a chord length, to a region with a constant value extending from 0.3 to 0.8 inches from the wall.

The turbulence fluctuations normal to the streamline are plotted in Figure 47. The main feature of these distributions is the absence of any demarcation between the two regions present in the distributions shown in Figures 45 and 46.

The peak value is reached at a greater distance from the wall, at 0.15 inches, and there is no apparent tendency for the position of the maximum to change with axial position.

5.3. Vorticity

As stated earlier in Section 5.2.1. the use of velocity to define the outer limit of the boundary layer is difficult because of the radial variation of the free stream velocity. A more precise definition of the boundary layer and information on its structure can be obtained by considering the vorticity of the flow.

Using the relationships given in Appendix 'D' the streamwise and normal vorticity components were calculated. These components are relative to the local flow direction and not to a mainstream direction. The distributions are shown in Figures 48 and 49.

The normal vorticity component dominates near the wall. The distribution is hyperbolic as would be expected from a logarithmic velocity distribution. However from 0.2 inches from the wall out the flow is dominated by streamwise vorticity. The streamwise component indicates two counter rotating vortices. The first with a centre at approximately 0.25 inches from the wall covering the region from 0.08 to 0.4 inches, and the second with a centre at approximately 0.6 inches from the wall and extending from 0.4 to 1.0 inches.

For points close to the wall, Figure 49 indicates considerable scatter. This is a result of the numerical differentiation of measurements. The small increments in distance from the wall in conjunction with unsmoothed measurements gives rise to this behaviour. However, if the flow angle is assumed to be constant through this region (see Section 5.2.2.) the streamwise component is of the order of 25, i.e. can be considered to be negligible.

The measured distribution indicates a small angle reduction in the viscous region close to the wall near the stator leading edge ; this indicates that there is a streamwise vorticity component in this region. This vorticity could be generated by the turning of the constant angle region. The flow angle in this region reduces by 2° as the flow moves from the rotor to the stator (Figure 43), this is small but in conjunction with the extremely high normal vorticity component near the wall could be responsible for a finite secondary flow which would result in further turning as is shown in Figure 44 at 0.67 and 0.83 chord lengths from the rotor trailing edge.

The streamwise component diffuses rapidly. The peak drops 50% in the region considered.

5.4. Discussion

The region which has been referred to as the hub boundary layer in this section cannot be considered as a boundary layer in the conventionally accepted sense. The portion of this region which has been generated as a result of the shear stress imposed by the hub wall extends only to approximately 0.4 inches from the wall. The disturbed region outside this shear region is related to the vorticity shed from the rotor some distance out from the wall. However it is convenient when considering the hub region of a machine to combine these two regions and use the general term hub boundary layer to cover the complete region of disturbed flow.

The experimental results presented in this section indicate that the boundary layer downstream of the rotor can be divided into three main sections.

(i) an inner region controlled by the wall shear stress.

(ii) a region dominated by the passage vortex.

(iii) a region on the outer edge of the boundary layer containing a vortex rotating in the opposite direction to the passage vortex.

In the region near the wall the flow direction is constant and the size of the region grows linearly with distance from the rotor trailing edge. This region can be considered as a new boundary layer growing on the stationary wall downstream of the rotor, inside the boundary layer or vorticity field which has resulted from the shedding of the boundary layer and associated disturbances from the rotor hub.

On the outer edge of the wall region the flow undergoes the normal overturning connected with the rotor passage vortex. Vorticity and flow angle distributions indicate that this vortex has its centre approximately 0.25 inches from the wall and controls the flow in the region between 0.1 and 0.4 inches from the wall.

Between 0.4 and the edge of the boundary layer at 1.2 inches from the wall, angle and vorticity measurements indicate a vortex rotating in the opposite direction to the passage vortex, with a centre at approximately 0.6 inches from the wall.

A plot of total pressure $\frac{1}{2}$ inch from the rotor trailing edge, Figure 50, taken from previous measurements carried out by the author on the Vortex Wind Tunnel reported in Reference 41, indicates a region of high loss with a centre at approximately 0.5 inches from the wall. This corresponds to the centre of the vortex discussed above. The most probable source of loss in the rotor would be from flow separation in the suction surface/hub corner, similar to that found in the stator row in Section 4.

As a result it would appear that the vortex originates in regions of flow separation on the rotor hub, because of the low energy (relative to the rotor) of the air it contains it is moved radially away from the hub by centrifugal effects and leaves the rotor at approximately 0.5 inches from the hub. The rotation in the opposite direction to the passage vortex could result from two influences. The passage vortex will when rotating along side the region of separation tend to induce a motion in the opposite direction to its own sense of rotation. Secondly, leakage flow will cause rotation in the opposite direction to the passage vortex in a manner similar to that in the stator.

The turbulence distribution cannot be completely reconciled with the mean flow model presented above. The cross product $\overline{u_1 u_2}$ distribution indicates two peaks separated by a region in which it almost falls to zero. This minimum coincides with the centres of the passage vortex region. The first peak coincides with the outer edge of the wall region and the high turbulence in this region is probably that shed from the rotor hub boundary layer. The second peak coincides with the centre of region 3 at approximately 0.5 inches from the wall.

When considering the turbulence distribution it must be remembered that the probe is not placed in a uniform flow field. Rotor wakes and various vortices shed from the rotor are passing the probe at approximately 300 cycles per second. The turbulence distributions discussed above are some mean of the turbulence associated with each of these.

6. TURBULENCE STRUCTURE OF BOUNDARY LAYER

6.1. Determination of Turbulance Components

6.1.1 Solution of Reynolds Equations

Using the hot wire anemometer it was possible to measure velocity, the flow direction, the R.M.S. values of the velocity fluctuations and the turbulance cross product in the axial-tangential plane. This leaves unmeasured the radial velocity, the R.M.S value of the radial velocity and the radial-axial and radial-tangential cross products.

To measure these components the wire must be inclined in the radial-axial and radial-tangential planes. Because of the size of the wire relative to the thickness of the boundary layer this was not possible.

An attempt has been made to obtain an estimate of the order of these terms by using the equations of motion . There are five quantities unmeasured, the four mentioned above plus static pressure. Reliable measurements of static pressure cannot be obtained because of the fluctuating flows mentioned in Section 3.5.

The relations available for the evaluation of the five unknown quantities are continuity and the three Reynolds equations. With only four equations for the solution of five unknown it was necessary to make the assumption that the axial static pressure gradient was negligible, thus providing in effect, a fifth equation.

These equations and the methods used to solve for the unknown quantities are given in Appendix E. The satisfactory solution of the equations depends on the obtaining of accurate axial derivatives. Due to the small changes in this direction, the axial derivatives control the accuracy of the solutions.

6.1.2 Discussion of Results.

The turbulence cross products in the radial-axial and radial-circumferential planes are shown in Figures 52 and 53. The radial-axial term reaches a high value within 0.002 inches from the wall. This region is dominated by viscous terms which contain the second derivatives of velocity. The small number of measurements obtained close to the wall and the validity of the wall correction on the anemometer results lead to some doubt on the accuracy of the results in this region. Later work by Walker (Ref. 45) indicates that velocities obtained with the Wills (Ref. 38) wall correction, used in this study, are considerably higher than the true value, As a result, derivatives and hence the calculated shear terms in this region are too high.

Outside the viscous region to approximately 0.3 inches from the wall, regions 1 and 2 of Section 5, the value of the shear terms is approximately constant. As a result of the integration technique the magnitude is fixed by the value in the wall viscous region.

The magnitude of the radial-circumferential term is controlled in a similar manner by the value at the wall. However, it does not remain constant through the inner section of the boundary layer but tends to decrease.

In the portion of the boundary layer designated region 3 in Section 4 the magnitude of the shear terms increases but not in an orderly manner. At 0.33 chord lengths from the rotor trailing edge it takes a large negative value while at 0.5 and 0.67 chord lengths it tends to a large positive value. A study of the various terms indicates that once outside the viscous layer the equations are dominated by the radial vorticity. The calculated values of the radial vorticity change sign as indicated above which shows the dependence on the calculations of accurate derivatives.

The radial velocity is of the order of 2 f.p.s. maximum and can be regarded as small. It was not possible to obtain the radial R.M.S. velocity. This required third derivatives of the measured information and these could not be obtained with sufficient accuracy.

The results presented in this section indicate that in the first 0.3 inches from the wall (regions 1 and 2) the Reynolds shear stresses in the radial-axial and radial-tangential planes are smaller than that in the axial-tangential plane and remain practically constant from the viscous layer out. This is illustrated in Figure 54. Outside this region no definite statements can be made about their distributions until more is known about the structure of region 3.

6.2. Component of Turbulence Resulting from Blade Wakes.

A stationary probe placed downstream of the rotor in the machine studied sees wakes passing approximately 300 times per second. The distrubances resulting from these wakes cannot be considered in the same sense as fluctuations found in a conventional boundary layer, which are considered to be random. These fluctuations in a machine will have certain directional properties which will be expected to show up in the structure of turbulence stresses.

6.2.1. "Turbulence Components" Downstream of Stator

For an observer stationed relative to a rotor the flow appears to be similar to that seen downstream of a stationary row, if rotational effects are neglected at this stage.

Properties based on a peripheral average downstream of the stator should behave in a similar manner to time averaged properties measured by a stationary probe downstream of the rotor.

To obtain an estimate of how much the wakes contribute to the magnitude and distribution of the turbulence components downstream of the rotor the stator was used as a model and the equivalent "turbulence components" were calculated using measurements taken 0.167 chord lengths downstream from the stator trailing edge.

An estimate of the radial velocity was obtained by using the continuity Equation

$$\frac{1}{r}\frac{\partial (V_r r)}{\partial r} + \frac{1}{r}\frac{\partial V_u}{\partial \theta} + \frac{\partial V_z}{\partial z} = 0 \qquad - \quad (44)$$

Assuming changes in the axial directions to be small compared with those in the circumferential direction the radial velocity is given by

$$V_r = \frac{1}{r}\int \frac{\partial V_u}{\partial \theta}\, dr \qquad - \quad (45)$$

Mean values of the velocity components and cross products were found using area averages.

The results of these calculations are shown in Figures 55 and 56. The components calculated are of the same magnitude as those measured and calculated downstream of the rotor and have similar distributions. The axial-circumferential cross product is dominant near the wall rising to a peak and then dropping rapidly to a value less than that of the other two cross products further from the wall. The axial and tangential R.M.S. velocities have high initial values rise to a peak 0.2 inches from the wall and then decrease.

Further measurements which have been completed by Merrington (Ref. 46) downstream of the stator with more sophisticated equipment indicate that the estimate of radial velocity used was approximately twice the actual value. The application of this correction would reduce the calculated radial-tangential and radial-axial components considerably.

The magnitude and distribution of the wake components calculated above would indicate that the wake accounts for the major portion of the turbulence components in the hub boundary layer downstream of the rotor. With superimposed random turbulence making up a minor portion. As a result of the dominance of the wakes, the turbulence component exhibit marked directional propoerties with components in the circumferential-axial plane dominating.

6.3. Boundary Layer Equations

In the boundary layer described in the previous section the rotor wakes dominate the turbulence structure. The radial-axial and radial-circumferential cross products are smaller than the axial-circumferential component and practially constant through the boundary layer with corresponding small axial and radial derivatives. The mean radial velocity has been found in Section 6.1 to be small. Deleting terms which measurements have shown to be small the equations of motion for the inner portion of this boundary layer become.

$$\rho \frac{\overline{V_\omega}^2}{r} = \frac{\partial P}{\partial r} - \rho \frac{\partial \overline{V_r'^2}}{\partial r}$$

$$\rho\left(\overline{V_r}\frac{\partial \overline{V_\omega}}{\partial r} + \overline{V_z}\frac{\partial \overline{V_\omega}}{\partial z}\right) = \mu \frac{\partial^2 \overline{V_\omega}}{\partial r^2} - \rho \frac{\partial \overline{V_\omega' V_z'}}{\partial z}$$

$$\rho\left(\overline{V_r}\frac{\partial \overline{V_z}}{\partial r} + \overline{V_z}\frac{\partial \overline{V_z}}{\partial z}\right) = -\frac{\partial P}{\partial z} + \mu \frac{\partial^2 \overline{V_z}}{\partial r^2} - \rho \frac{\partial \overline{V_z'^2}}{\partial z} \qquad - \quad (46)$$

As in other turbulent boundary layer equations, one would neglect the turbulance terms where the viscous terms dominate and vice versa.

Measurements of static pressure (Ref. 41) through the boundary layer, shown in Figure 57, with pressure probes, indicate that it is not constant. The decrease near the wall can be accounted for in part by the high tangential component of velocity in the layer but the increase in gradient near the wall may be due to the radial variation of the direct Reynolds stress in the radial direction. This component has not been measured or estimated. The probability of instrument error in this region of high shear must be considered when examining the information in Figure 57.

The axial decay of the wakes is accounted for by the axial derivative of the axial-tangential shear stress in the second equation and the direct stress in the third equation.

These equations apply only to regions 1 and 2 of the boundary layer described in Section 5.4. In the outer portion the behaviour of the Reynolds components has not been defined and no definite statements can be made.

7. CONCLUSIONS

1. The statement that the present inviscid secondary flow theories for the turning of rotational flow in a blade passage are not sufficient to describe the conditions in a machine has been substantiated by this work.

The present theories do not include the viscous effects such as the flow separation which occurs in suction surface - end wall junction of a blade passage, which appear to be a dominant feature. A study of this separation region would appear to be the logical next step in this field of research.

2. A model of the hub boundary layer between the rotor and stator as a quasi-turbulent boundary layer in which the rotor wakes play a dominant part in the distribution of the turbulance stresses has been presented.

3. Solution of the boundary layer equation for the hub boundary layer must await better predictions of the secondary flow within a blade passage, which in turn are dependant on prediction of separation of this boundary layer.

4. The appropriate boundary layer equations required to describe the (inner part) hub boundary layer in regions of axial symmetry have been identified in Section 6.3. The order of magnitude study of the general equations required to reduce them to this form has been based on the measurements made.

APPENDIX 'A'

The main dimensions of the Vortex Wind Tunnel are given below

	I.G.V.	Rotor	Stator
No. of Blades	38	37	38
Core Diameter	27"	27"	27"
Shell Diameter	45"	45"	45"
Clearance at Core	0.020-0.060"	0.030"	0.030"
Clearance at Shell	0.025"	0.033"	0.020"
S/C at Mid Blade Height	0.99	1.02	0.99
Hub Stagger	17.2°	4.2°	37.2°
Mid Blade Stagger	13.9°	29.5°	29.5°
Tip Stagger	11.25°	42.15°	25.1°
Hub Camber	34.40°	52.5°	32.9°
Mid Blade Camber	27.8°	31.1°	31.1°
Tip Camber	24.25°	19.1°	29.4°

APPENDIX 'B'

To determine the turbulence components the method presented by Hinze (Ref. 37) was used.

Consider a uniform flow with mean velocity U and turbulence components u_1, u_2 and u_3 which are small compared with U.

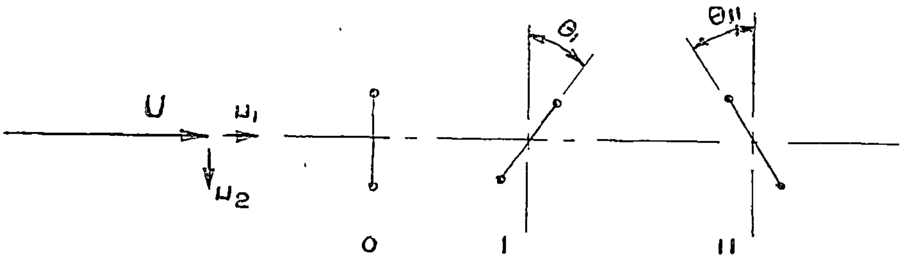

Fig. B.1

When the wire is placed in the u_1 u_2 plane as shown in figure B.1, u_1 is found directly when the wire is normal to the flow and u_2 by using the directional sensitivity of the wire by rotating in the u_1 u_2 plane. The third component u_3 can be found by inclining the wire in the u_1 u_3 plane.

The cooling of the wire is determined mainly by the velocity component normal to the wire, the longitudial component only assuming importance when the normal component is small. When the wire is rotated through an angle θ from the normal to the flow direction the effective velocity indicated by the wire can be obtained from

$$U_{eff}^2 = U^2 \left(\cos^2\theta + a^2 \sin^2\theta \right) \qquad - \quad (47)$$

Hinze and Webster (Ref. 43) have found the value a to be between 0.1 and 0.3. For practical purposes in the range of angles used it is sufficient to use the normal component only, neglecting the $a^2 \sin^2\theta$ term.

The cooling of the wire can be described by the relationship given by King (Ref. 44).

$$\frac{V^2}{R_w(R_w - R_a)} = A + BU^n \qquad - \quad (48)$$

where R_w - wire operating resistance

R_a - wire resistance at ambient temperature

V - D.C. voltage

A & B - Constants for a particular wire.

Using a constant temperature anemometer system R_a and R_w are constant and the relationship simplifies to

$$V^2 = A + BU^n$$

With the wire in the u_1 u_2 plane at an angle θ to the flow the velocity normal to the wire is given by

$$\left\{\left[(U + u_1)\cos\theta + u_2 \sin\theta\right]^2 + u_3\right\}^{1/2} \qquad - \quad (49)$$

When it is assumed that $U \gg u_1, u_2$ and u_3 we have

$$V^2 = A + B\,(U\cos\theta)^n \qquad - \quad (50)$$

For a small velocity change dU the change in voltage is given by

$$\begin{aligned} e = dV &= nB(U\cos\theta)^{n-1}(\cos\theta\, dU + U\sin\theta\, d\theta)/2V \\ &= \frac{nB(U\cos\theta)^n . u_1}{2V} + \frac{nB(U\cos\theta)^{n-1}\sin\theta . u_2}{2V} \\ &= S_1 u_1 + S_2 u_2 \qquad - \quad (51) \end{aligned}$$

where S_1 and S_2 are sensitivities of the hot wire to the velocity components u_1 and u_2.

To measure these two components the wire is set in three positions relative to the flow as is shown in Fig (B.1). The voltage changes are

$$e_0 = (S_1)_0 u_1$$

$$e_1 = (S_1)_1 u_1 + (S_2)_1 u_2$$

$$e_{11} = (S_1)_{11} u_1 + (S_2)_{11} u_2 \qquad - (52)$$

where the additional suffices indicate the sensitivities at different angles.

The values e_0, e_1 and e_{11} are obtained indirectly from the R.M.S. values indicated by a thermocouple and are expressed as

$$(\overline{e^2})_0 = (S_1)_0^2 \, \overline{u_1^2}$$

$$(\overline{e^2})_1 = (S_1)_1^2 \, \overline{u_1^2} + (S_2)_1^2 \, \overline{u_2^2} + 2(S_1)_1 (S_2)_1 \, \overline{u_1 u_2}$$

$$(\overline{e^2})_{11} = (S_1)_{11}^2 \, \overline{u_1^2} + (S_2)_{11}^2 \, \overline{u_2^2} + 2(S_1)_{11} (S_2)_{11} \, \overline{u_1 u_2} \qquad - (53)$$

which can be solved for $\overline{u_1^2}$, $\overline{u_2^2}$ and $\overline{u_1 u_2}$.

APPENDIX 'C'

To obtain suitable relationships between the pressure measured in the three holes of a cobra yaw meter and yaw, velocity and total pressure when the yaw meter is used away from the nulled position, consider inviscid flow around a cylinder with three equispaced holes yawed at an angle α to the flow, with a free stream velocity U.

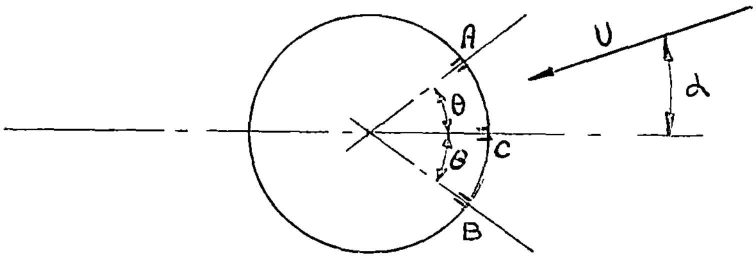

Fig. C.1

The surface of the cylinder is a streamline hence the total head is given by

$$\begin{aligned} h_0 &= h_A + \left[2U\sin(\theta+\alpha)\right]^2/2g \\ &= h_C + \left[2U\sin\alpha\right]^2/2g \\ &= h_B + \left[2U\sin(\theta-\alpha)\right]^2/2g \end{aligned} \quad - \quad (54)$$

where h_A, h_B and h_C are the heads indicated at the three tappings.

A little rearrangement gives

$$\frac{h_A - h_C}{h_B - h_C} = F(\alpha)$$

The same form is applicable to the cobra yaw meter, F still being a function of α only. This relationship enables yaw and hence flow direction to be determined.

When the yaw angle is known the velocity is determined from

$$U = \left| 2g \left(h_A - h_C \right) \right|^{1/2} G_1(\alpha)$$

$$\text{or} \quad U = \left| 2g \left(h_B - h_C \right) \right|^{1/2} G_2(\alpha) \qquad - \quad (56)$$

where G_1 and G_2 are also functions of α only.

The difference between the centre hole reading and true total head can be found when the velocity and yaw angles are known, by using the relationship

$$h_0 - h_C = \frac{U^2}{2g} H(\alpha) \qquad - \quad (57)$$

APPENDIX 'D'

Components of Vorticity

In cylindrical polar cordinates the three components of vorticity are

$$\begin{aligned} &\text{Axial} && W_z = \frac{1}{r}\frac{\partial(V_u r)}{\partial r} - \frac{1}{r}\frac{\partial V_r}{\partial \theta} \\ &\text{Tangential} && W_u = \frac{\partial V_u}{\partial z} - \frac{\partial V_z}{\partial r} \\ &\text{Radial} && W_r = \frac{1}{r}\frac{\partial V_z}{\partial \theta} - \frac{\partial V_u}{\partial z} \end{aligned} \qquad - (58)$$

Assuming that V_z and $V_u > V_r$ (section 6.1.2.) and $\frac{\partial}{\partial r}$ and $\frac{\partial}{\partial \theta}$ $> \frac{\partial}{\partial z}$ these relationships approximate to

$$\begin{aligned} W_z &= \frac{1}{r}\frac{\partial(V_u r)}{\partial r} \\ W_u &= -\frac{\partial V_z}{\partial r} \\ W_r &= \frac{1}{r}\frac{\partial V_z}{\partial \theta}. \end{aligned} \qquad - (59)$$

If the radial flows are small the streamlines can be considered parallel to the wall and the streamwise and normal to streamwise components in the plane parallel to the wall become

$$\begin{aligned} W_s &= U\frac{\partial \alpha}{\partial r} + \frac{U}{r}\sin\alpha\cos\alpha \\ W_n &= -\frac{U}{r}\sin^2\alpha - \frac{\partial U}{\partial r} \end{aligned} \qquad - (60)$$

Downstream of the rotor where axial symmetry exist the radial component is negligible compared with the two components in plane parallel with the wall.

APPENDIX 'E'

Solution of Reynolds Equation

E.1. Reynolds Equation

In cylindrical polar co-orindates and assuming axial symmetry the Reynolds equations become

$$\overline{V_r}\frac{\partial \overline{V_r}}{\partial r} - \frac{\overline{V_\omega}^2}{r} + \overline{V_z}\frac{\partial \overline{V_r}}{\partial z} = -\frac{1}{\rho}\frac{\partial P}{\partial r} + \nu\left(\frac{\partial^2 \overline{V_r}}{\partial r^2} + \frac{1}{r}\frac{\partial \overline{V_r}}{\partial r} - \frac{\overline{V_r}}{r^2} + \frac{\partial^2 \overline{V_r}}{\partial z^2}\right) - \left(\frac{\partial \overline{V_r'^2}}{\partial r} + \frac{\partial \overline{V_r' V_z'}}{\partial z} - \frac{\overline{V_\omega'^2}}{r} + \frac{\overline{V_r'^2}}{r}\right) \qquad - (61)$$

$$\overline{V_r}\frac{\partial \overline{V_\omega}}{\partial r} + \overline{V_z}\frac{\partial \overline{V_\omega}}{\partial z} + \frac{\overline{V_\omega}\,\overline{V_r}}{r} = \nu\left(\frac{\partial^2 \overline{V_\omega}}{\partial r^2} + \frac{1}{r}\frac{\partial \overline{V_\omega}}{\partial r} - \frac{\overline{V_\omega}}{r^2} + \frac{\partial^2 \overline{V_\omega}}{\partial z^2}\right) - \left(\frac{\partial \overline{V_r' V_\omega'}}{\partial r} + \frac{\partial \overline{V_\omega' V_z'}}{\partial z} + 2\,\frac{\overline{V_\omega' V_r'}}{r}\right) \qquad - (62)$$

$$\overline{V_r}\frac{\partial \overline{V_z}}{\partial r} + \overline{V_z}\frac{\partial \overline{V_z}}{\partial z} = -\frac{1}{\rho}\frac{\partial P}{\partial z} + \nu\left(\frac{\partial^2 \overline{V_z}}{\partial r^2} + \frac{1}{r}\frac{\partial \overline{V_z}}{\partial r} + \frac{\partial^2 \overline{V_z}}{\partial z^2}\right) - \left(\frac{\partial \overline{V_r' V_z'}}{\partial r} + \frac{\partial \overline{V_z'^2}}{\partial z} + \frac{\overline{V_z' V_r'}}{r}\right) \qquad - (63)$$

The mean value continuity relation is

$$\frac{\partial \overline{V_r}}{\partial r} + \frac{\overline{V_r}}{r} + \frac{\partial \overline{V_z}}{\partial z} = 0 \qquad - (64)$$

Pressure is unknown, this can be removed by forming the vorticity equations by taking the curl of the Reynolds equations. Because the flow is considered to be essentially axially symmetrical this reduces the number of useful equations to two. Equations (61) and (63) combine to give Equation (65) but Equations (66) and (67) are respectively the axial and radial derivatives of Equation (62).

$$W_\omega \frac{\partial \overline{V_r}}{\partial r} + \overline{V_r}\frac{\partial W_\omega}{\partial r} + W_\omega \frac{\partial \overline{V_z}}{\partial z} + \overline{V_z}\frac{\partial W_\omega}{\partial z} + 2\,\frac{\overline{V_\omega}\,W_r}{r}$$

$$= \nu\left(\frac{\partial^2 W_\omega}{\partial r^2} + \frac{\partial W_\omega}{r\,\partial r} - \frac{W_\omega}{r^2} + \frac{\partial^2 W_\omega}{\partial z^2}\right) - \left(\frac{\partial^2 \overline{V_r'^2}}{\partial z\,\partial r} - \frac{\partial^2 \overline{V_z'^2}}{\partial r\,\partial z} - \frac{\partial \overline{V_\omega'^2}}{r\,\partial z}\right.$$

$$\left. - \frac{\partial \overline{V_r'^2}}{r\,\partial z} + \frac{\partial^2 \overline{V_r' V_z'}}{\partial z^2} - \frac{\partial^2 \overline{V_r' V_z'}}{\partial r^2} - \frac{\partial \overline{V_z' V_r'}}{r\,\partial r} + \frac{\overline{V_r' V_z'}}{r^2}\right) \qquad - (65)$$

$$\frac{\partial(\overline{V_r}\,W_z)}{\partial z} - \frac{\partial(\overline{V_z}\,W_r)}{\partial z} = \nu\left(\frac{\partial^2 W_r}{\partial r^2} + \frac{\partial W_r}{r\,\partial r} - \frac{W_r}{r^2} + \frac{\partial^2 W_r}{\partial z^2}\right)$$

$$-\left(\frac{\partial^2 \overline{V_r' V_\omega'}}{\partial r\,\partial z} + \frac{\partial^2 \overline{V_\omega' V_z'}}{\partial z^2} + \frac{\partial \overline{V_\omega' V_r'}}{\partial z}\right) \qquad - (66)$$

$$\frac{\partial(\overline{V_r}\,W_z)}{\partial r} - \frac{\partial(\overline{V_z}\,W_r)}{\partial r} + \frac{\overline{V_r}\,W_z}{r} - W_r\frac{\partial \overline{V_z}}{\partial r} = \nu\left(\frac{\partial^2 W_z}{\partial r^2} + \frac{\partial W_z}{r\,\partial z}\right.$$

$$\left. + \frac{\partial^2 W_z}{\partial z^2}\right) - \left(\frac{\partial^2 \overline{V_r' V_\omega'}}{\partial r^2} + \frac{\partial^2 \overline{V_\omega' V_z'}}{\partial r\,\partial z} + \frac{\partial \overline{V_\omega' V_z'}}{r\,\partial z} + 3\,\frac{\partial \overline{V_\omega' V_r'}}{r\,\partial r}\right) \qquad - (67)$$

In Equations (65), (66) and (67) the vorticity components are given by Equations (58) of Appendix 'D'.

Axially $\quad W_z = \dfrac{1}{r}\dfrac{\partial(V_\omega r)}{\partial r}$

Tangentially $\quad W_\omega = \dfrac{\partial V_r}{\partial z} - \dfrac{\partial V_z}{\partial r}$

Radially $\quad W_r = -\dfrac{\partial V_\omega}{\partial z}$

E.2 Evaluation of Reynolds Stresses

A value of the radial velocity was obtained from the continuity Equation (64) which was rewritten as

$$\overline{V_r} = \frac{1}{r}\int \frac{\partial \overline{V_z}}{\partial z}\, r\, dr \qquad - (68)$$

The radial-tangential turbulence cross product $\overline{V_r' V_\omega'}$ was then obtained from Equation (62) by re-arranging as follows

$$\frac{\partial(\overline{V_r' V_\omega'}\, r^2)}{r^2\,\partial r} = \overline{V_r}\frac{\partial \overline{V_\omega}}{\partial r} + \overline{V_z}\frac{\partial \overline{V_\omega}}{\partial z} + \frac{\overline{V_\omega}\,\overline{V_r}}{r}$$

$$-\nu\left(\frac{\partial^2 \overline{V_\omega}}{\partial r^2} + \frac{\partial \overline{V_\omega}}{r\,\partial r} - \frac{\overline{V_\omega}}{r^2} + \frac{\partial^2 \overline{V_\omega}}{\partial z^2}\right) - \frac{\partial \overline{V_\omega' V_z'}}{\partial z} \qquad - (69)$$

From this equation the cross product itself is given by

$$\overline{V_\omega' V_r'} = \frac{1}{r^2}\int r^2 f_1(r)\,dr$$

where f, is a function of r only at a particular value z and is the right hand side of Equation (69).

Only four equations are available for the solution of five unknowns. To obtain an estimate of the radial-axial turbulence cross product it was assumed that the axial pressure gradient was small and equation (63) used in the form

$$\frac{1}{r}\frac{\partial(r\overline{V_r'V_z'})}{\partial r} = \bar{V}_r\frac{\partial \bar{V}_z}{\partial r} + \bar{V}_z\frac{\partial \bar{V}_z}{\partial z} + \nu\left(\frac{\partial^2 \bar{V}_z}{\partial r^2} + \frac{1}{r}\frac{\partial \bar{V}_z}{\partial r} + \frac{\partial^2 \bar{V}_z}{\partial z^2}\right) - \frac{\partial \overline{V_z'^2}}{\partial z} \quad - \quad (70)$$

which gives the cross product as

$$\overline{V_r'V_z'} \approx \frac{1}{r}\int r f_2(r)\,dr$$

where f_2 is the right hand side of equation (70).

Both f_1 and f_2 are functions of the radial position only and were evaluated from the measurements at a particular axial station.

To obtain an estimate of the radial R.M.S. velocity equation (65) was used as follows

$$- \frac{\partial}{\partial z}\left(\frac{\partial(\overline{V_r'^2}\,r)}{r\,\partial r}\right) = -\left(W_\omega\frac{\partial \bar{V}_r}{\partial r} + \bar{V}_r\frac{\partial W_\omega}{\partial r} + W_\omega\frac{\partial \bar{V}_z}{\partial z} + \bar{V}_z\frac{\partial W_\omega}{\partial z} + 2\bar{V}_\omega\frac{W_r}{r}\right) + \nu\left(\frac{\partial^2 W_\omega}{\partial r^2} + \frac{\partial W_\omega}{r\,\partial r} - \frac{W_\omega}{r^2} + \frac{\partial^2 W_\omega}{\partial z^2}\right) - \frac{\partial}{\partial z}\left(\frac{\partial \overline{V_z'^2}}{\partial r} + \frac{\partial \overline{V_r'V_z'}}{\partial z}\right) + \frac{\partial}{\partial r}\left(\frac{\partial(\overline{V_z'V_r'}\,r)}{r\,\partial r}\right) \quad - \quad (71)$$

Integration of Equation (71) give the direct stress as

$$\overline{v_r'^2} = \int r \int f_3(r)\, dr\, dz \qquad - (72)$$

where f_3 is the right hand side of Equation (71) and is again, a function of the radius only.

These relations offer a means of obtaining an estimate of the unknown terms. However there are some computational difficulties.

Consider the solution of Equation (62) for the radial-tangential shear stress. The dominant terms which are left in the equation after discarding those which have been shown by the measurements to be small leave the equation in the form

$$\overline{V_r}\frac{\partial \overline{V_\omega}}{\partial r} + \overline{V_z}\frac{\partial \overline{V_\omega}}{\partial z} = \nu \frac{\partial^2 \overline{V_\omega}}{\partial r^2} - \frac{\partial \overline{V_r' V_\omega'}}{r^2 \partial r} \qquad - (73)$$

The left hand side is dominated by derivatives in the axial direction. The radial velocity is obtained from the continuity equation (Equation 64), and is dependent on the axial derivative of the axial velocity. Changes in this direction are small approaching the magnitude of the experimental error making the accurate determination of derivatives difficult.

The viscous term on the right hand side dominates when close to the wall. The accurate determination of radial gradients in this region is necessary but measurements closer than 0.001" from the wall were not possible and the validity of the correction for the proximity of the wall as discussed in Section 3.3. is uncertain.

The evaluation of the equations was programmed for computation on anElliott 503 digital computor. Derivatives were obtained by a method equivalent to fitting a parabola to three points, that is, assuming the slope varies linearly between points. The derivative at a point being the weighted mean of the slopes at the mid point of the two adjacent intervals. This method is equivalent to using second order central difference but extended to non uniform intervals.

Integration was carried out using the trapezoidal method. This may appear crude, taking into account the accuracy of the numbers being used, it was considered acceptable.

In an effort to overcome the problem of inaccuracy in the calculation of axial derivatives a correction was placed on the velocity measurements by checking the mass flow at each station. It was assumed that the most likely source of error was a parallel shift in the velocity calibration curve of the wire as would have occurred if the wire had been strained by touching on the wall or by the collection of dust, and that the measurement of flow angle was correct. The average axial velocity was calculated at each axial station and a factor applied to bring it to a standard value.

NOTATION

x, y, z	Cartesian co-ordinates
r, θ, z	Cylindrical polar co-ordinates
U	Absolute velocity
Um	Peripheral velocity of rotor at mid blade height
V_r, V_u, V_z	Velocity components, cylindrical polar co-ordinates
Vr^1, Vu^1, Vz^1	Turbulence components, cylindrical polar co-ordinates
W_r, W_u, W_z	Vorticity components, cylindrical polar co-ordinates
W_s, W_n	Vorticity components relative to streamline
α	Flow angle
i	Incidence angle
ϵ	Flow deflection
Po	Total pressure
P	Static pressure
c	Blade chord
s	Blade spacing
h	Blade height
t	Blade tip clearance
A	Blade aspect ration (h/c)
ρ	Density
μ	Viscosity
ν	Kinematic viscosity
τ_0	Wall shear stress
ϕ	Flow coefficient (Vu/Um)
ψ	Pressure coefficient $(P / \frac{1}{2} \rho U^2_m)$

C_L	Lift coefficient
C_D	Drag coefficient
C_{DP}	Profile drag coefficient
C_{DS}	Secondary drag coefficient
C_{DA}	Annulus drag coefficient
C_{DSP}	Passage secondary flow drag coefficient
C_{DST}	Mainstream secondary flow drag coefficient
C_{DSC}	Clearance flow drag coefficient
Re	Reynolds number
M	Mach number
R	Degree of reaction
δ	Boundary layer thickness
δ^*	Boundary layer displacement thickness

REFERENCES

1. SERVOY, G.K. Recent Progress in Aerodynamic Design of Axial Flow Compressors in the United States. *Trans A.S.M.E.,* Vol. 88, Series A. No.3 July, 1966, pp. 251 - 261.

2. HOWELL, A.R. Fluid Dynamics of Axial Compressors *Proc. Instn. Mech. Engrs.*, Vol. 153, 1945, pp. 441 - 452.

3. HORLOCK, J.H. Axial Flow Compressors. *Butterworths Scientific Publications*, 1958.

4. LAKSHMINARAYANA, B. AND HORLOCK, J.H. Review : Secondary Flows and Losses in Cascades and Axial Flow Turbomachines. *Int. J. Mech. Sci.,* Vol. 5 1963, pp. 287 - 307.

5. HOWELL, A.R. The Present Basis of Axial Flow Compressor Design Part. 1. Cascade Theory and Performance *A.R.C. R and M* 2095, 1942.

6. CARTER, A.D.S. Three-dimensional-flow Theories for Axial Compressors and Turbines. *Proc. Instn Mech. Engrs.* Vol. 159, 1948, pp. 255 - 268.

7. WALLIS, R.A. Axial Flow Fans, Newnes 1961.

8. ARMSTRONG, W.D. The Secondary Flow in a Cascade of Turbine Blades, *A.R.C. R and M* 2979 1955.

9. HERZIG, H.Z. HANSEN, A.G. AND COSTELLO, G.R. Visualization Study of Secondary Flows in Cascades. *N.A.C.A. Report* 1163, 1954.

10. SQUIRE, H.B. AND WINTER K.G. The Secondary Flow in a Cascade of Aerofoils in a Non Uniform Stream. *J. Aero Sci.* Vol. 18, 1951, pp. 271 - 277.

11. HAWTHORNE, W.R. Secondary Circulation in Fluid Flow. *Proc. Roy. Soc.* Series A, Vol. 206 1951, pp. 374 - 387.

12. PRESTON, J.H. A Simple Approach to the Theory of Secondary Flow. *Aero Quart.* Vol. 5 1954, pp. 218 - 234.

13. SMITH, L.H. Secondary Flow in Axial Flow Turbomachinary. *Trans A.S.M.E.* Vol. 77, 1955, pp. 1065 - 1076.

14. MARRIS, A.W. The Generation of Secondary Vorticity in an Incompressible Fluid. *Trans A.S.M.E.*, Vol. 30, Series E, No. 4, 163, pp. 525 - 531.

15. LAKSHMINARAYANA, B. AND HORLOCK, J.H. Effect of Shear Flow on the Outlet Angle in Axial Compressor Cascades - Methods of Prediction and Correlation with Experiments. Trans A.S.M.E. Series D, Vol. 89, 1967, pp. 191 - 200.

16. HORLOCK, J.H.
LOUIS, J.F.
PERCIVAL, P.M.E.
AND LAKSHMINARAYANA, B. Wall Stall in Compressors. Trans A.S.M.E. Series D, Vol. 88, 1966, pp. 637 - 648.

17. LOUIS, J.F. Secondary Flow and Losses in a Compressor Cascade. A.R.C. R and M 3136, 1958.

18. HANLEY, W.J. A Correlation of End Wall Losses in Plane Compressor Cascades. Trans A.S.M.E. Series A, Vol. 90, 1968 pp. 251 - 257.

19. OLIVER, A.R. Comparison Between Sand Cast and Machined Blades in the Vortex Wind Tunnel. A.R.L. M.E. 103, 1961

20. WALLIS, R.A. Private Communication 1969.

21. MELDAHL, A. End Losses of a Turbine Blade. Brown Boveri Review, Vol. 28, 1941

22. EHRICH, F.F. AND DETRA R.W. Transport of the Boundary Layer in Secondary Flow. *J. Aero Sci.* Vol. 21, 1954, pp. 136 - 138.

23. FUJIE, K. A Study of the Flow through the Rotor of an Axial Compressor. *Bul. of J.S.M.E.* Vol. 5, 1962, pp. 292 - 301.

24. EHRICH, F.F. Secondary Flows in Cascades of Twisted Blades. *J. Aero Sci*. Vol. 22, 1955, pp. 51 - 60.

25. MARTIN, P.M.E. *A.R.C. C.P.* 425, 1959

26. TSIEN, H.S. Loss in a Compressor or Turbine due to Twisted Blades. *J. Chinese Inst. Engrs*. 1947.

27. VON KARMAN, T. *General Elec. Co. Report.* 1941

29. LAKSHMINARAYANA, B. AND HORLOCK, J.H. Leakage Flows in Compressor Cascades *A.R.C. R and M* 3483, 1965.

30. LAKSHMINARAYANA, B. AND HORLOCK, J.H. Tip Clearance Flow and Losses for an Isolated Compressor Blade. *A.R.C. R and M* 3316, 1962

31. VAVRA, M.H. Aero-Thermodynamics and Fluid Flow in Turbomachines. *John Wiley*, New York , 1960.

32. RAINS, D.A. — *Hydro and Mech. Lab. C.I.T. Report* No. 5, 1954.

33. BETZ, A. — Hydraulische Probleme V.D.I., 1925

34. HORLOCK, J.H. — Some Recent Research in Turbo Machinery, *Proc. Inst. Mech. Engrs*. Vol. 182, 1968.

35. KOFSKEY, G AND ALLEN, H.W. — Smoke Study of Nozzle Secondary Flows in a Low-Speed Turbine *N.A.C.A. TN*. 3260, 1954.

36. Aerodynamic Design of Axial Flow Compressors, N.A.S.A. SP-36, 1965.

37. HINZE, J.O. — Turbulence, An Introduction to its Mechanism and Theory, *McGraw-Hill Book Co.*, 1959.

38. WILLS, J.A.B. — The Correction of Hot Wire Readings for Proximity to a Solid Boundary. *J.F.M.* Vol. 12, 1962, pp. 388 - 396

39. MACMILLAN, F.A. — Experiments on Pitot Tubes in Shear Flow. *A.R.C. R and M* 3208, 1956.

40. YOUNG, A.D. AND MAAS, J.N. — The Behaviour of a Pitot Tube in Transverse Total Pressure Gradients *A.R.C. R and M* 1770, 1936

41. RUSSELL, B.A. Hub Boundary Layer in Vortex Wind Tunnel, Honours Degree Thesis, *University of Tasmania*, 1965

42. NEUSTEIN, J. Low Reynolds Number Experiments in an Axial-Flow Turbomachine. *Trans A.S.M.E.,* Vol. 86, Series A, 1964, pp. 257 - 295.

43. WEBSTER, C.A.G. A Note on the Sensitivity to yaw of a Hot Wire Anemometer. *J.F.M.* Vol. 13, 1963, pp. 307 - 312.

44. KING, L.V. Convection of Heat from Small Cylinders in a Stream of Fluid. *Phil. Trans. Roy. Soc.* Vol. 214, 1914, pp. 378.

45. WALKER, G.J. The Correction of Hot Wire Anemometer Measurements for Proximity to a Solid Boundary. Symposium on Wind Tunnel Technique and Scale Comparisons, Monash University, 1968.

46. MERRINGTON, G.L. Unpublished Data, *University of Tasmania.*

47. MAGER, A.
MALONEY, J.J.
AND BUDINGER, R.E. Discussion of Boundary-Layer Characteristics Near the Wall of an Axial Flow Compressor. *N.A.C.A. Rep.* 1085, 1952.

48. ROHLIK, E. KOFSKY, M.G. ALLEN, H.W. AND HERZIG, H.Z. Secondary Flows and Boundary Layer Accumulation in Turbine Nozzles. *N.A.C.A. Rep.* 1168, 1954.

49. HORLOCK, J.H. Annulus Wall Boundary Layers in Axial Compressor Stages. *Trans A.S.M.E.* Vol. 85, Series D, 1963.

50. SCHUBAUER, G.B. AND KLEBANOFF, P.S. *N.A.C.A.* Wartime Rep. No. ACR.5K.27, 1946.

52. OWER, E. The Measurement of Air Flow, *Chapman and Hall Ltd.*

53. PANKHURST, R.C. AND HOLDER, D.W. Wind Tunnel Technique, *Pitman*, 1952

54. SCHLICHTING, H. Boundary Layer Theory. *McGraw Hill Book Co.*, 1960

55. TOWNSEND, A.A. The Structure of Turbulent Shear Flow. *Cambridge University Press* 1956.

56 LAMB, H. Hydrodynamics. *Cambridge University Press.*

57. ROSENHEAD, L. Laminar Boundary Layers. *Oxford University Press,* 1963

58. HAWTHORNE, W.R. Aerodynamics of Turbines and Compressors. *Oxford University Press* 1964.

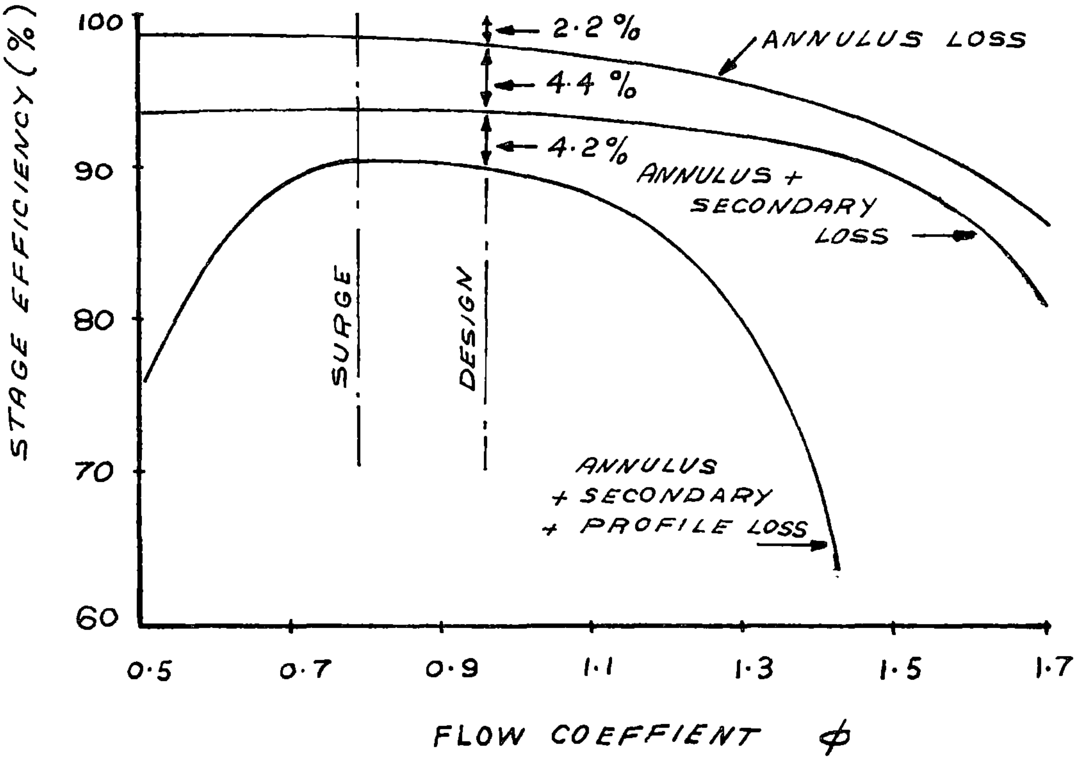

FIG. 1

LOSSES IN AN AXIAL FLOW COMPRESSOR STAGE (REF. 2)

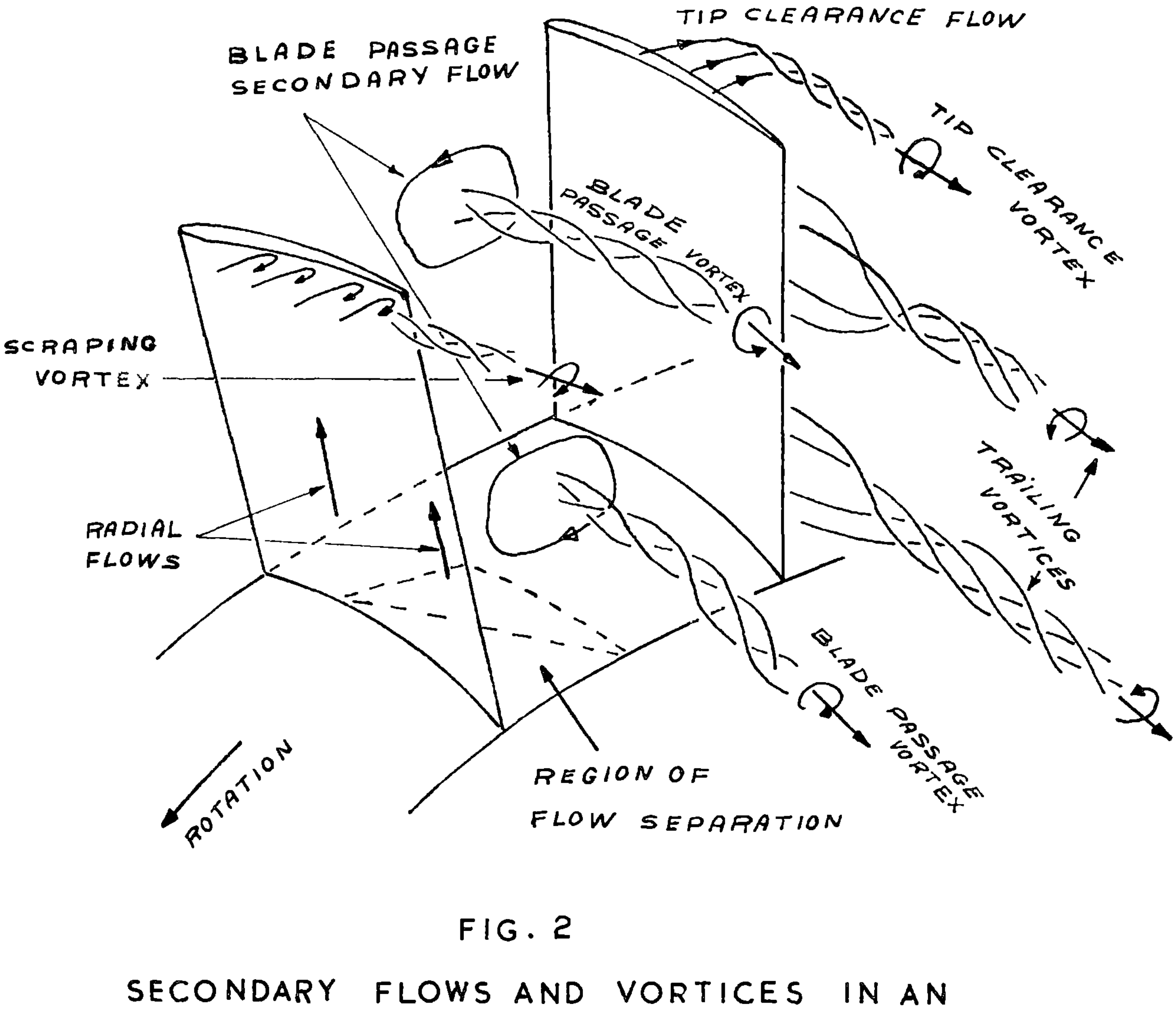
TIP CLEARANCE FLOW
BLADE PASSAGE SECONDARY FLOW
TIP CLEARANCE VORTEX
BLADE PASSAGE VORTEX
SCRAPING VORTEX
RADIAL FLOWS
TRAILING VORTICES
BLADE PASSAGE VORTEX
ROTATION
REGION OF FLOW SEPARATION

FIG. 2

SECONDARY FLOWS AND VORTICES IN AN AXIAL FLOW COMPRESSOR ROTOR (REF. 4)

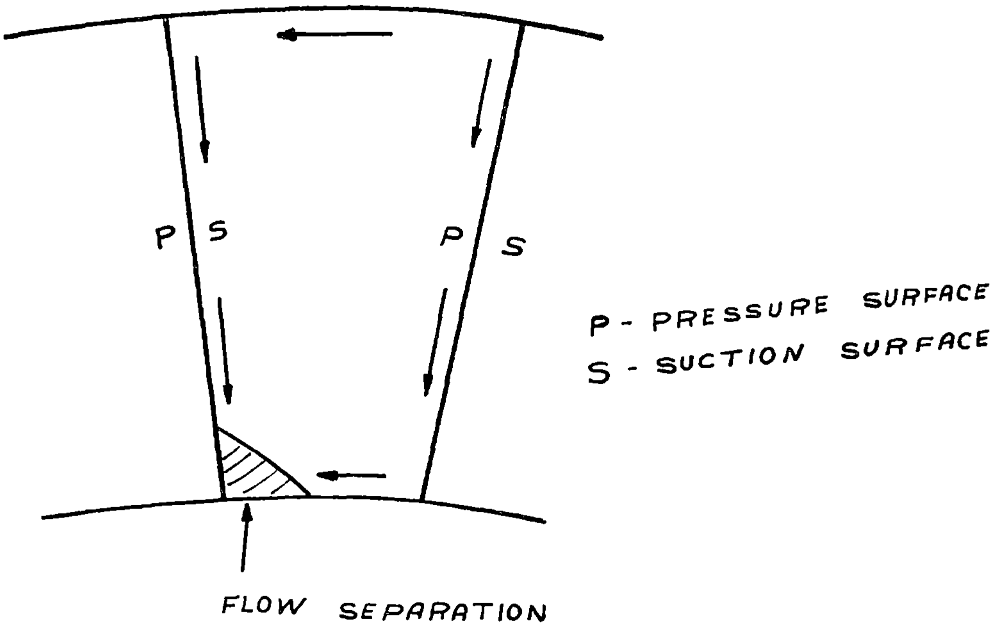
P
S
P
S
P - PRESSURE SURFACE
S - SUCTION SURFACE
FLOW SEPARATION

FIG. 3

SECONDARY FLOWS FEEDING LOW ENGERGY AIR INTO SUCTION SURFACE-HUB CORNER IN A STATOR ROW

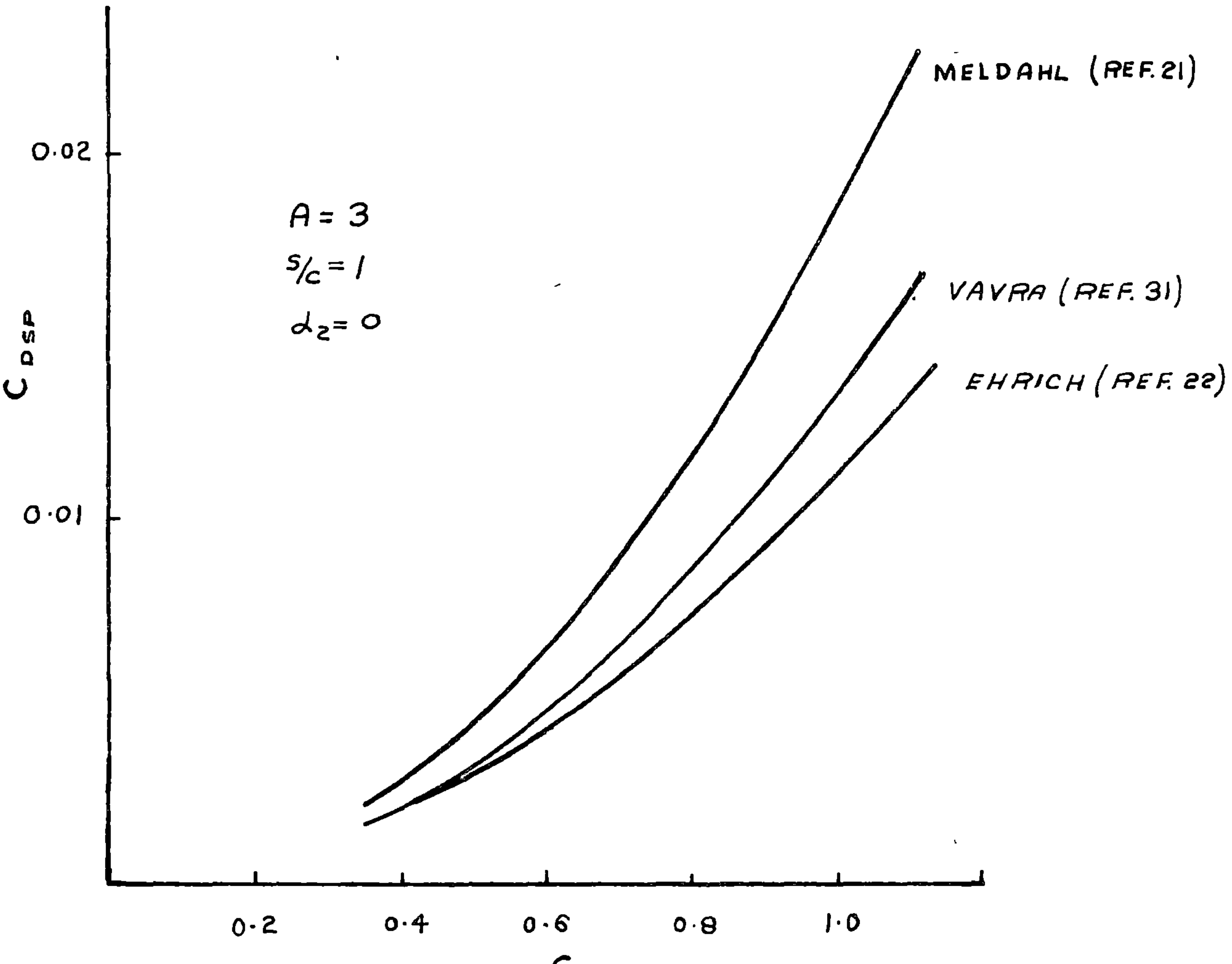

FIG. 4

COMPARISON OF PASSAGE SECONDARY FLOW DRAG COEFFICIENTS

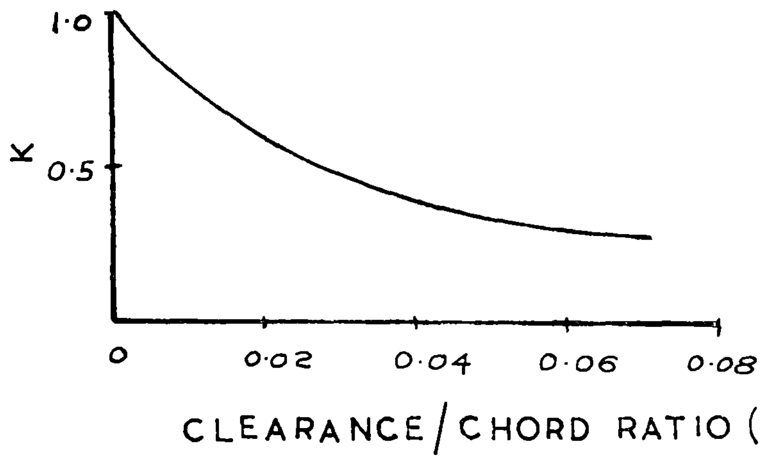

FIG. 5

LIFT RETAINED AT TIP OF BLADE (REF. 29)

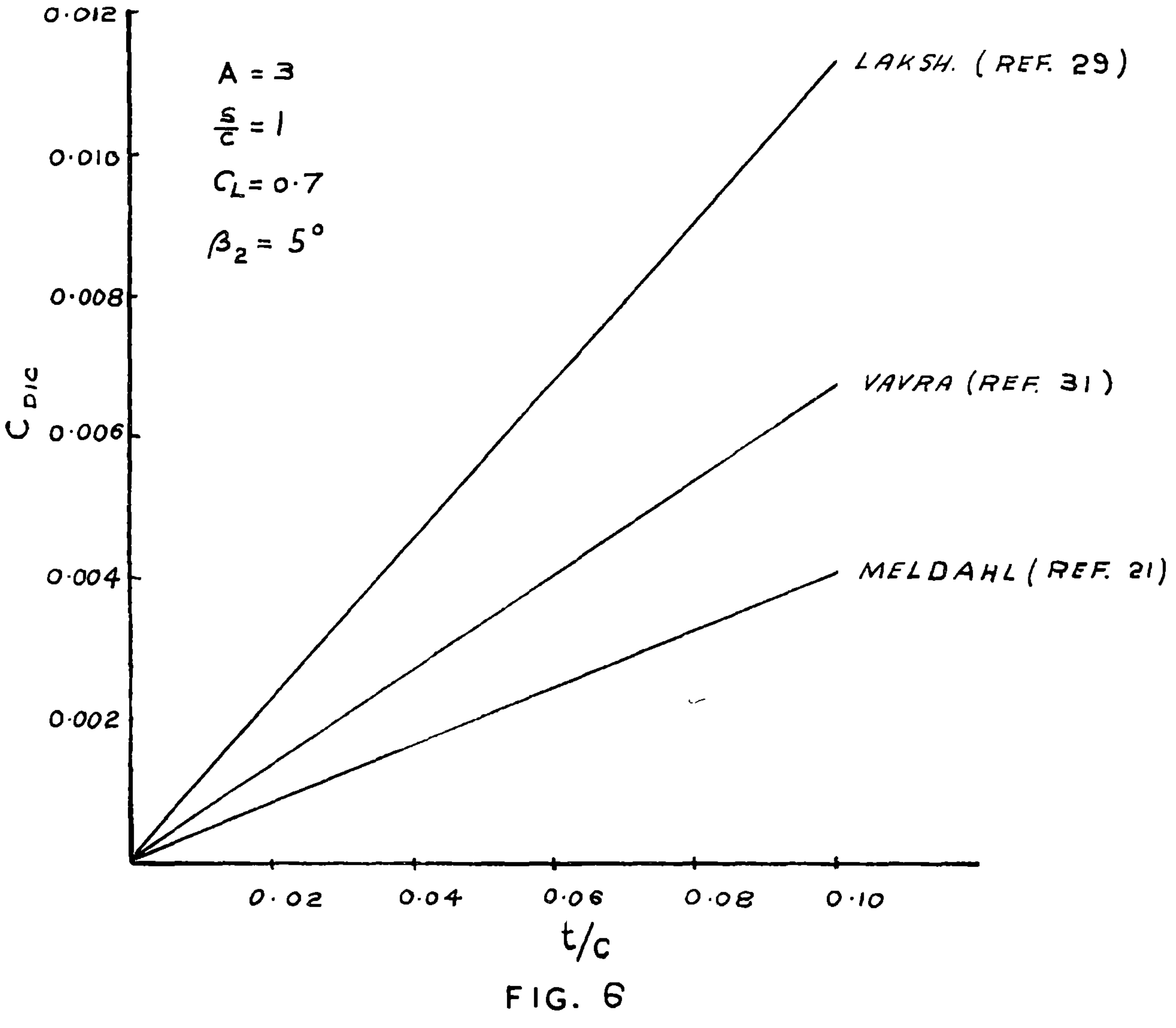

FIG. 6

COMPARISON OF TIP CLEARANCE DRAG COEFFIENTS

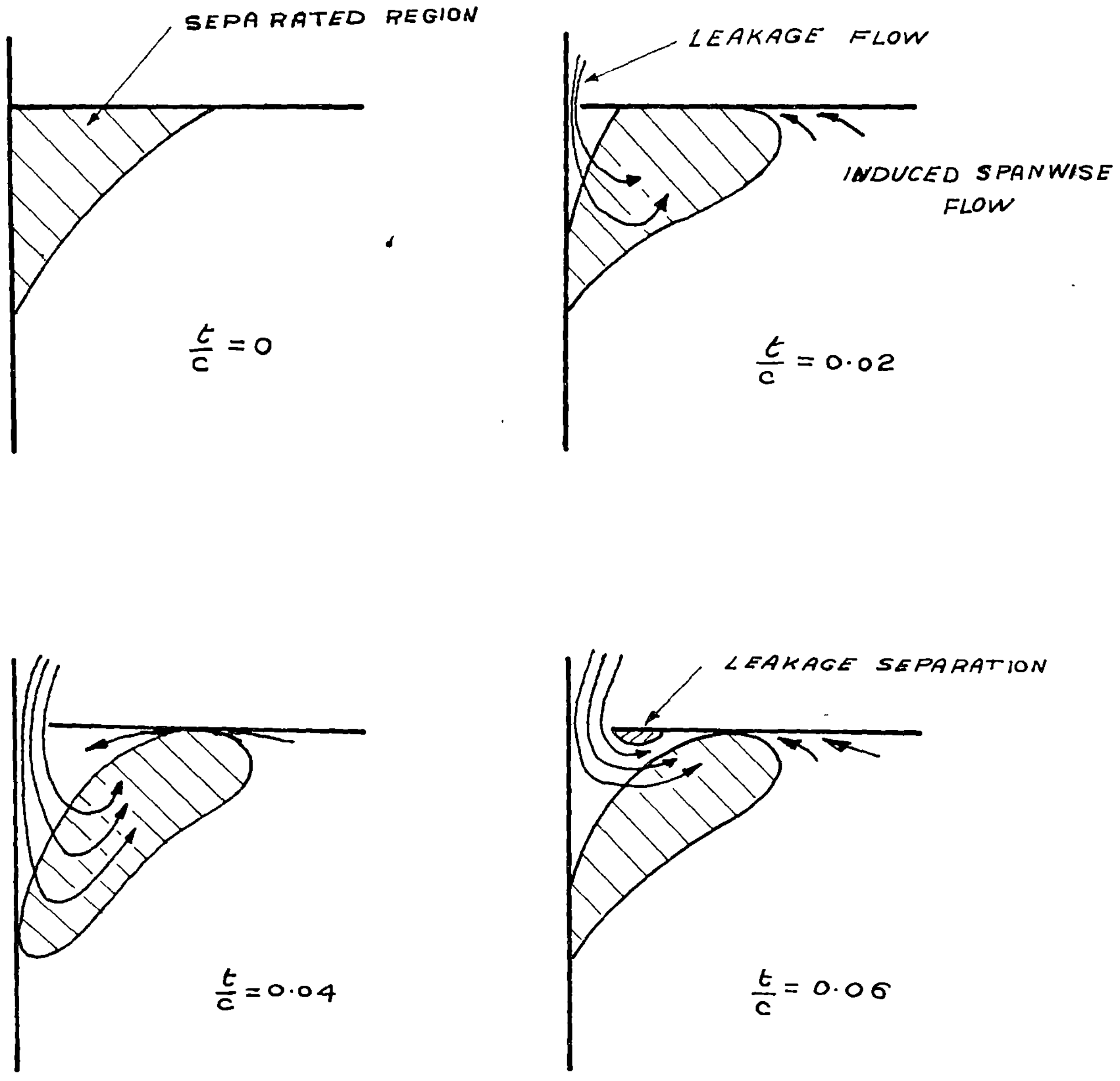
SEPARATED REGION
$\frac{t}{c} = 0$
LEAKAGE FLOW
INDUCED SPANWISE FLOW
$\frac{t}{c} = 0{\cdot}02$
$\frac{t}{c} = 0{\cdot}04$
LEAKAGE SEPARATION
$\frac{t}{c} = 0{\cdot}06$

FIG. 7

INTERACTION OF LEAKAGE FLOW AND SEPARATED REGION IN A BLADE PASSAGE (REF. 29)

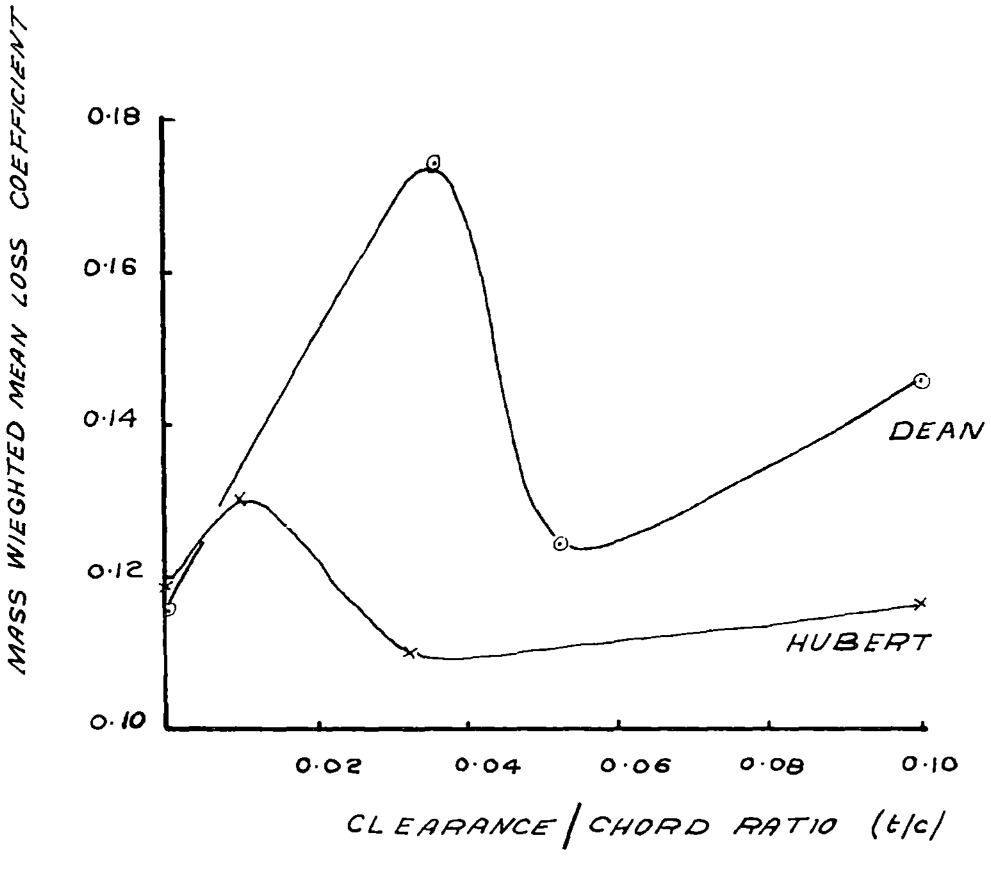

FIG. 8

VARIATION OF LOSS COEFFIENT
WITH TIP CLEARANCE
(REF. 29)

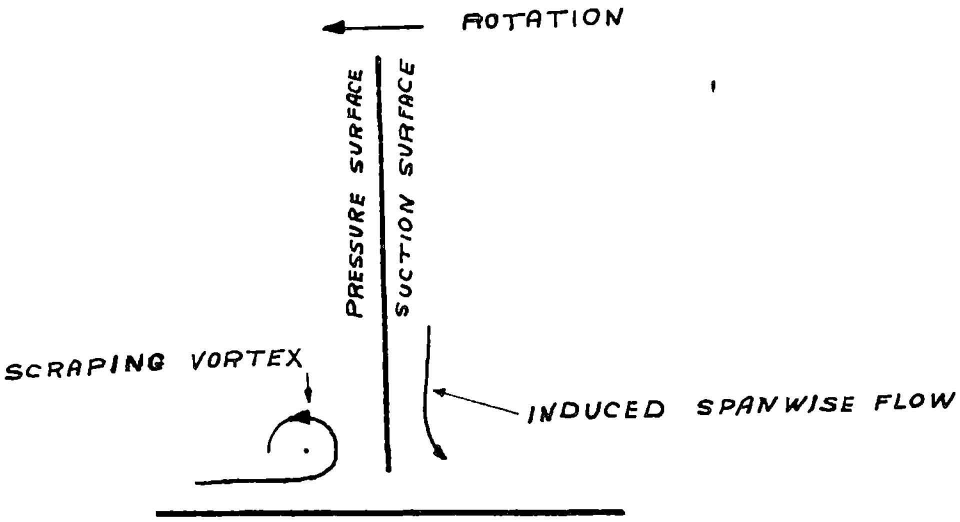
ROTATION
PRESSURE SURFACE
SUCTION SURFACE
SCRAPING VORTEX
INDUCED SPANWISE FLOW

FIG. 9

EFFECT OF RELATIVE MOTION BETWEEN BLADE TIP AND WALL

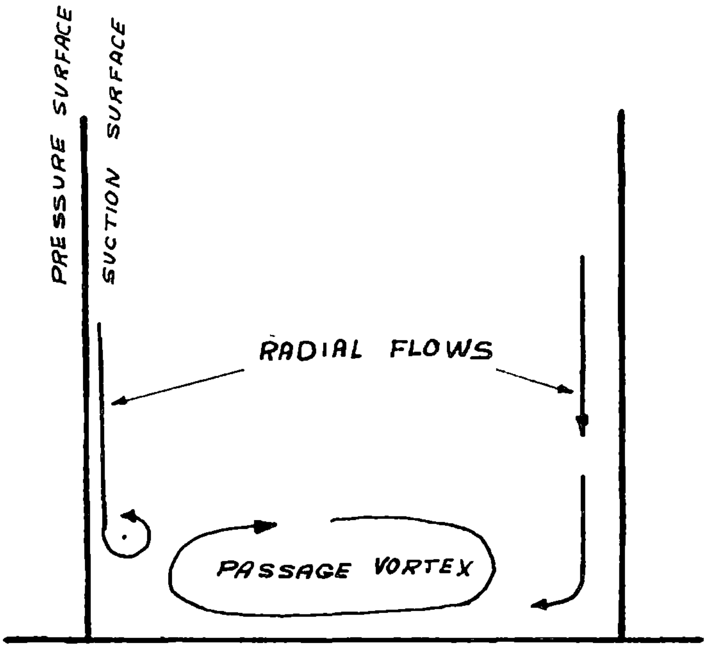
PRESSURE SURFACE
SUCTION SURFACE
RADIAL FLOWS
PASSAGE VORTEX

FIG. 10

RADIAL FLOW VORTEX

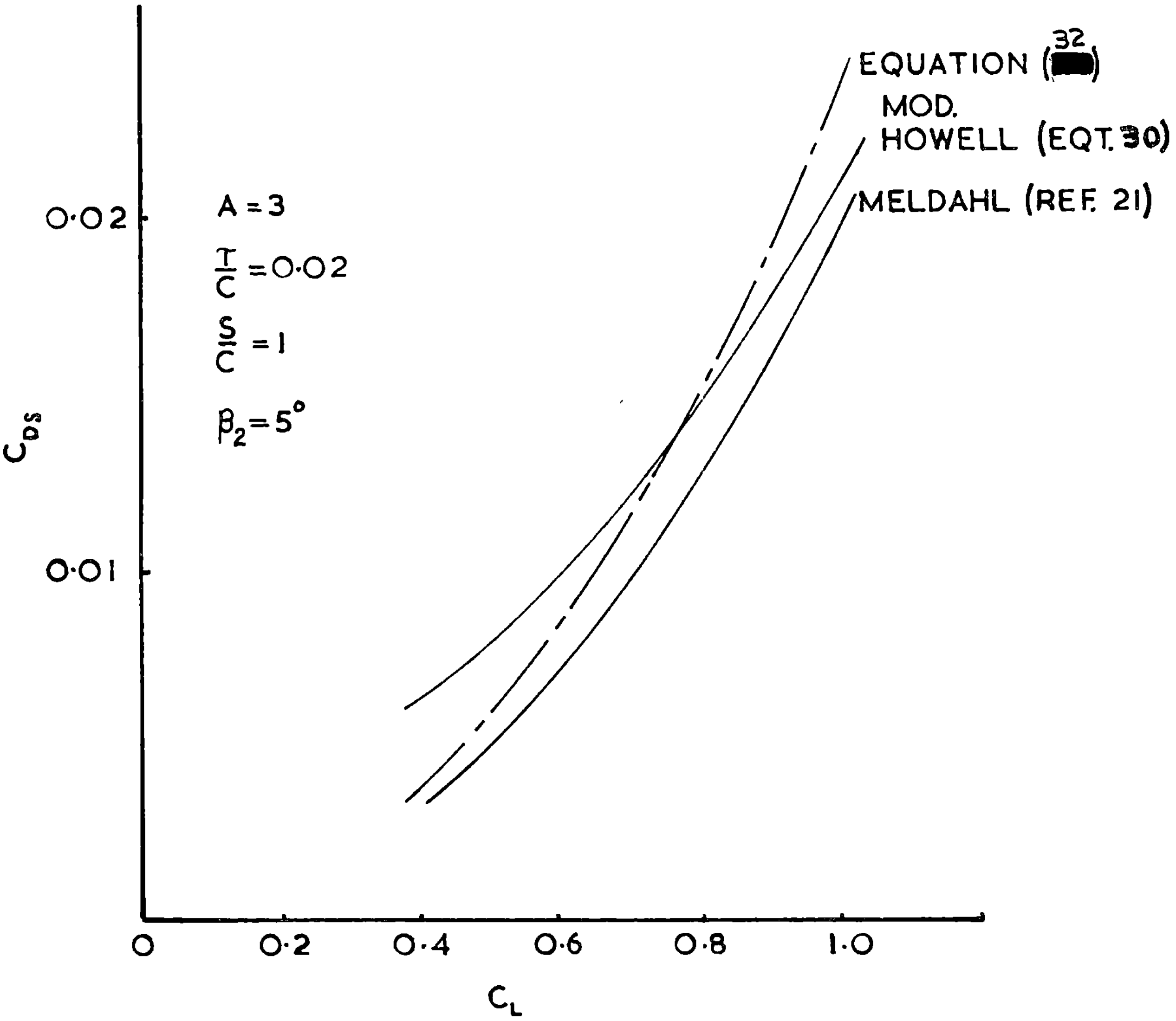

FIG. 11

COMPARISON OF SECONDARY DRAG RELATIONSHIPS

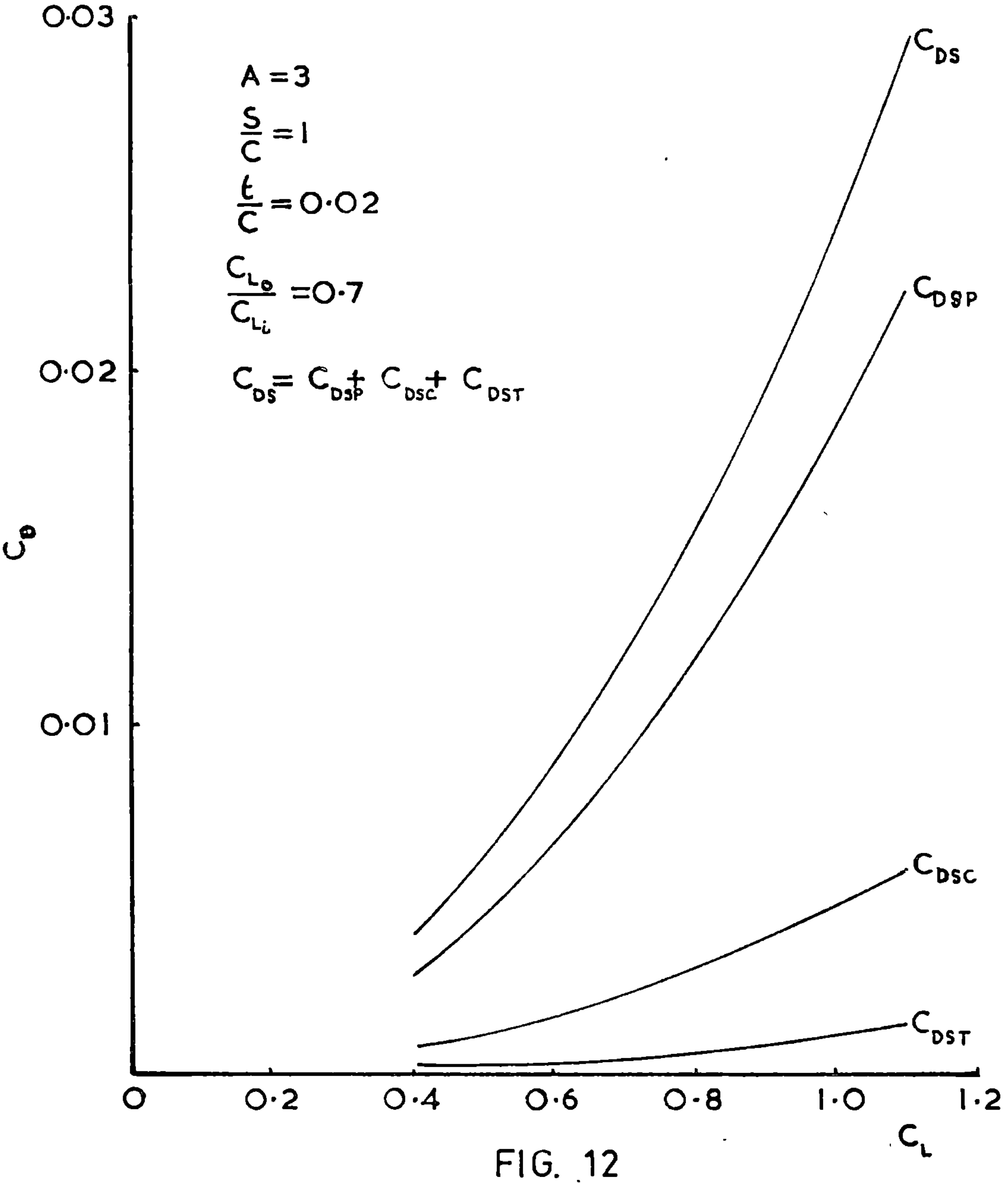

FIG. 12

COMPONENTS OF SECONDARY DRAG IN AN AXIAL FLOW COMPRESSOR

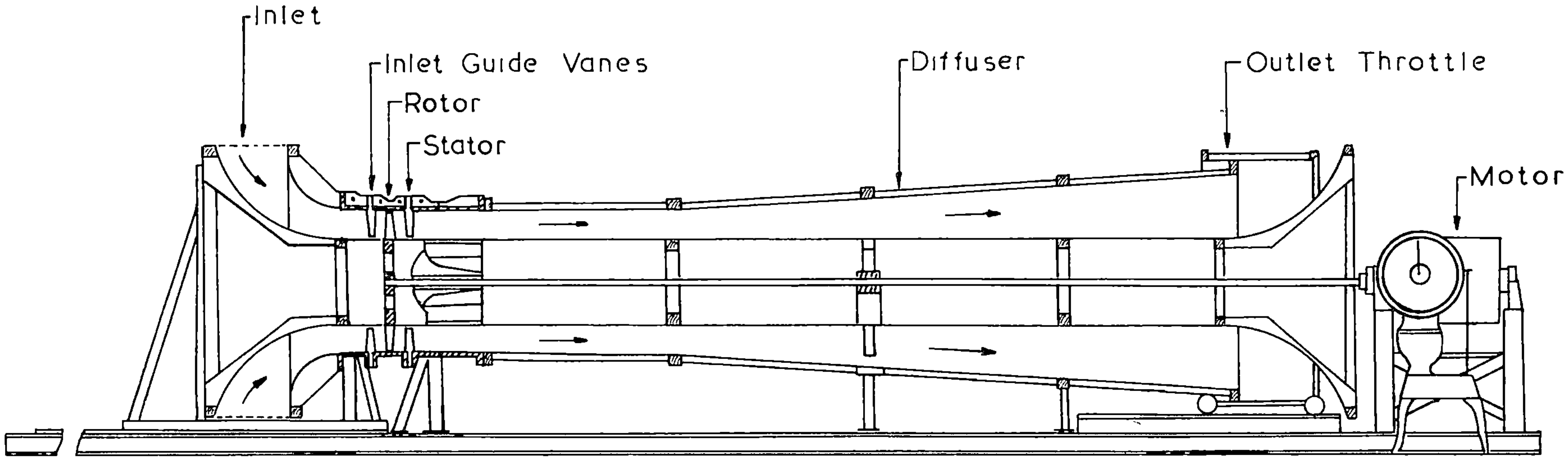
Inlet
Inlet Guide Vanes
Rotor
Stator
Diffuser
Outlet Throttle
Motor

VORTEX WIND TUNNEL

Fig. **13**

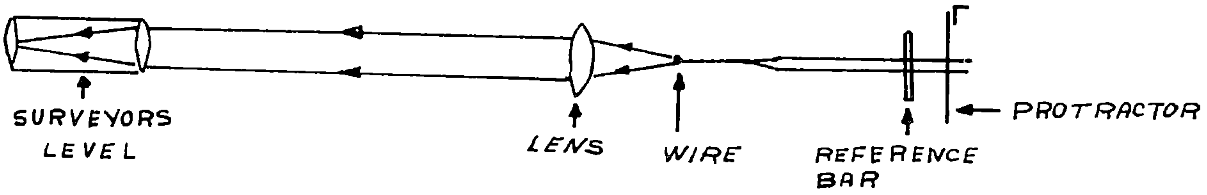
SURVEYORS
LEVEL
LENS
WIRE
REFERENCE
BAR
PROTRACTOR

FIG. 14
MEASUREMENT OF ANGLE DATUM

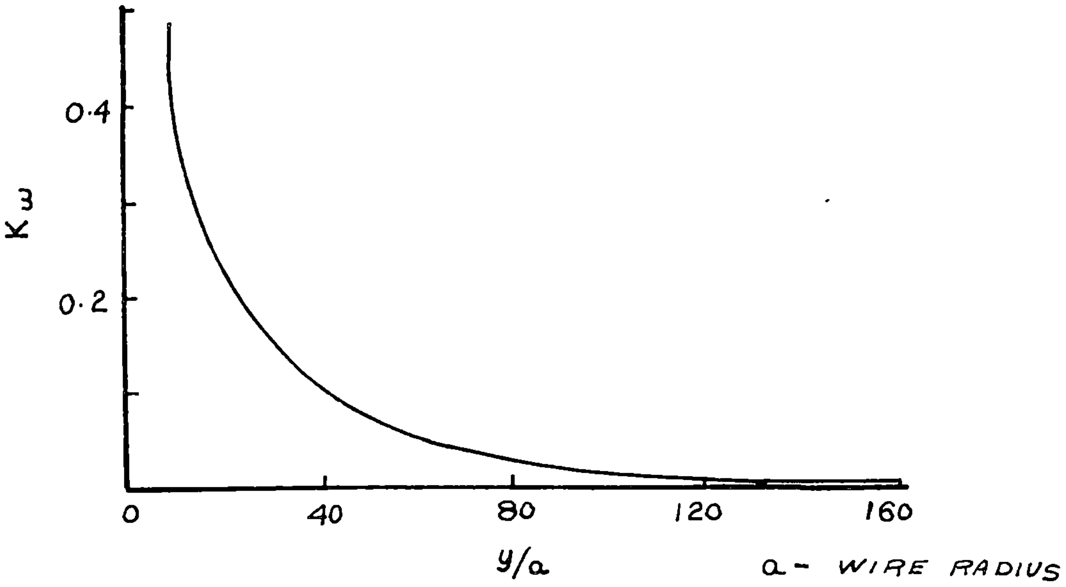

FIG. 15
WALL CORECTION FACTOR

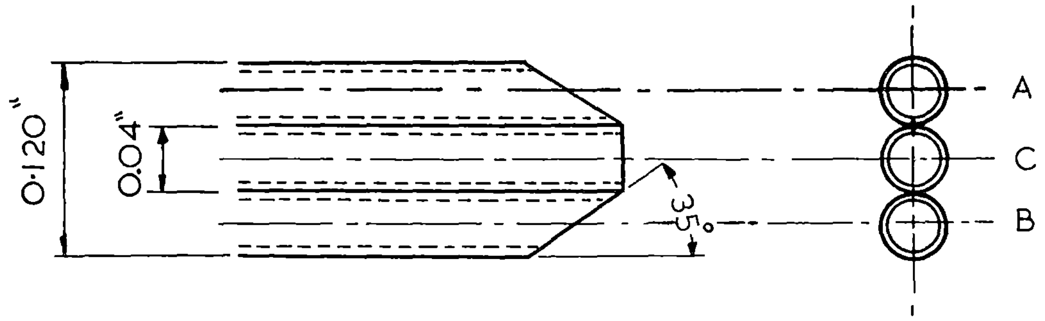
0·120"
0.04"
35°
A
C
B

YAW METER HEAD

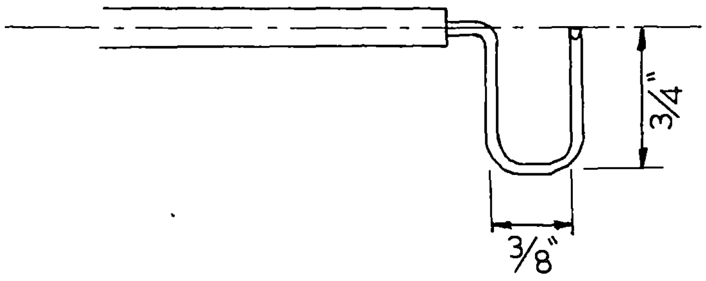

YAW METER NO. 1

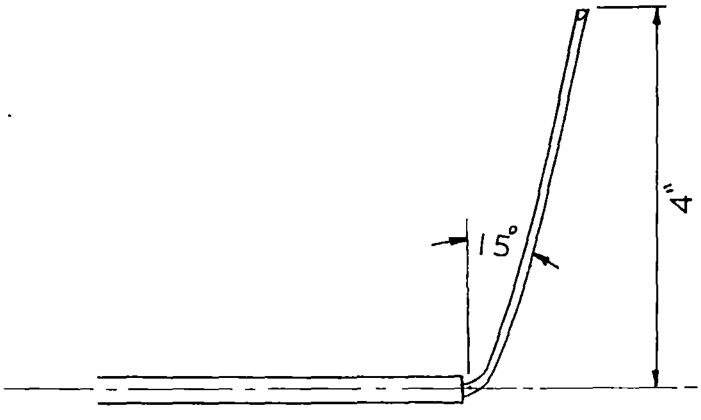

YAW METER NO. 2

COBRA YAW METERS

Fig. 16

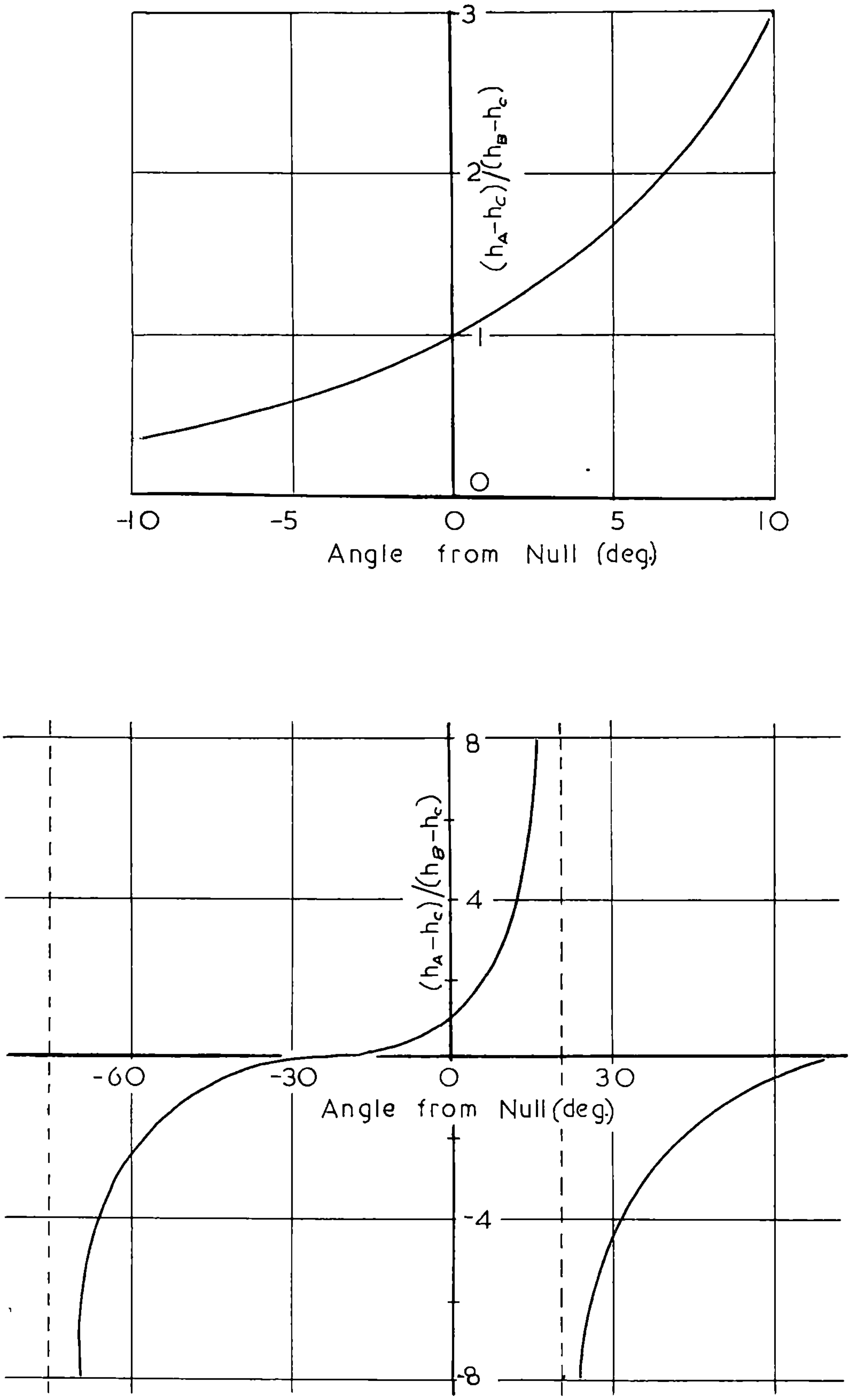

PROBE NO. 2

COBRA YAW METER ANGLE CALIBRATION

Fig. 17

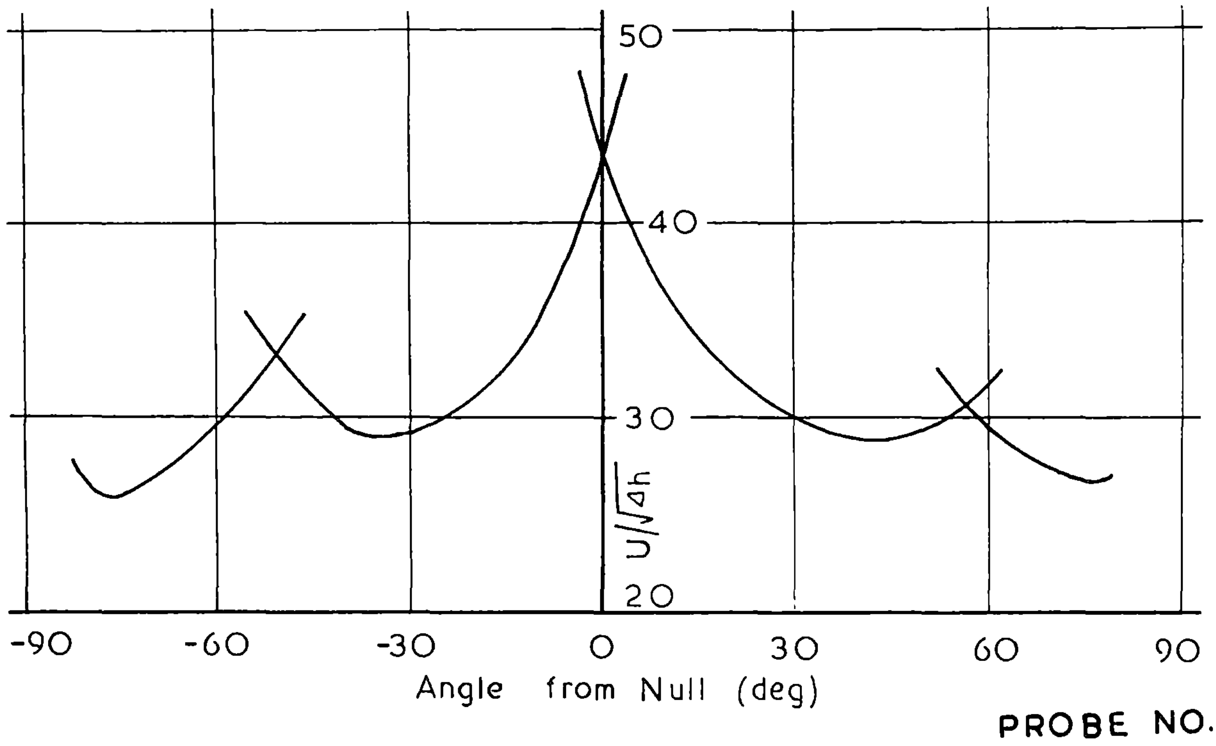

COBRA YAW METER VELOCITY CALIBRATION

Fig. 18

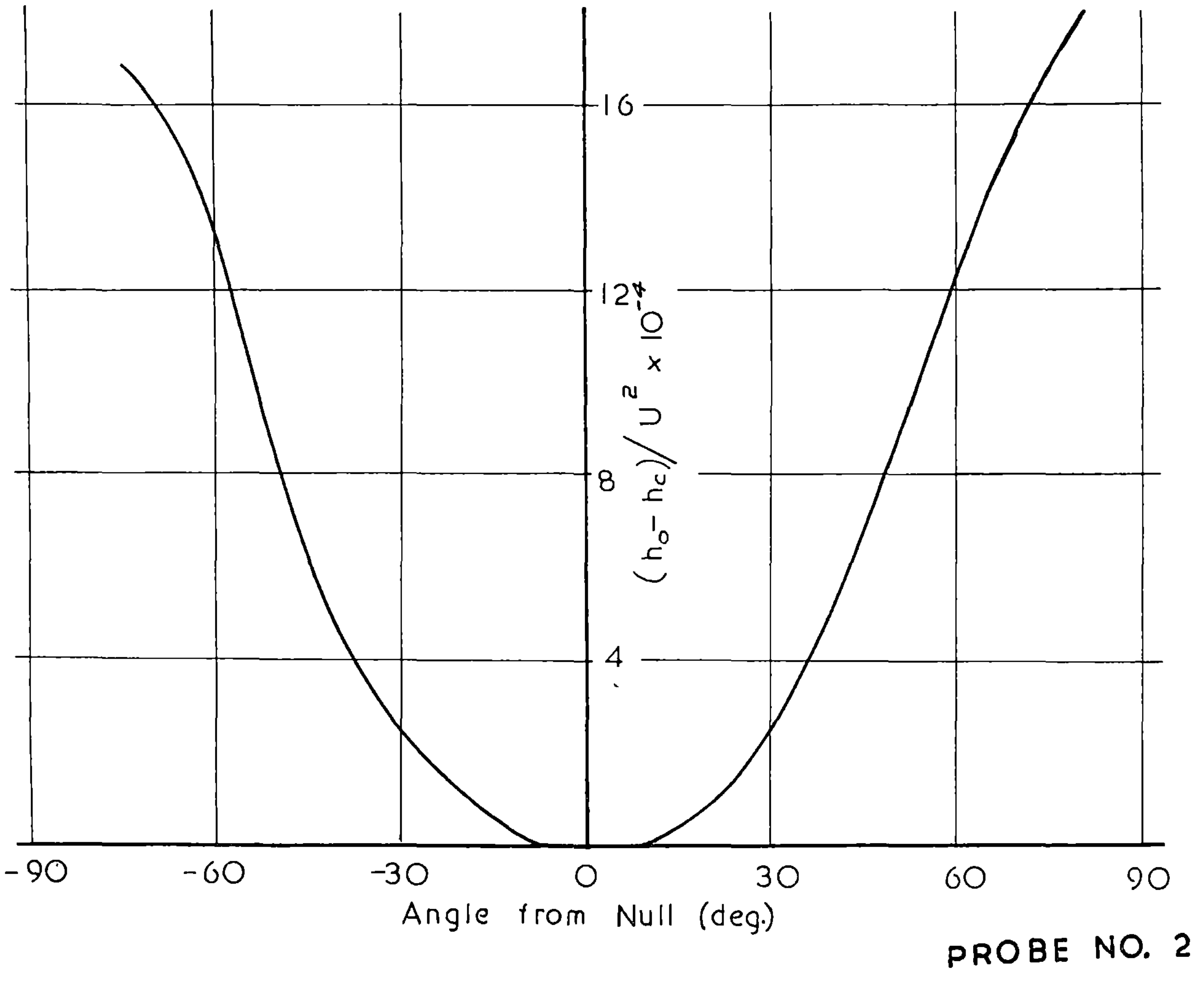

COBRA YAW METER TOTAL PRESSURE CALIBRATION

Fig. 19

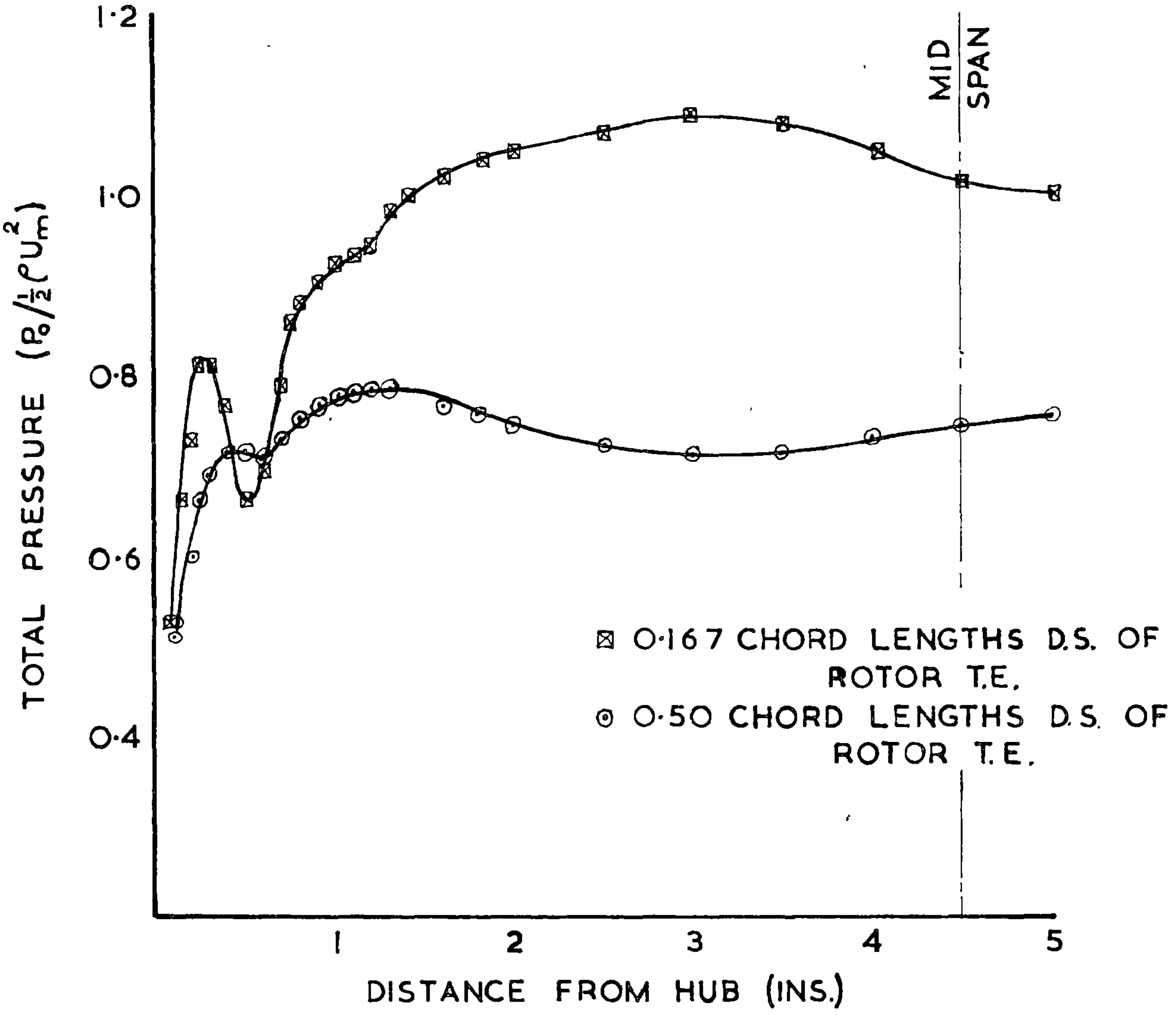

FIG. 20

TOTAL PRESSURE DOWNSTREAM OF ROTOR MEASURED WITH COBRA YAW METER

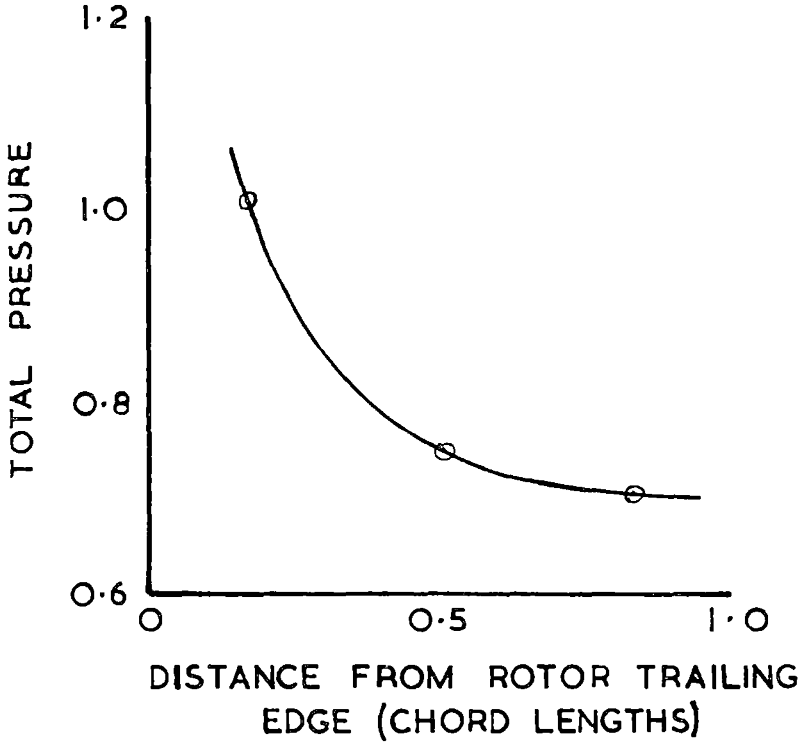

FIG. 21

VARIATION OF TOTAL PRESSURE AT MID SPAN INDICATED BY A COBRA YAW METER,~DISTANCE FROM ROTOR

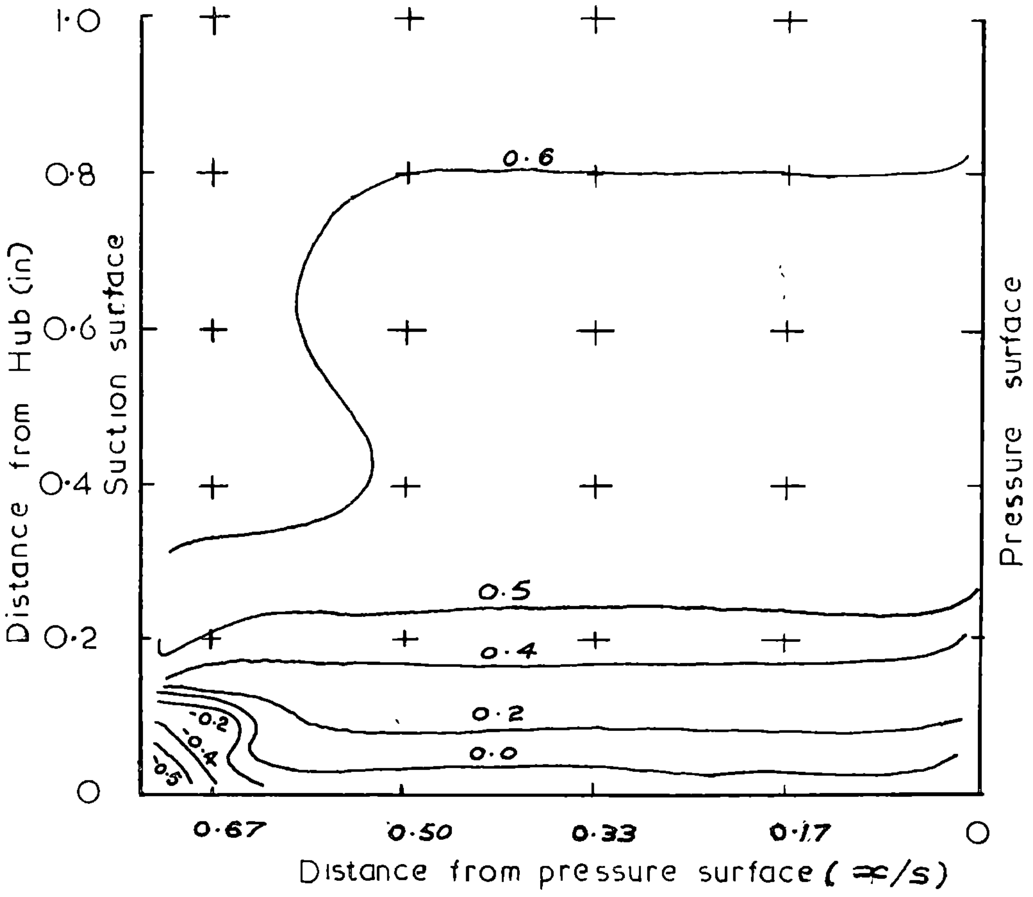

0·67 C U.S. of T.E.

Fig. 22

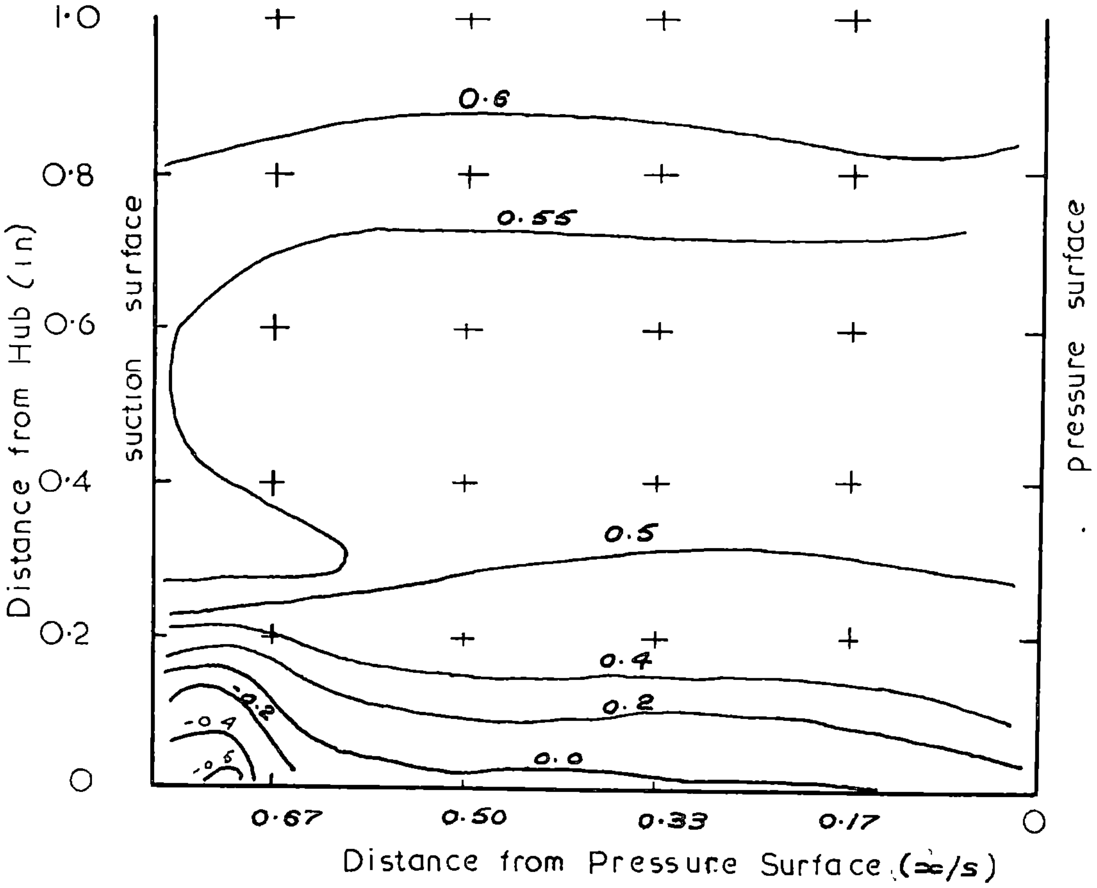

0·50 C U.S. of T.E.

Fig. 23

C = 3 INS.
S = 3 INS.

CONTOURS OF TOTAL PRESSURE ($P_o/\frac{1}{2}\rho U_m^2$)
THROUGH STATOR

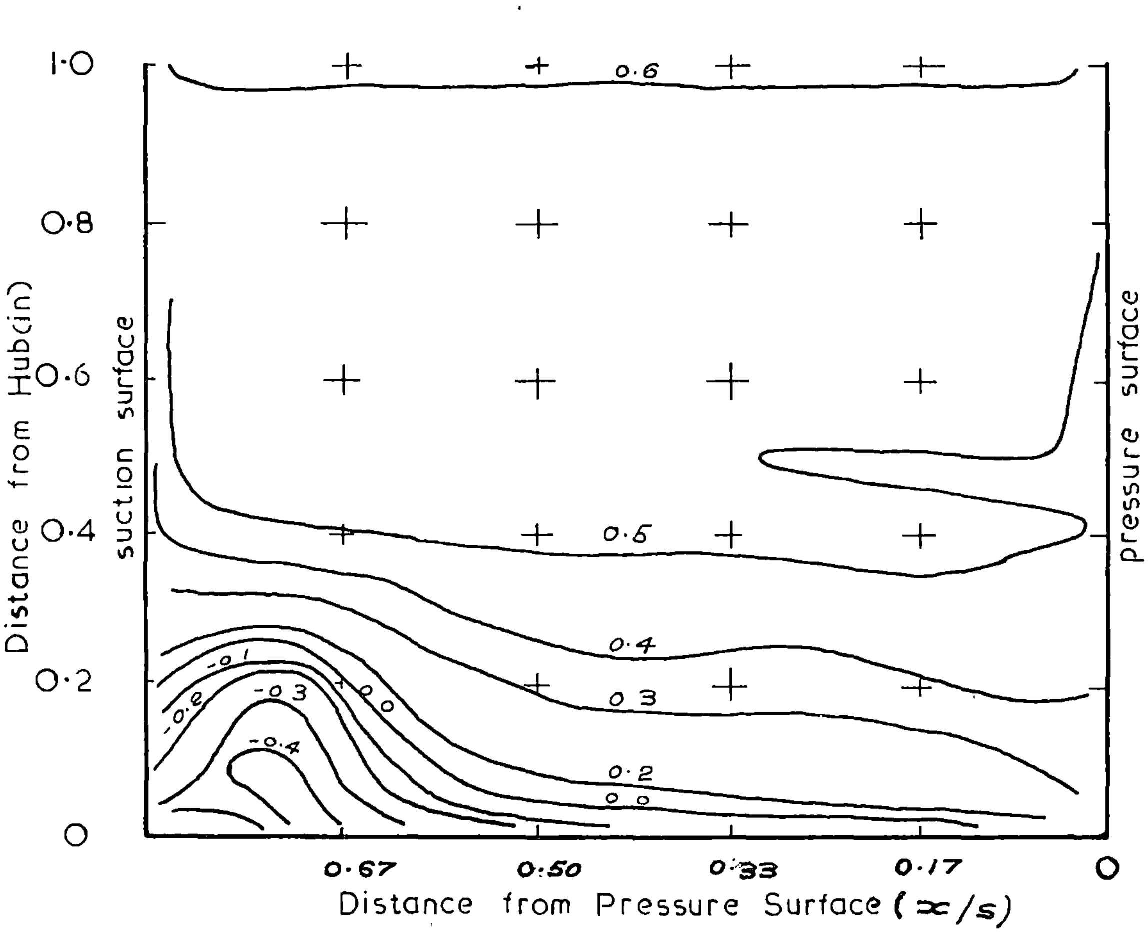

0·33 C U.S. of T.E.

Fig. **24**

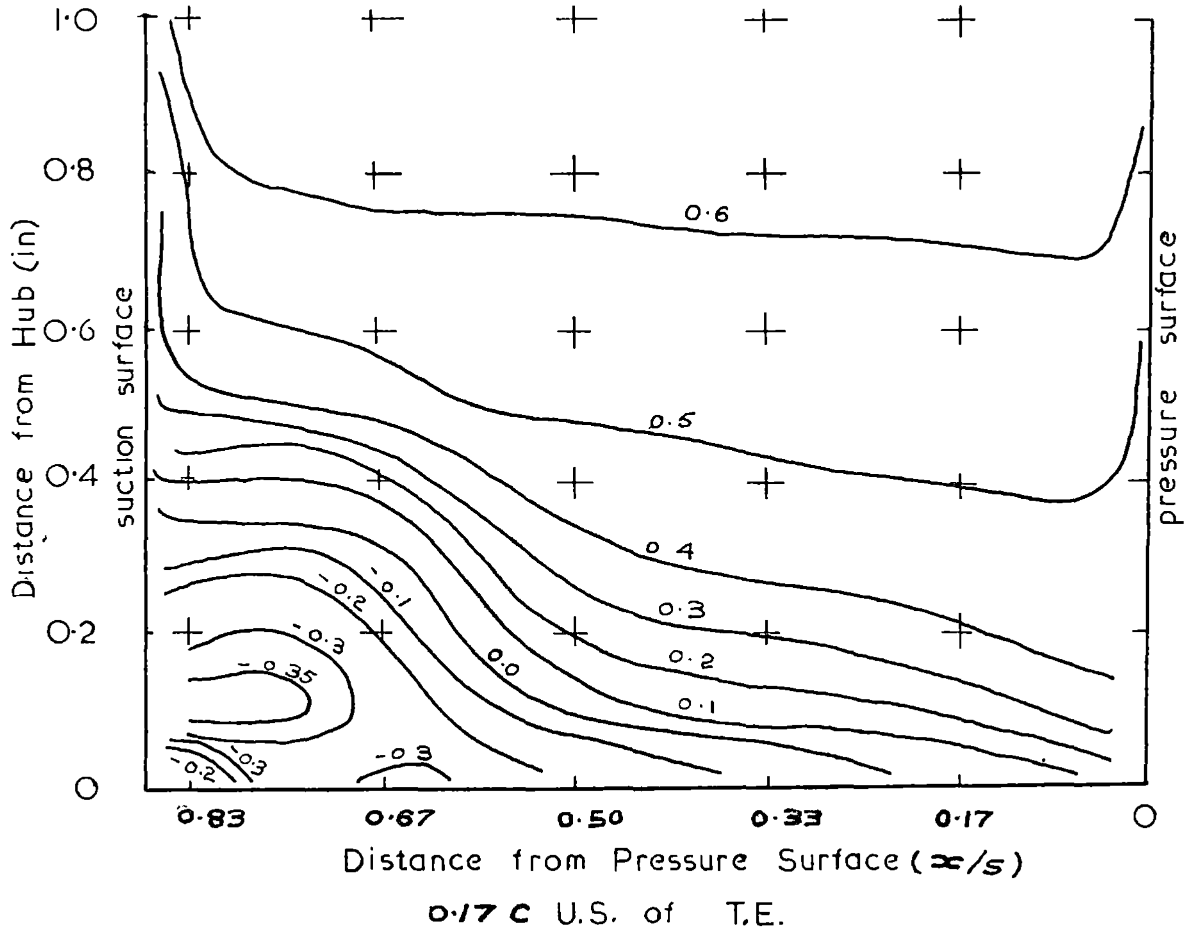

0·17 C U.S. of T.E.

Fig. **25**

CONTOURS OF TOTAL PRESSURE THROUGH STATOR

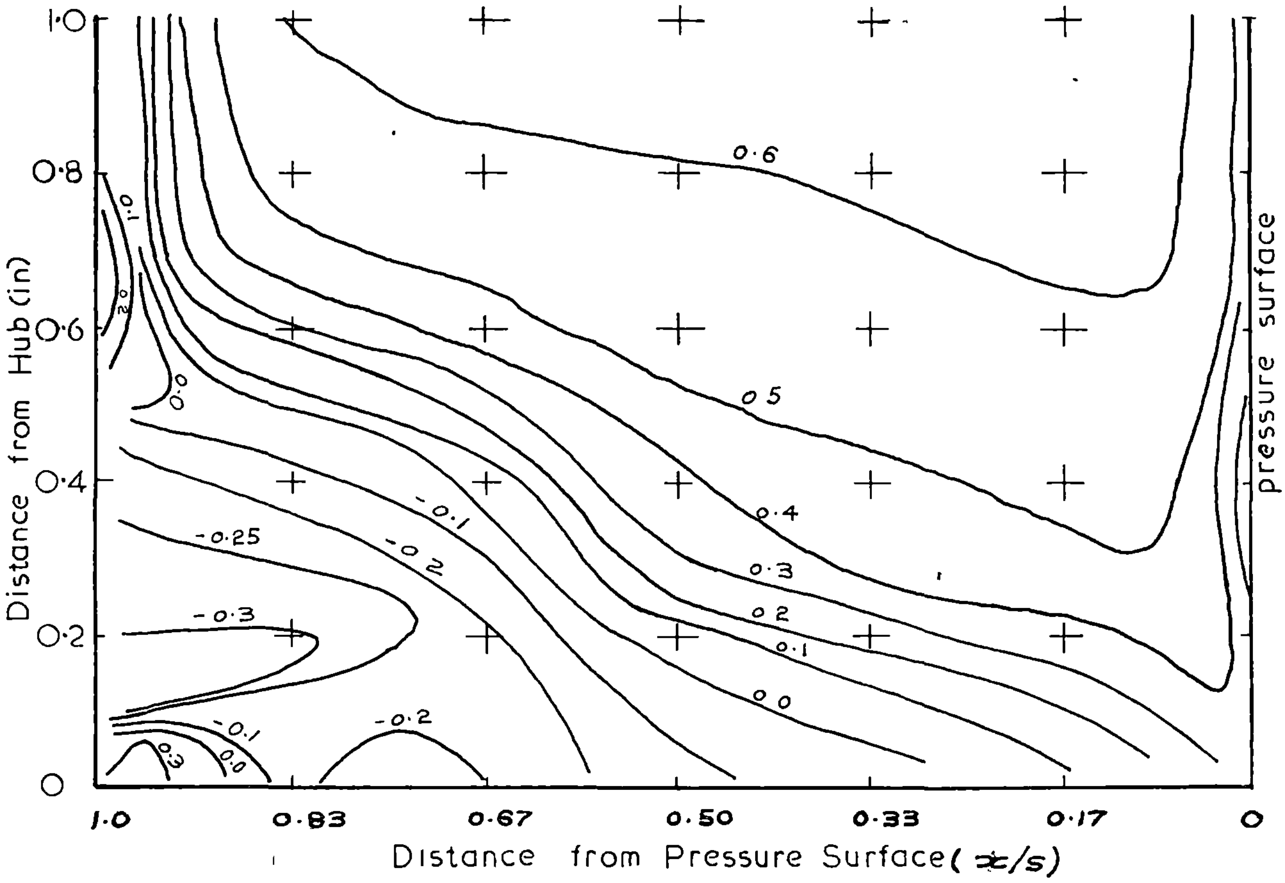

STATOR T.E.
Fig. **26**

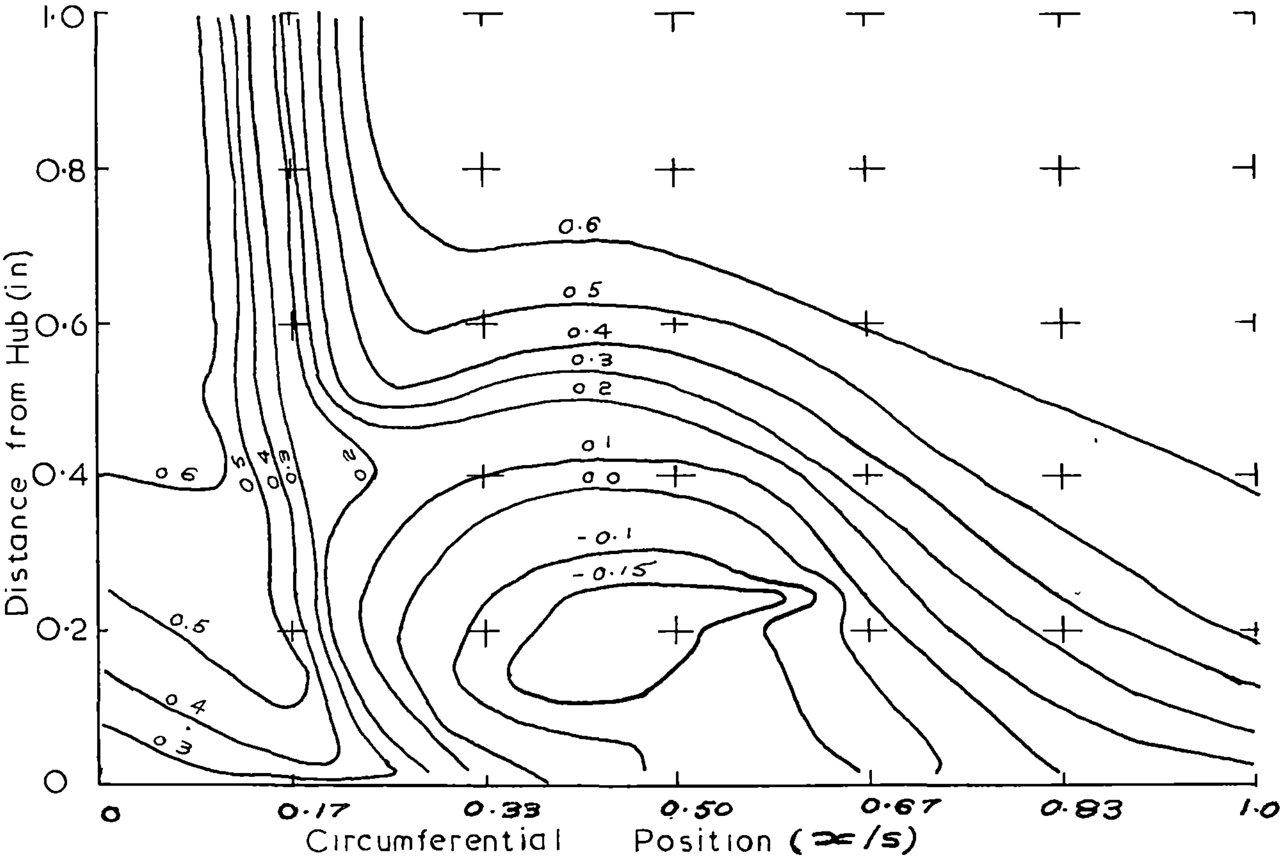

0·17 C D.S. of Stator T.E.
Fig. **27**

CONTOURS OF TOTAL PRESSURE

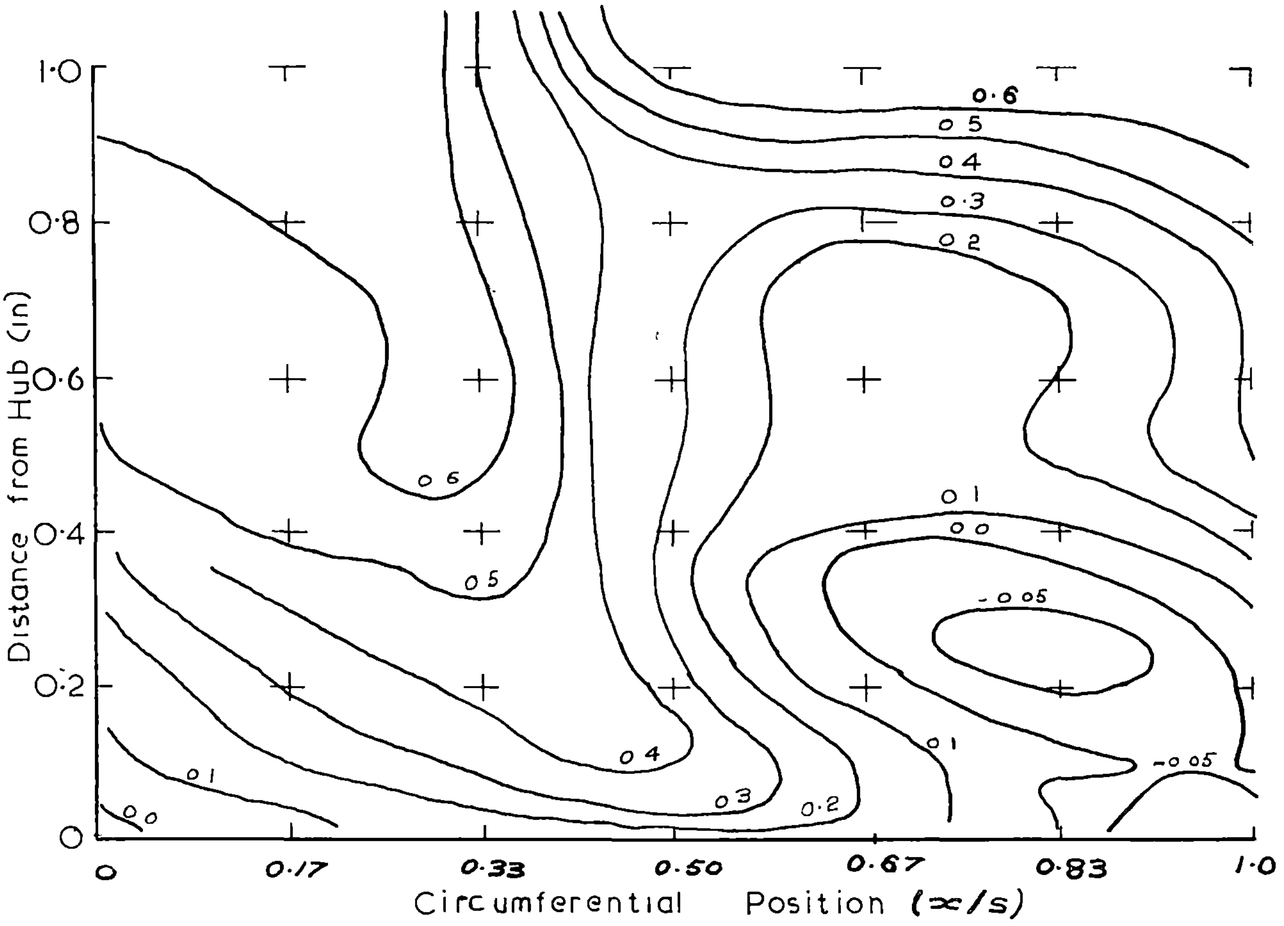

CONTOURS OF TOTAL PRESSURE 0·5C D.S. OF STATOR T.E.

Fig. **28**

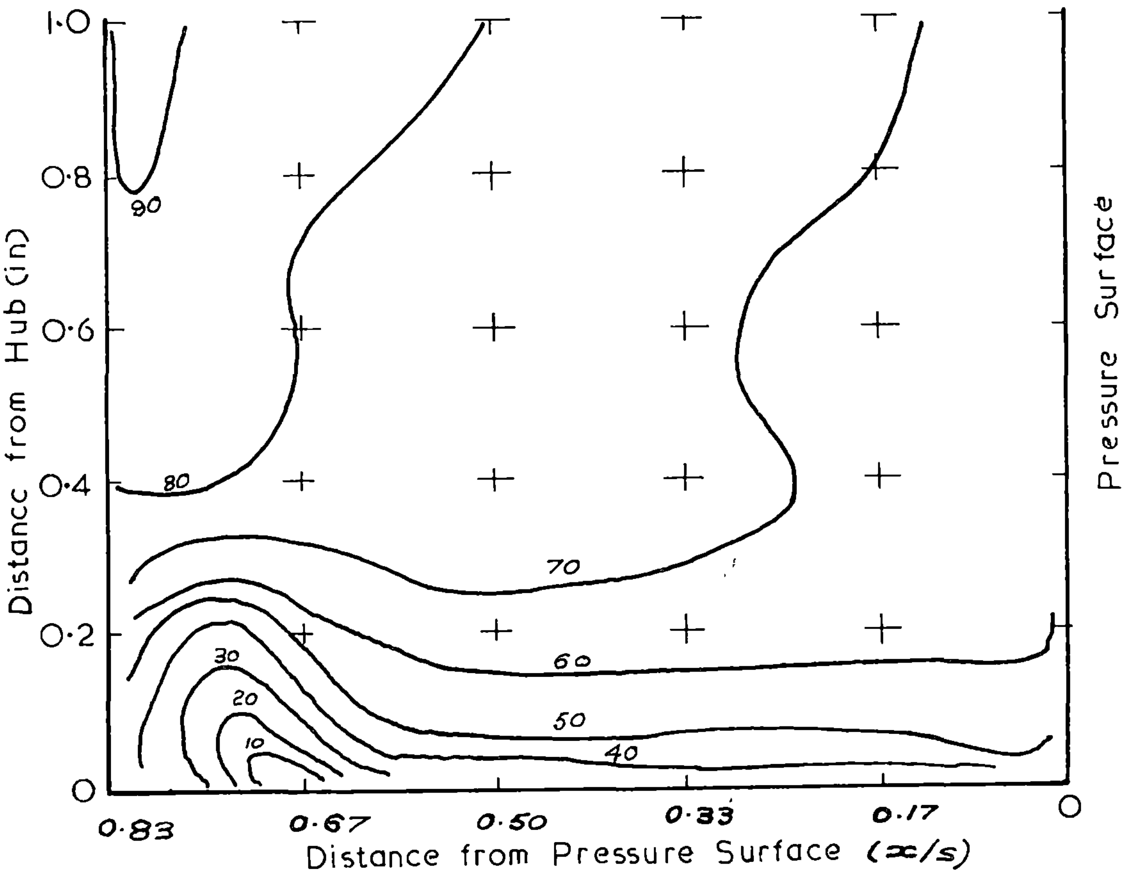

CONTOURS OF VELOCITY 0·33C U.S. OF STATOR T.E.

Fig. **29**

C = 3 INS.
S = 3 INS.

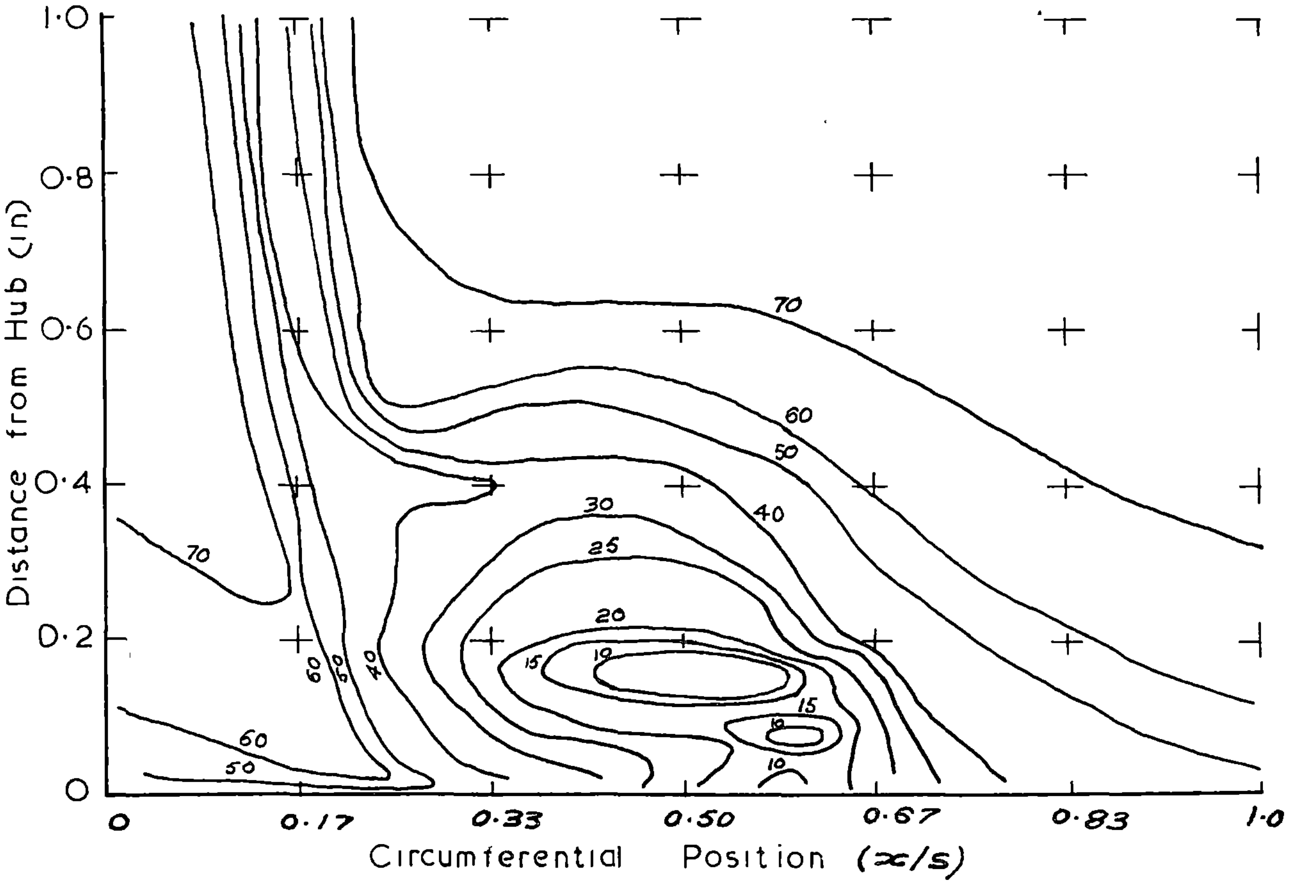

0·17 C D.S. of STATOR T.E.

Fig. 30

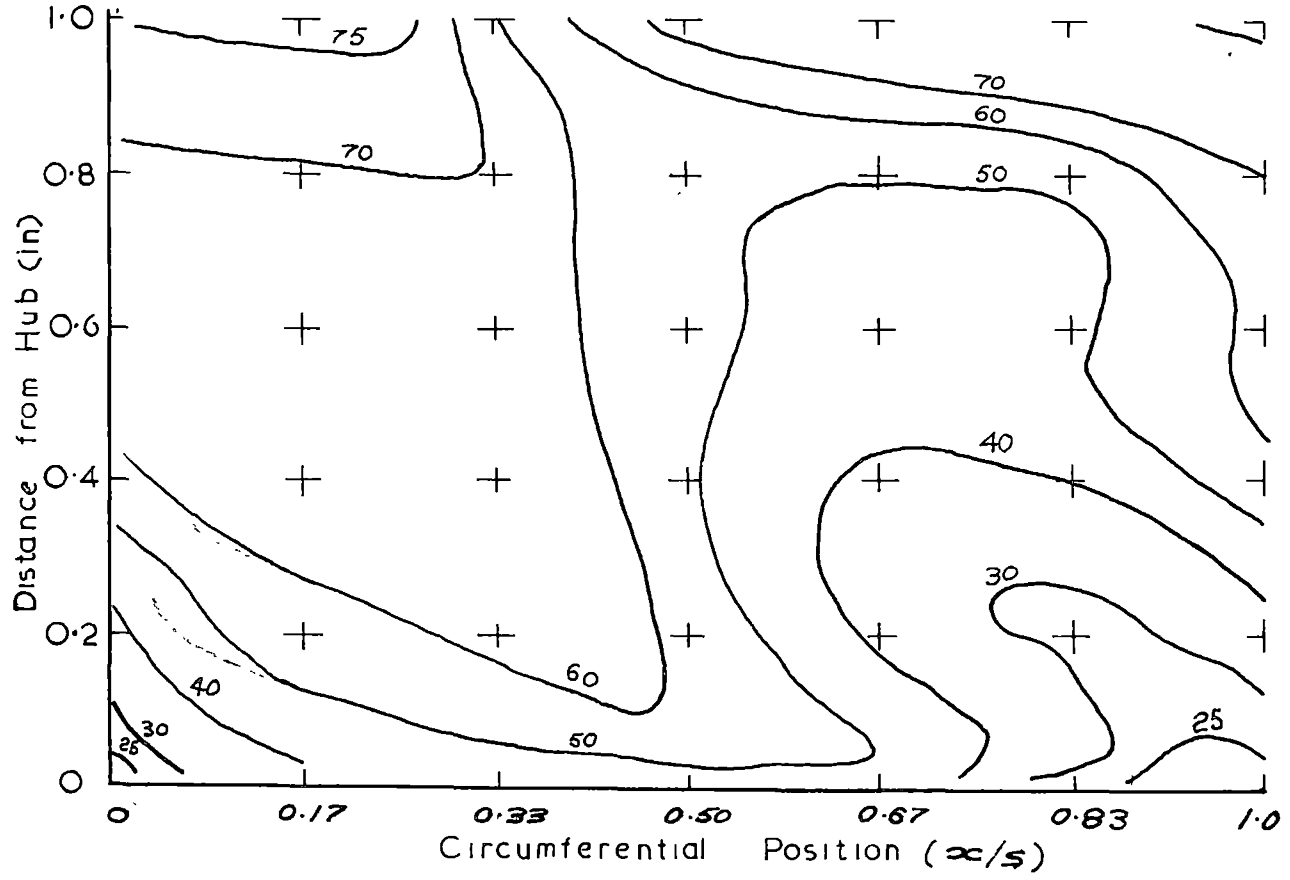

0·50 C D.S. of STATOR T.E.

Fig. 31

CONTOURS OF VELOCITY (f.p.s.)

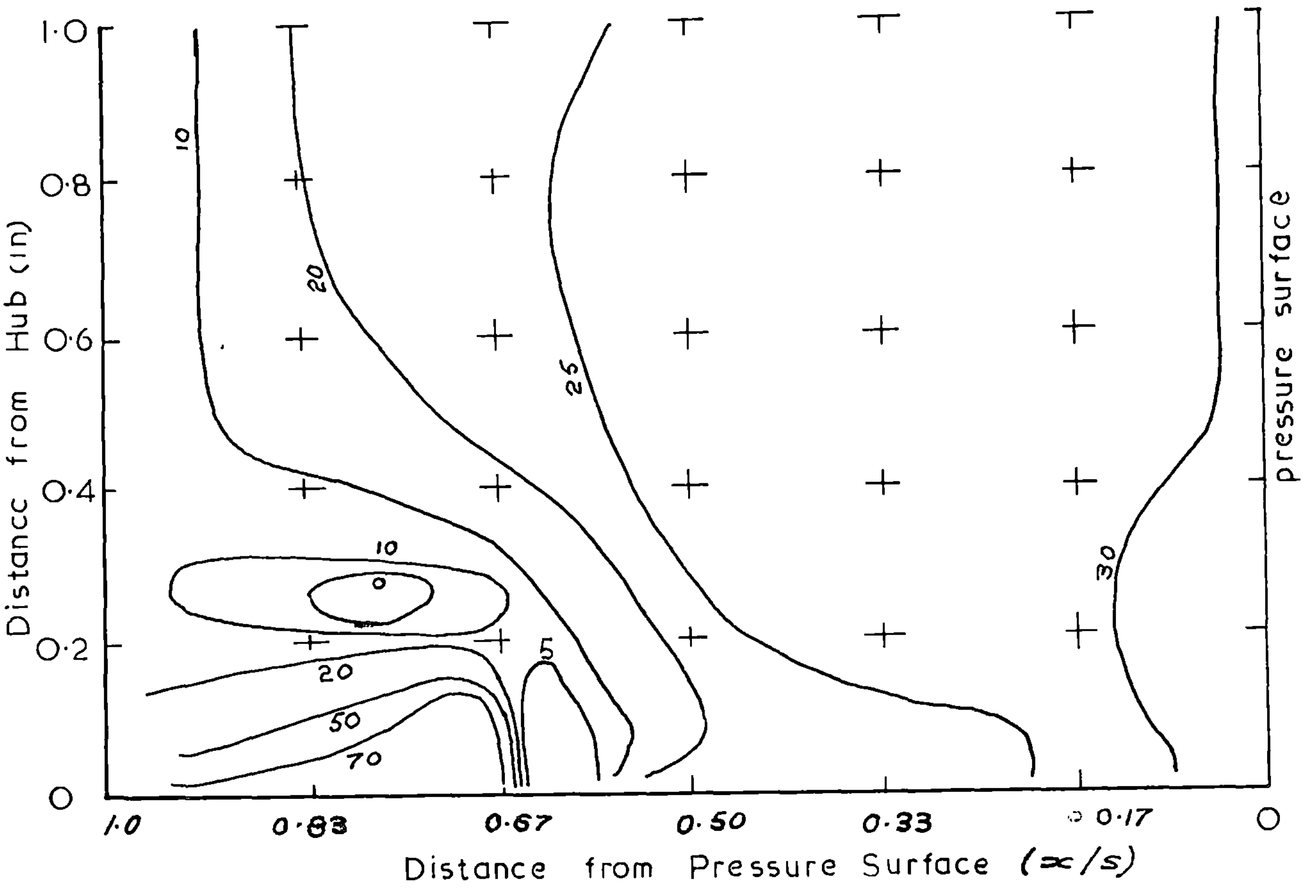

AT STATOR T.E.
Fig. **32**

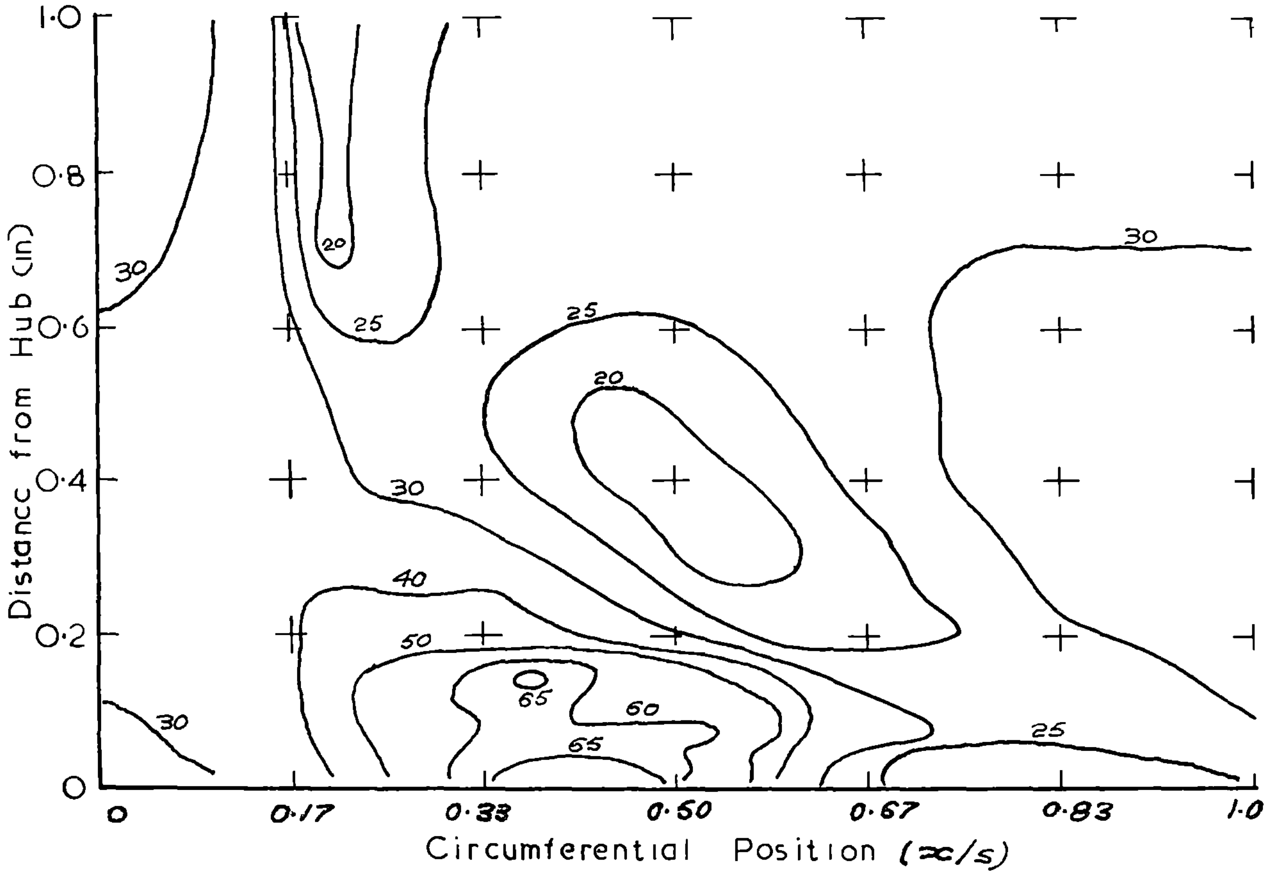

0·17C D.S. of STATOR T.E.
Fig. **33**

C = 3 INS.
S = 3 INS.

CONTOURS OF FLOW ANGLE (°)

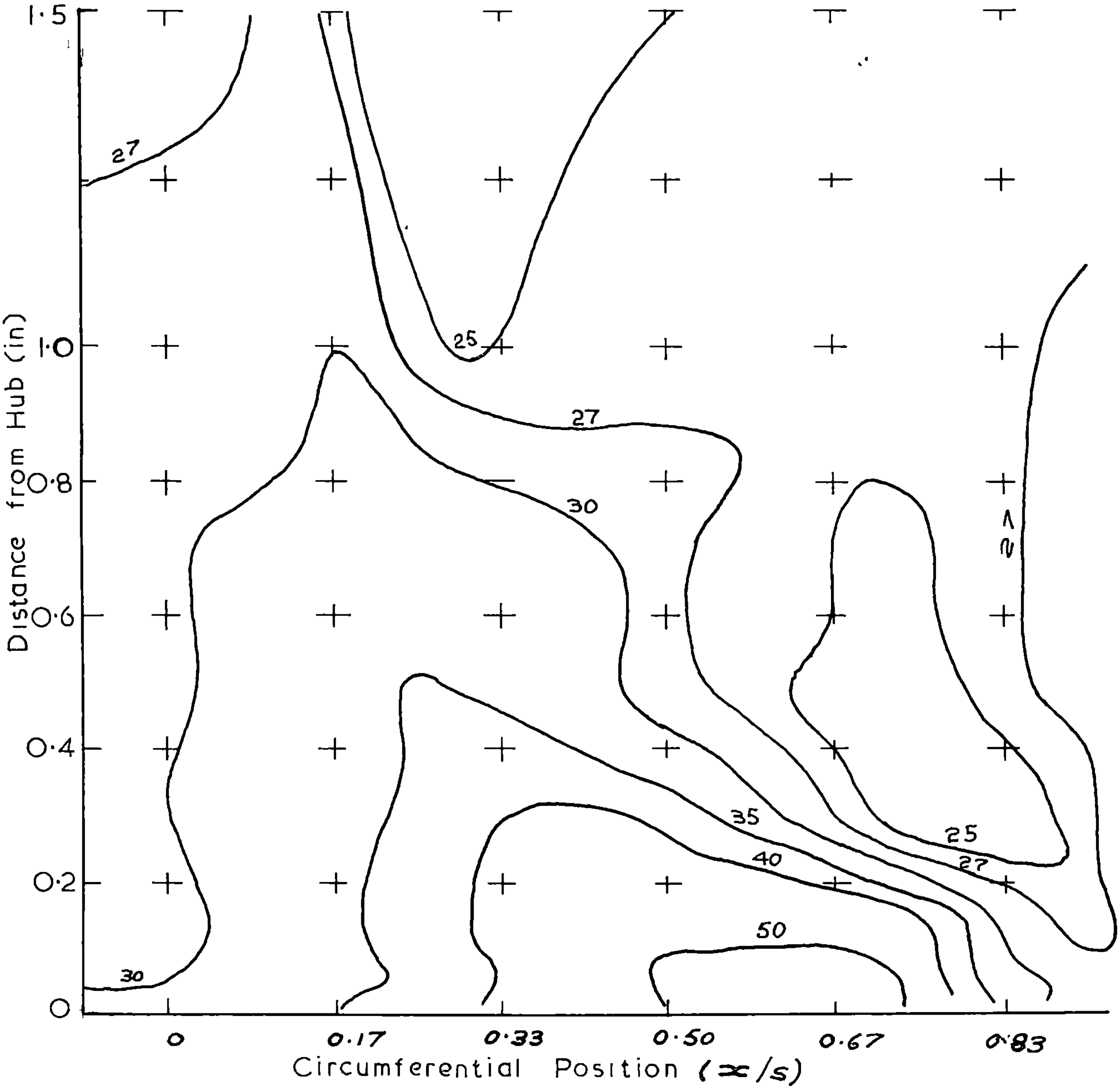

0·50 C D.S. of STATOR T.E.

Fig. 34

CONTOURS OF FLOW ANGLE (°)

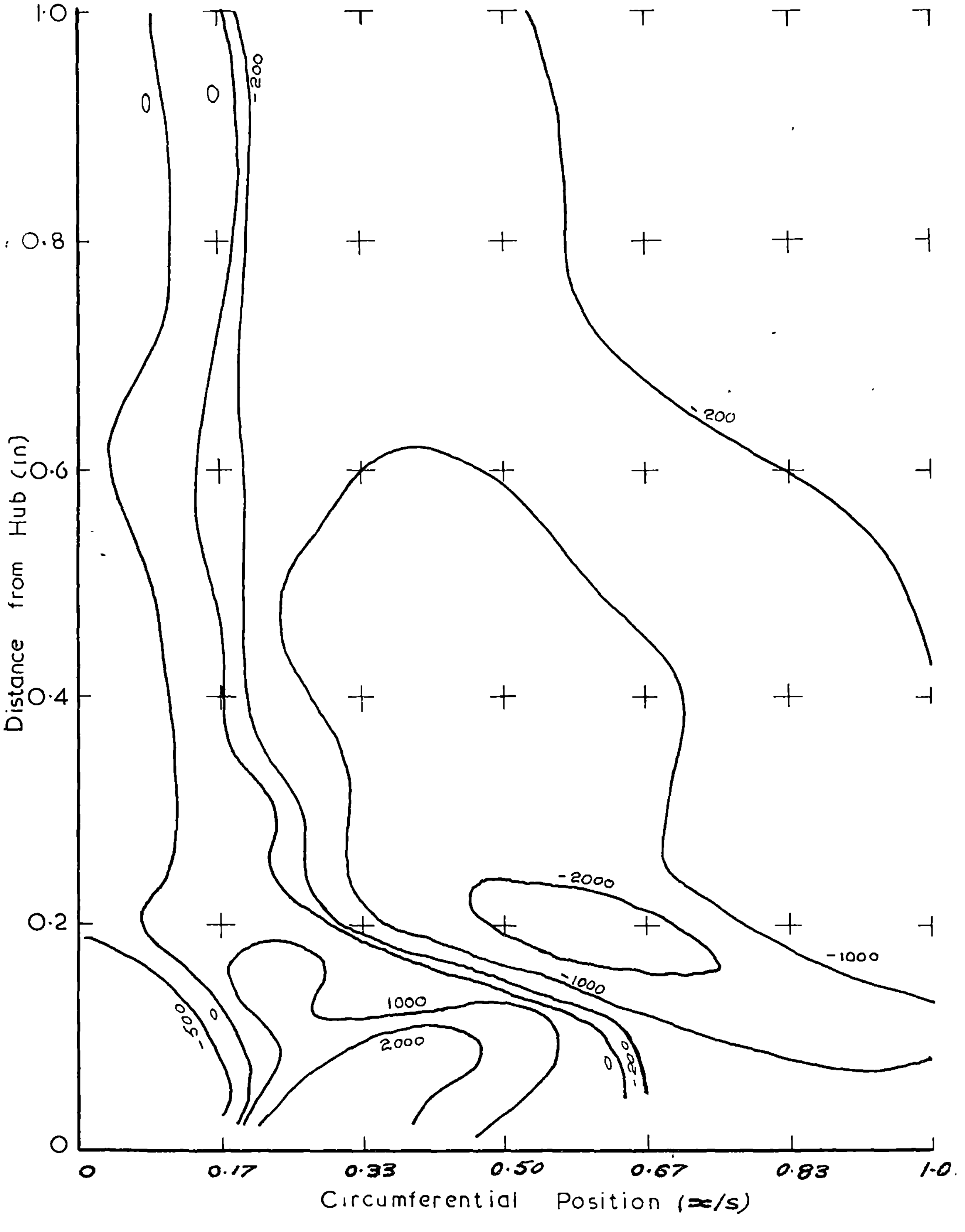

VORTICITY NORMAL TO STREAMLINE (Rad./sec)

0·17C D.S. OF STATOR T.E.

Fig. **35**

C = 3 INS.
S = 3 INS.

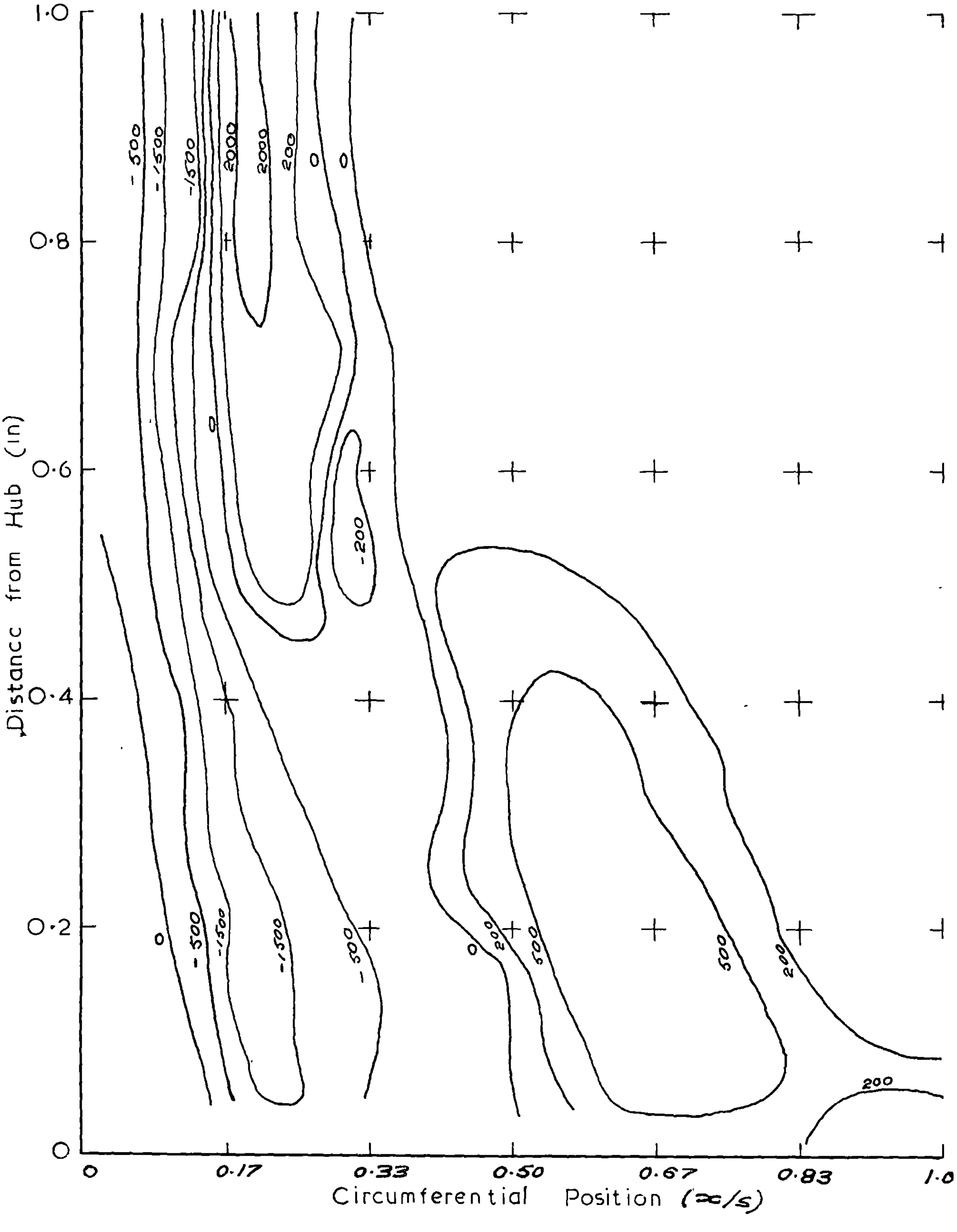

RADIAL VORTICITY 0·17 C DS OF STATOR T. E.
(Rad. / Sec)

Fig. 36

C = 3 INS.
S = 3 INS.

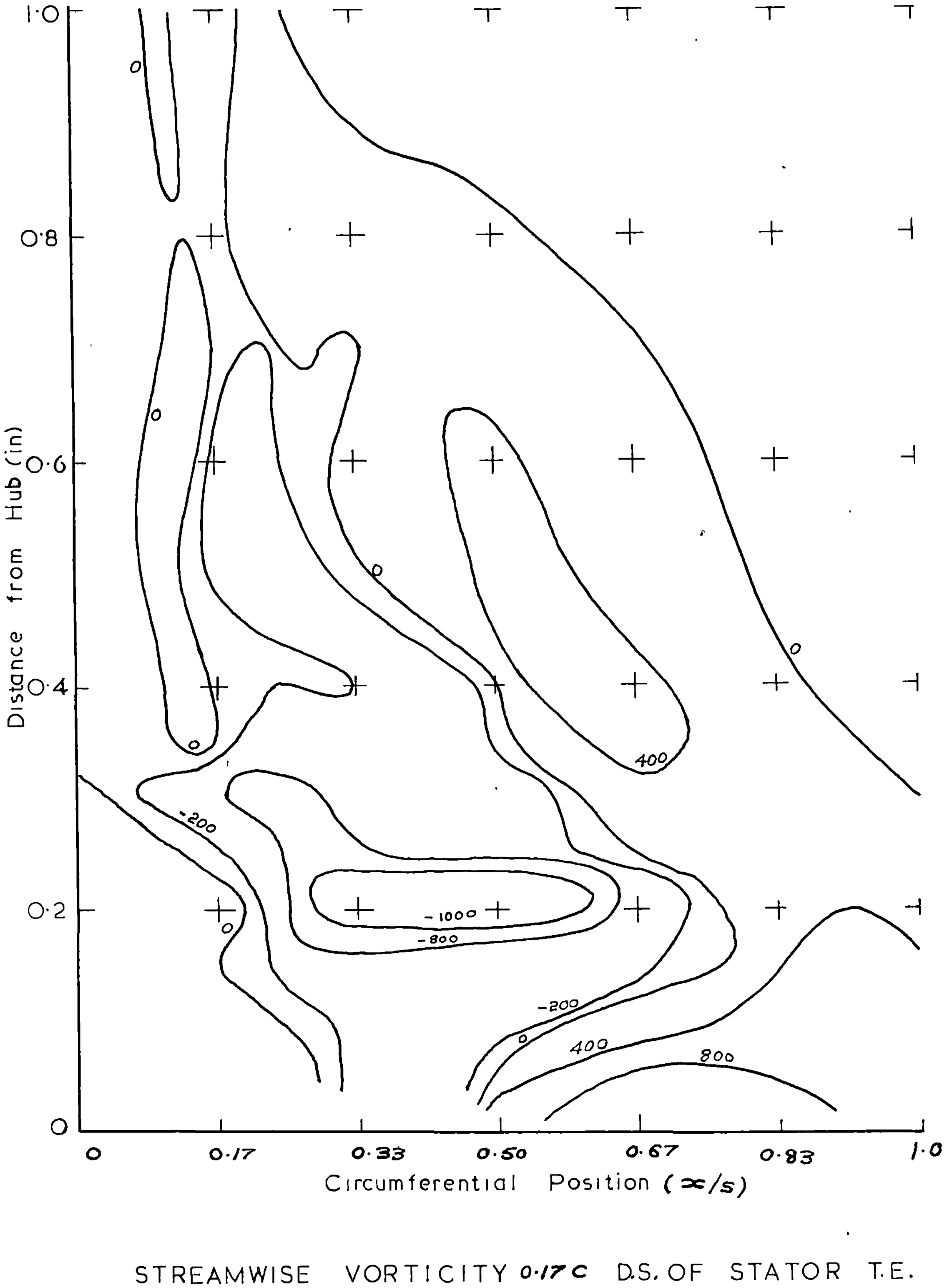

STREAMWISE VORTICITY 0·17C D.S. OF STATOR T.E.
(Rad. / sec)

Fig. 37

C =3 INS.
S =3 INS.

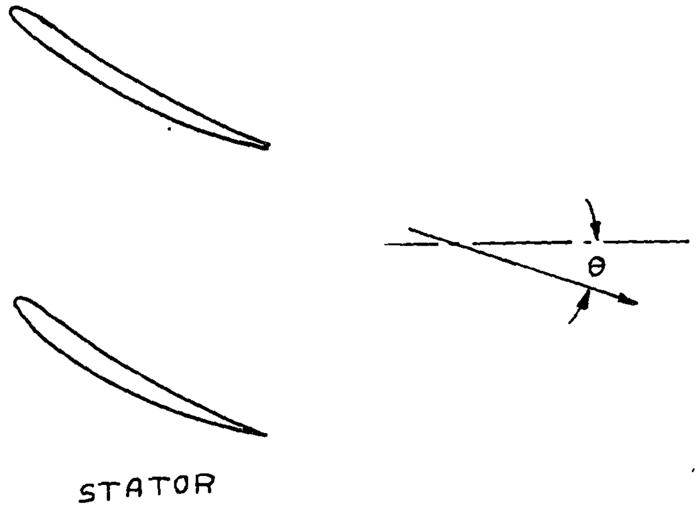

DEFINITION OF FLOW DIRECTION

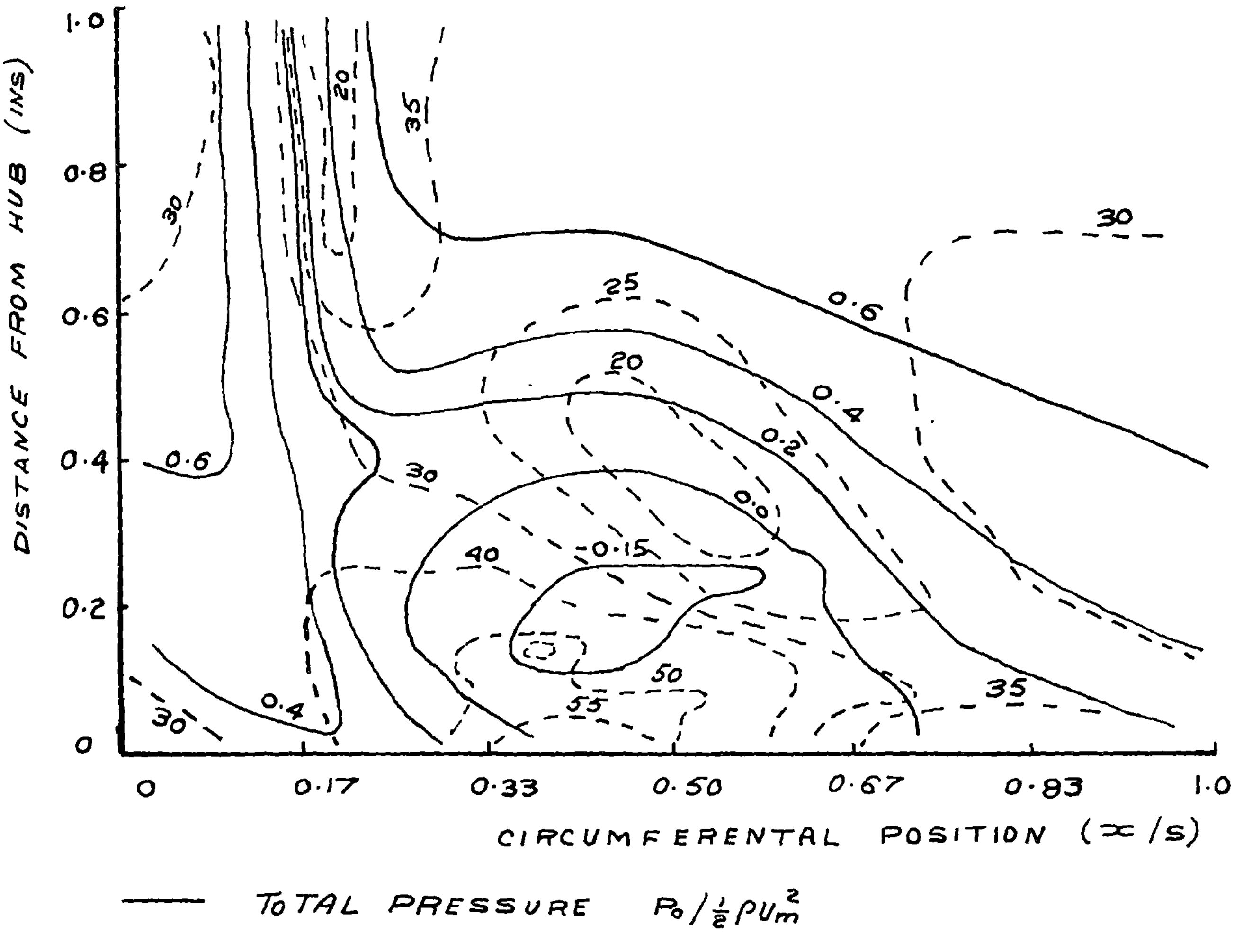

FIG. 38

FLOW ANGLE AND TOTAL PRESSURE DISTRIBUTION 0·17 CHORD LENGTHS DOWNSTREAM OF ROTOR T.E.

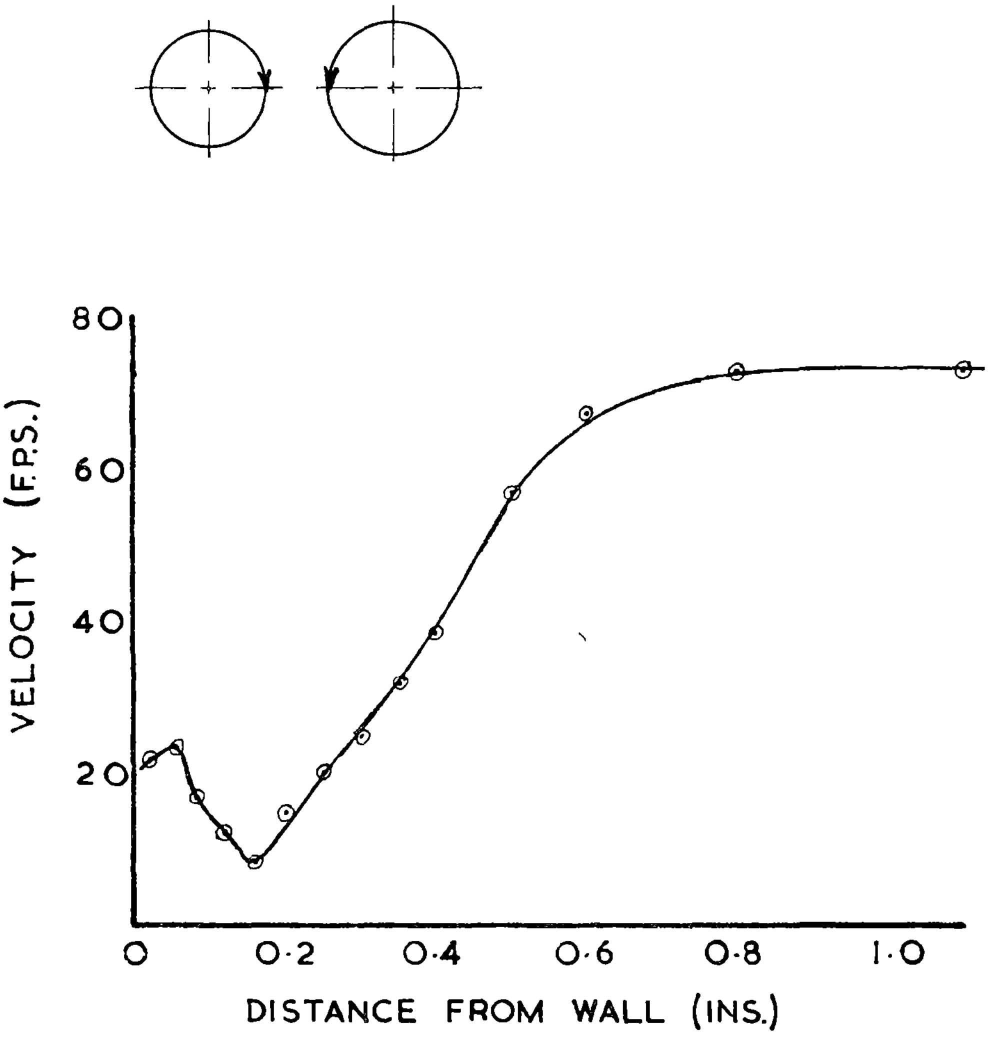

FIG. 39

[redacted] VELOCITY DISTRIBUTION 0·167 CHORD LENGTHS DOWNSTREAM OF STATOR T.E. CIRCUMFERENTIAL POSITION

$x/s = 0{\cdot}5$

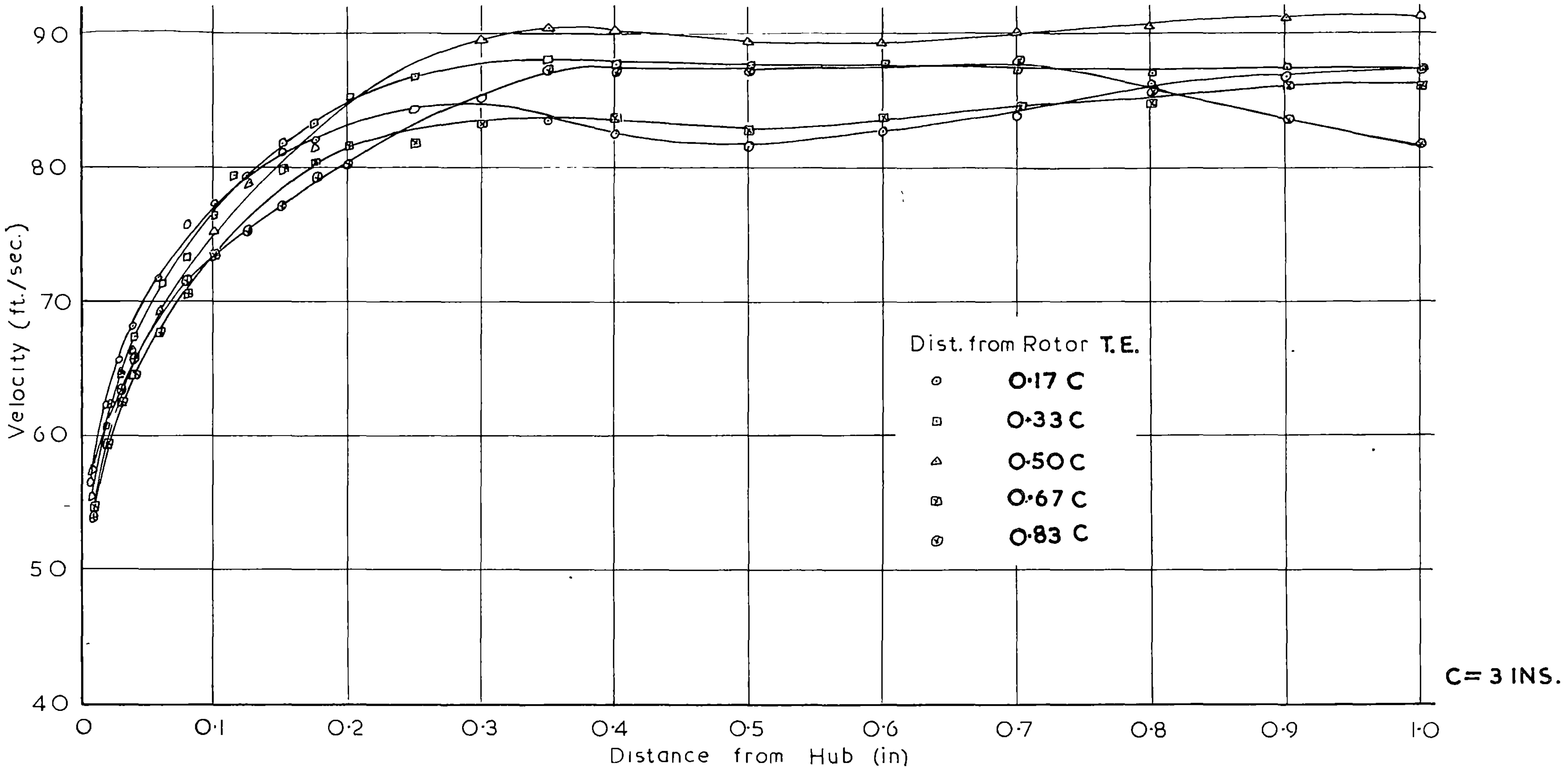

VELOCITY D.S. OF ROTOR

Fig. **40**

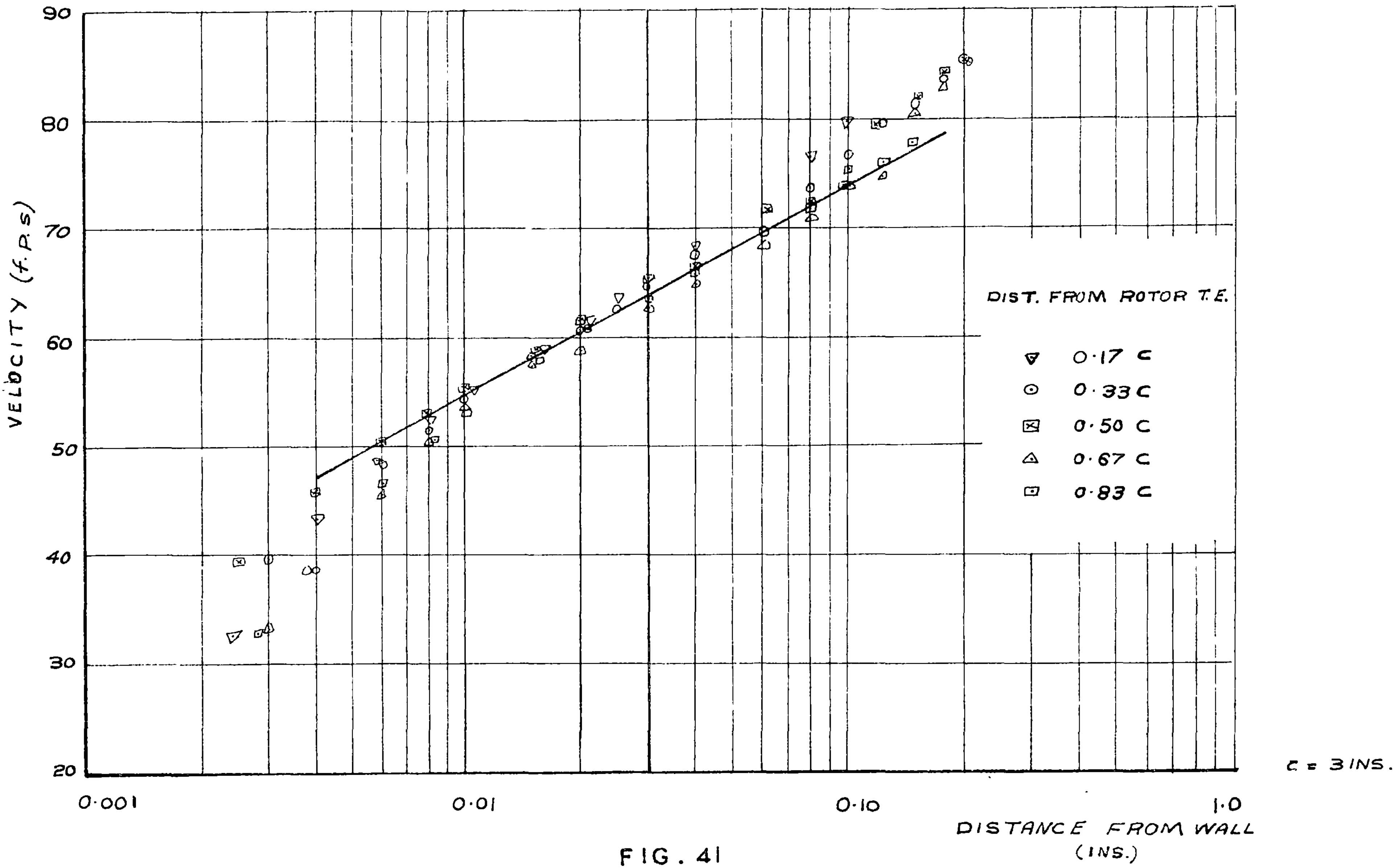

FIG. 41
VELOCITY DISTRIBUTION

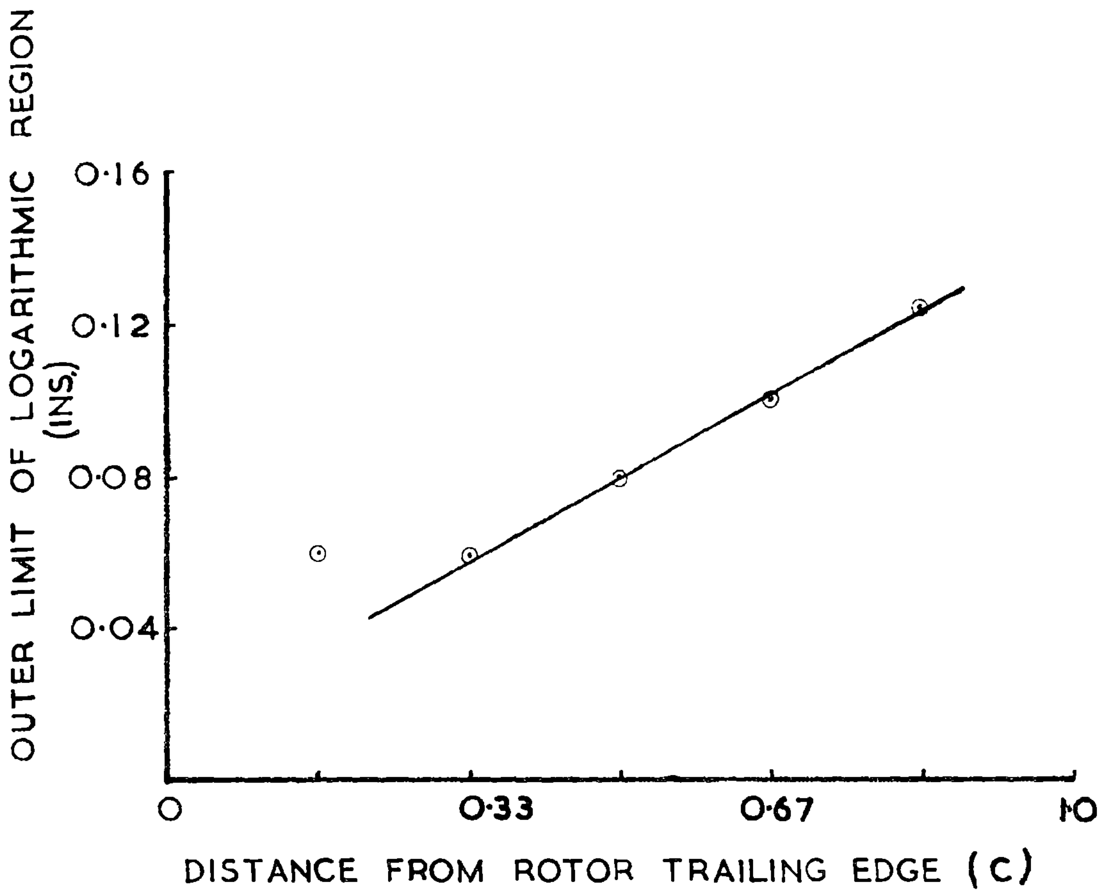

FIG. 42

VARIATION OF OUTER LIMIT OF LOGARITHMIC VELOCITY REGION WITH DISTANCE FROM ROTOR

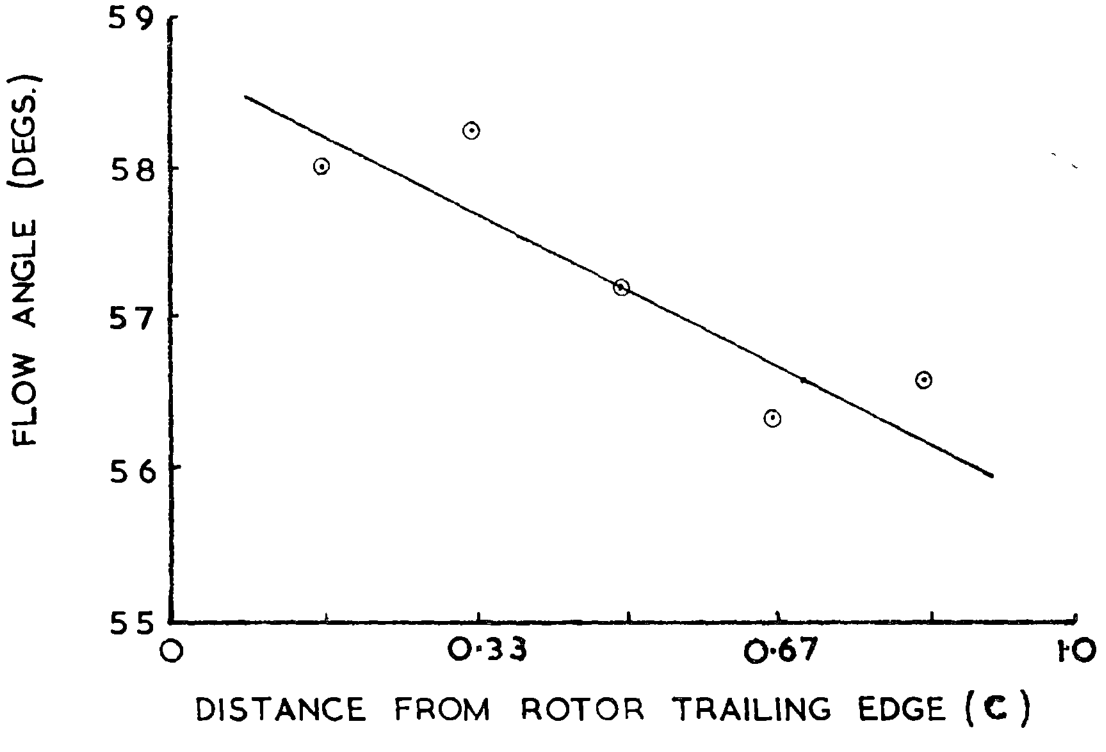

FIG. 43

VARIATION OF FLOW ANGLE IN LOGARITHMIC VELOCITY REGION

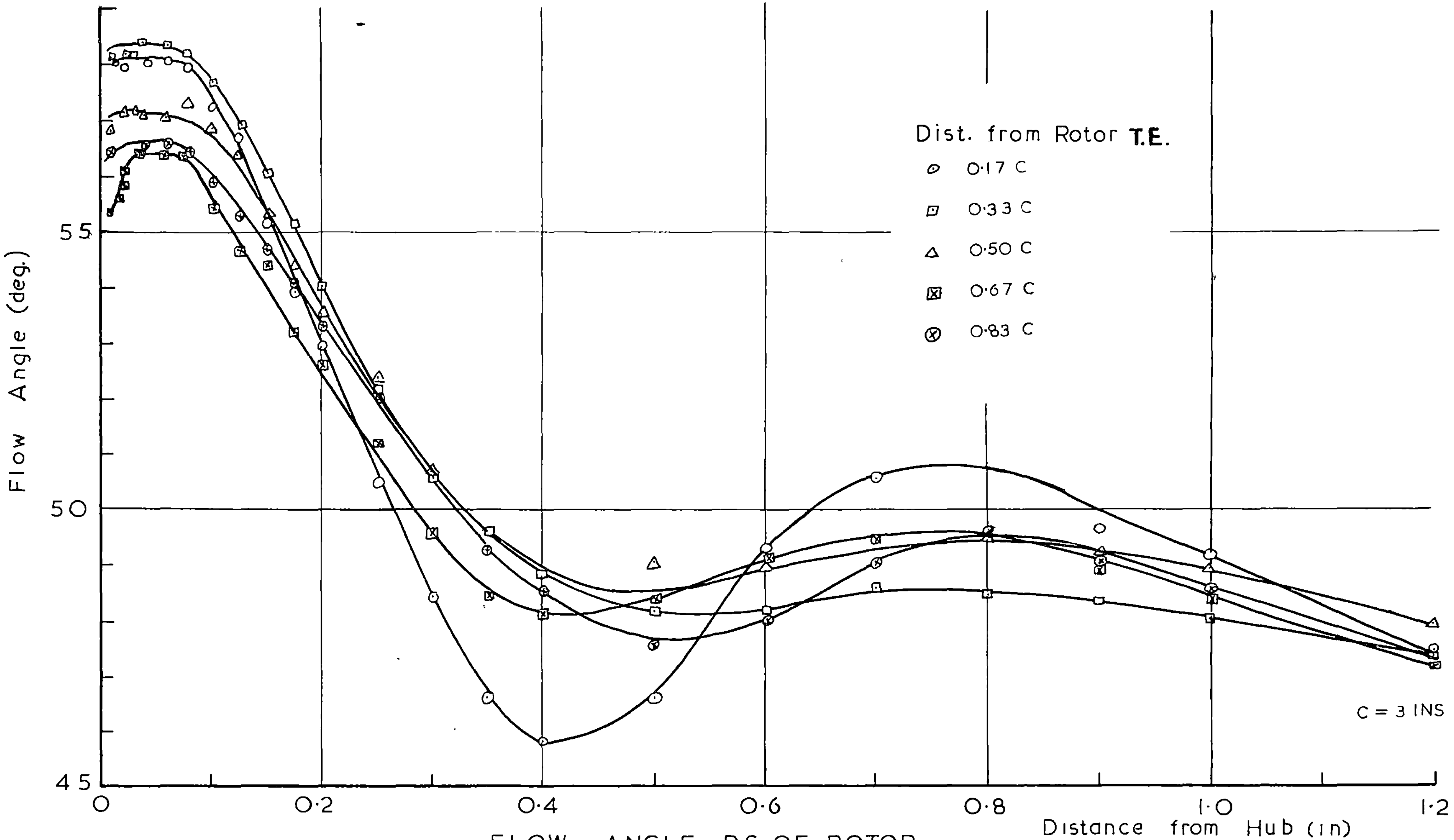

FLOW ANGLE D.S. OF ROTOR

Fig. 4[illegible]4

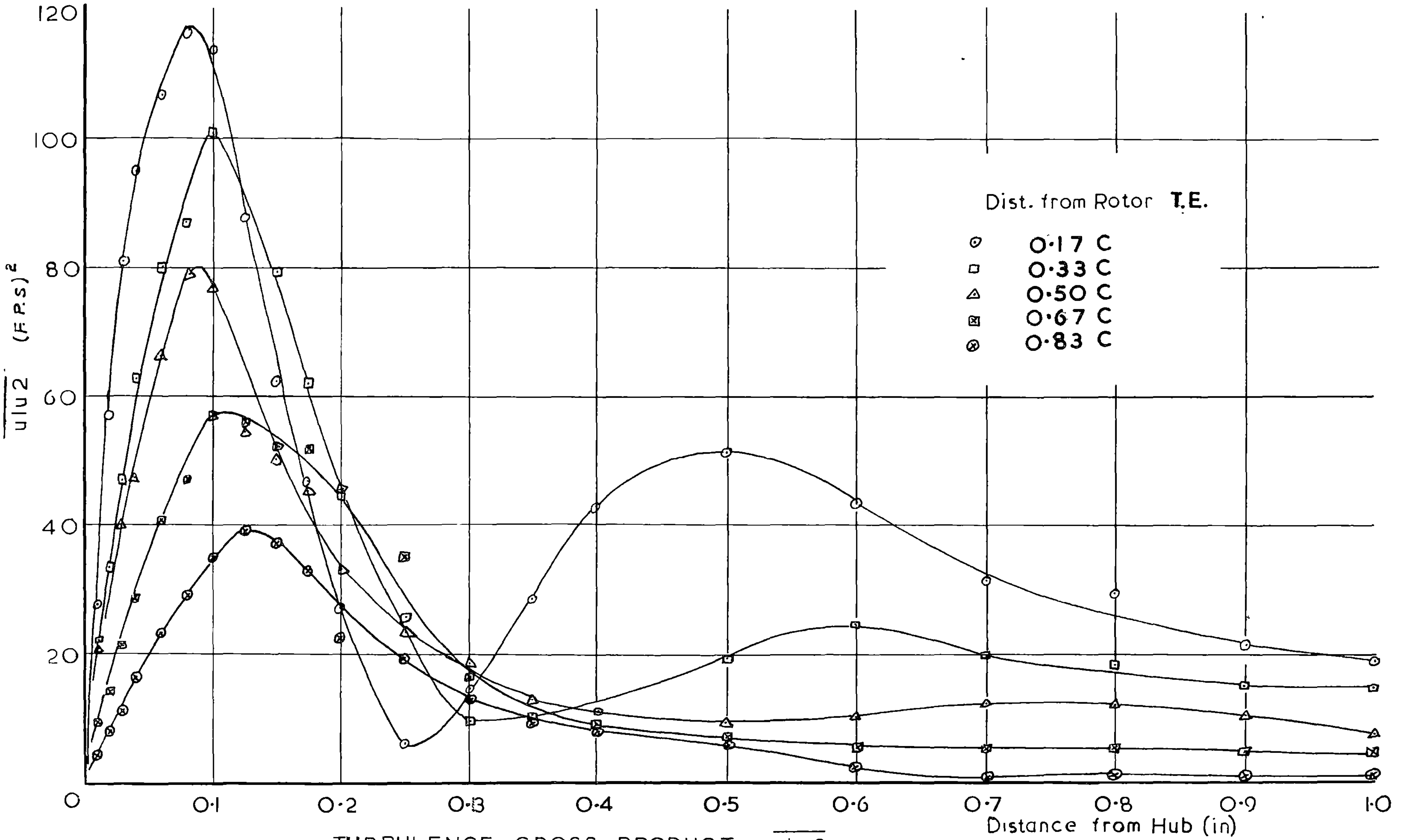

TURBULENCE CROSS PRODUCT $\overline{u1u2}$

Fig. 45

C = 3 INS.

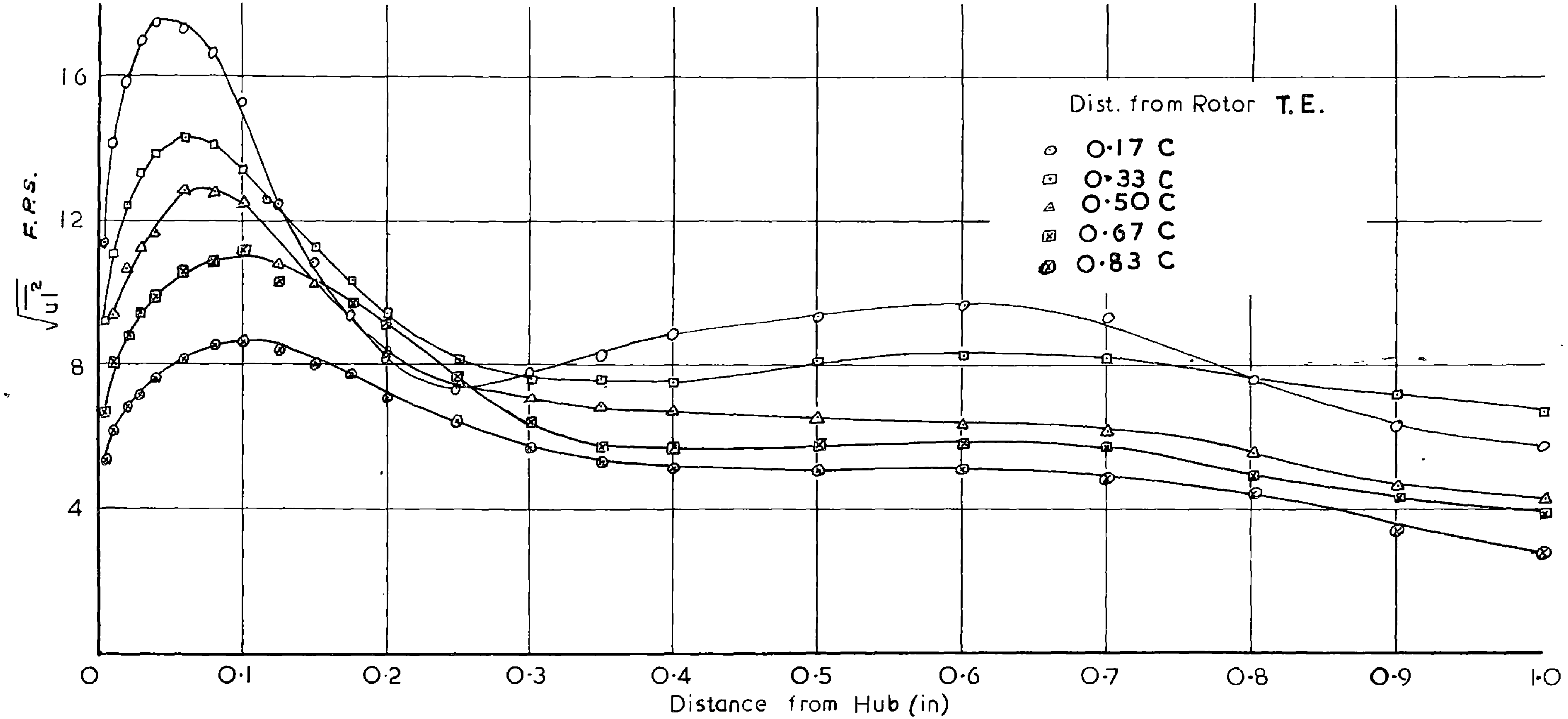

STREAMWISE TURBULENCE COMPONENT C = 3 INS.

Fig. **46**

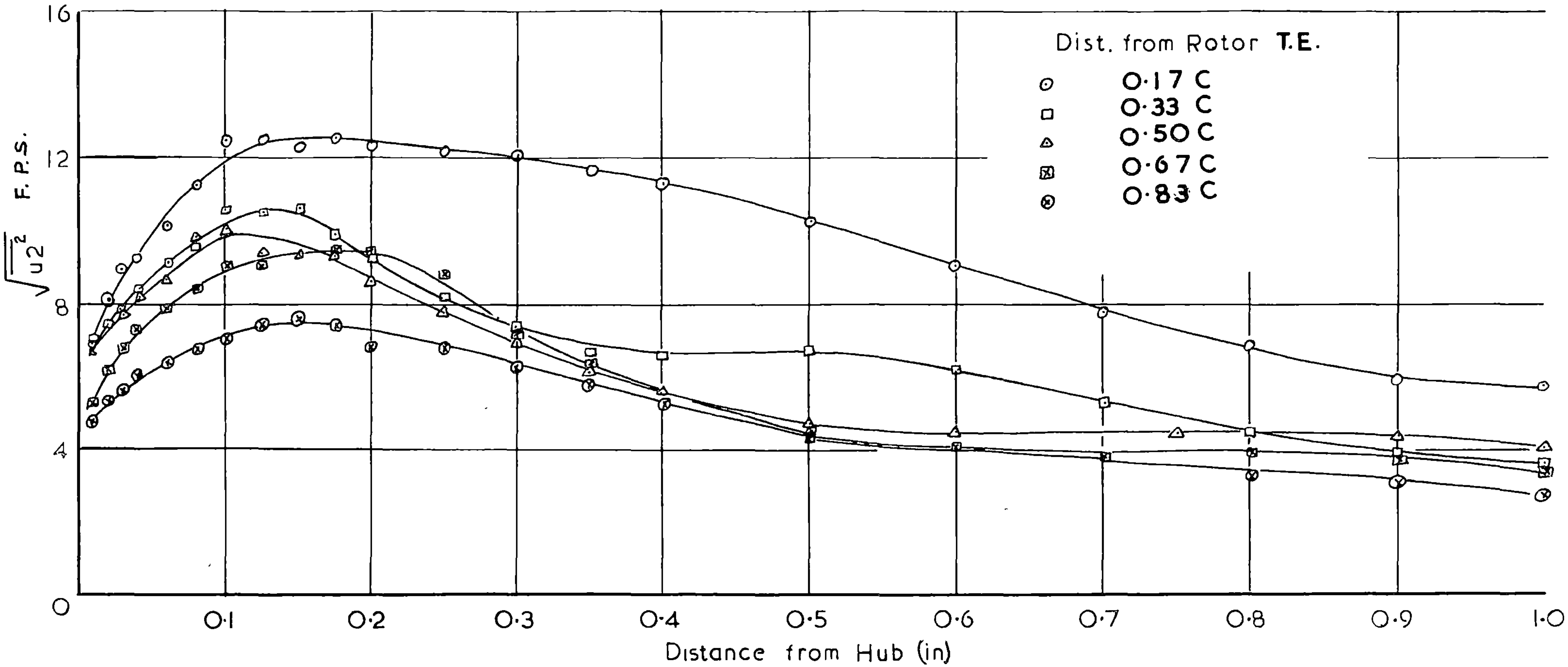

TURBULENCE COMPONENT NORMAL TO STREAMLINE

C = 3 INS.

Fig. 47

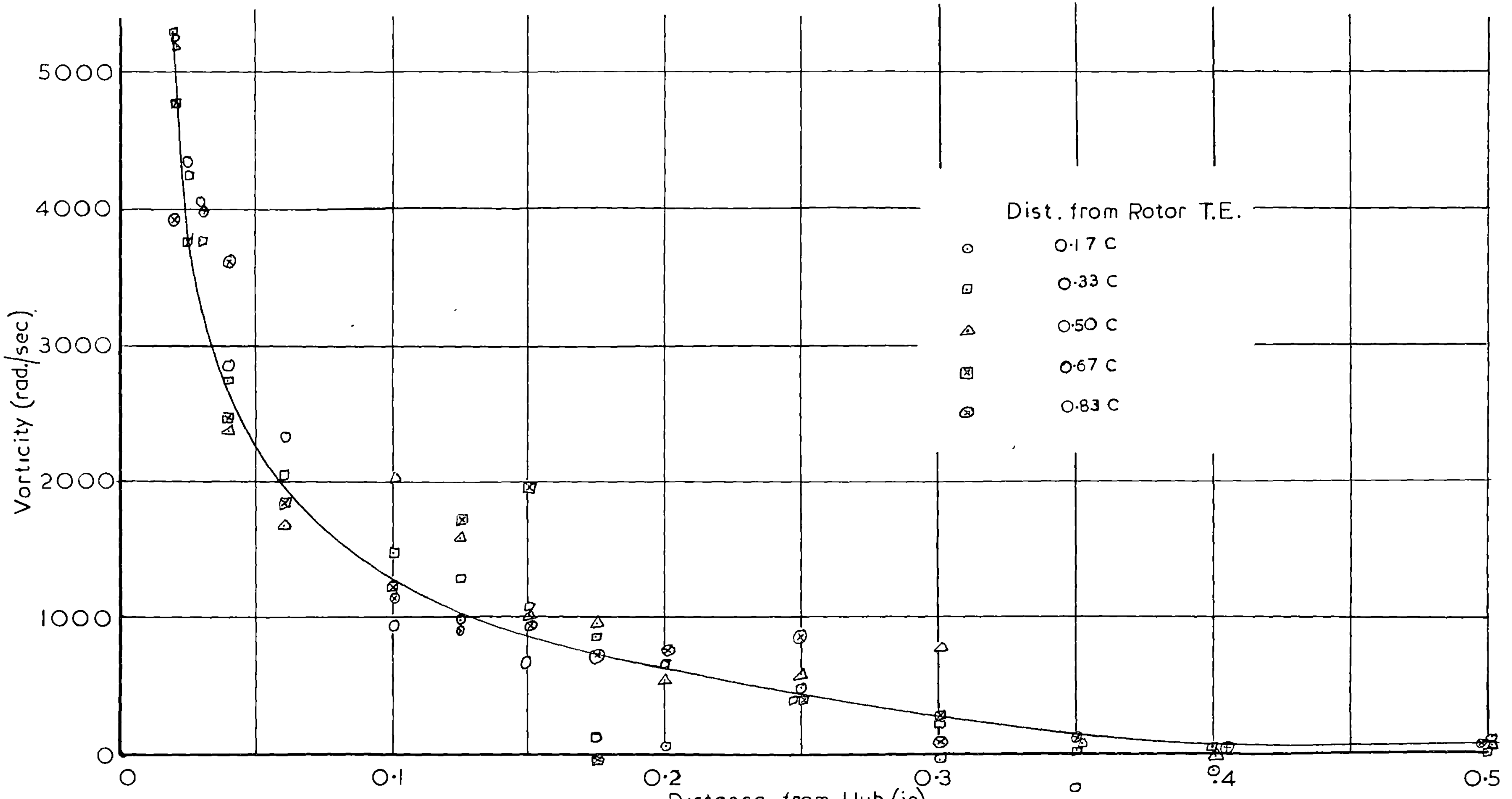

VORTICITY NORMAL TO STREAMLINE

C = 3 INS.

Fig. 48

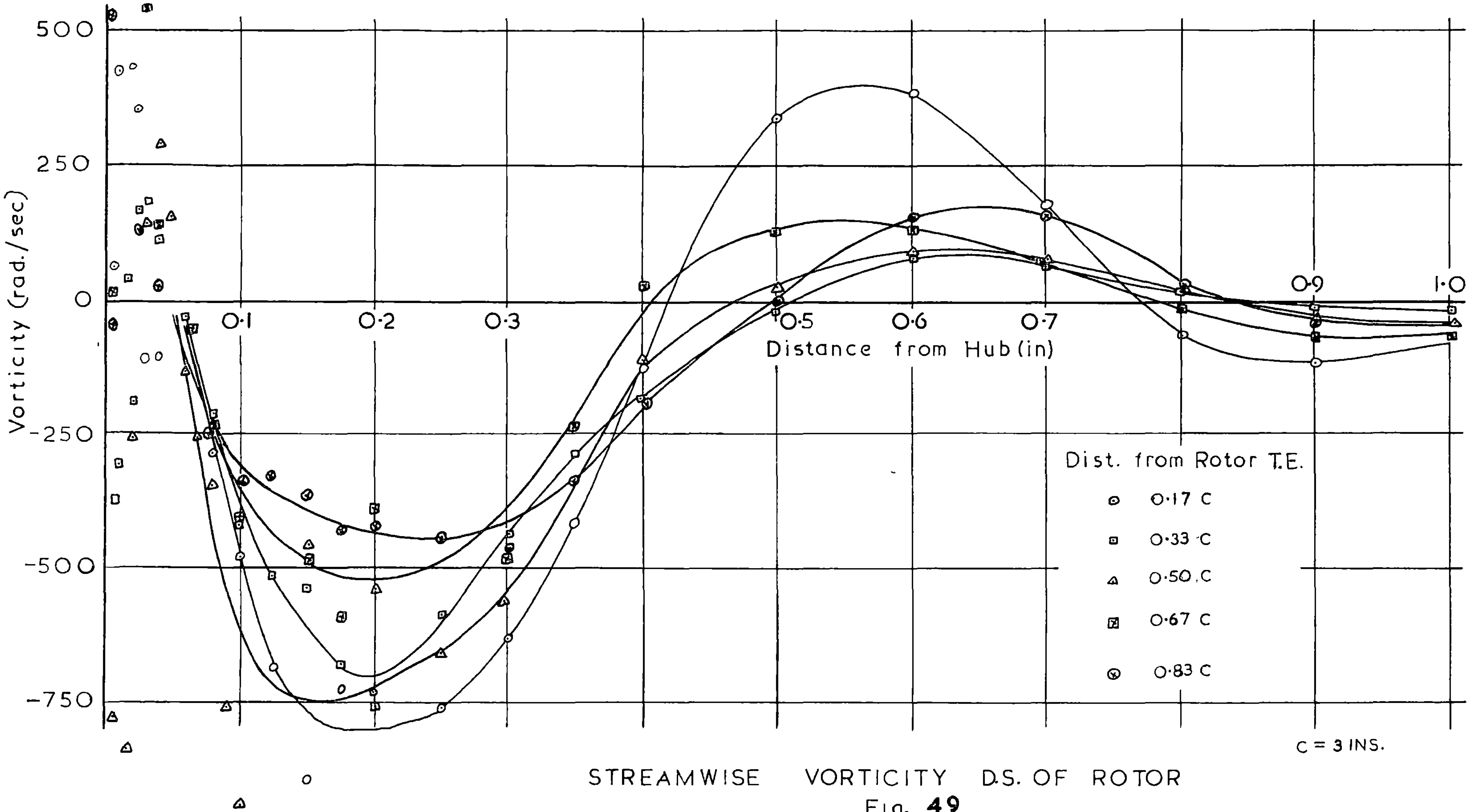

STREAMWISE VORTICITY D.S. OF ROTOR

Fig. 49

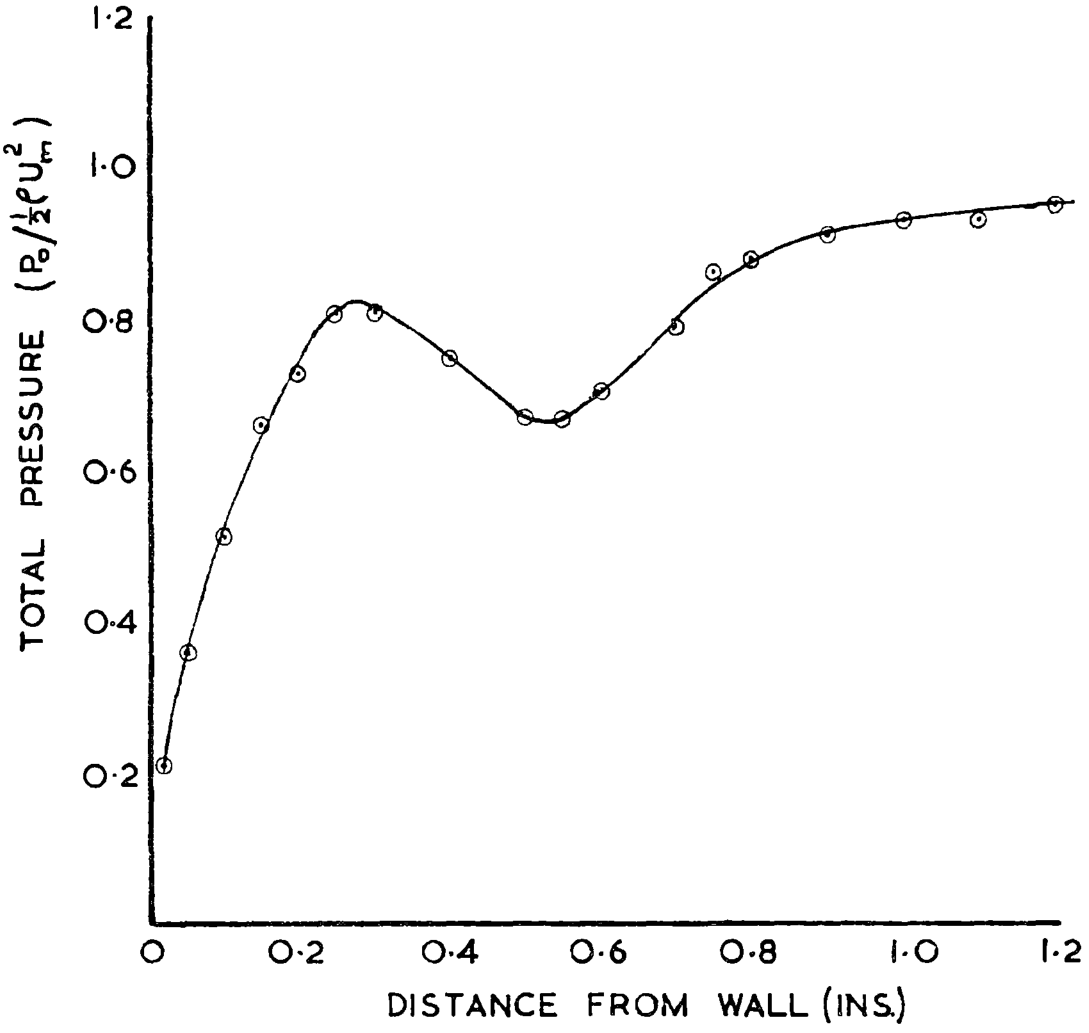

FIG. 50

TOTAL PRESSURE 0·17C DOWNSTREAM OF ROTOR TRAILING EDGE (REF. 41)

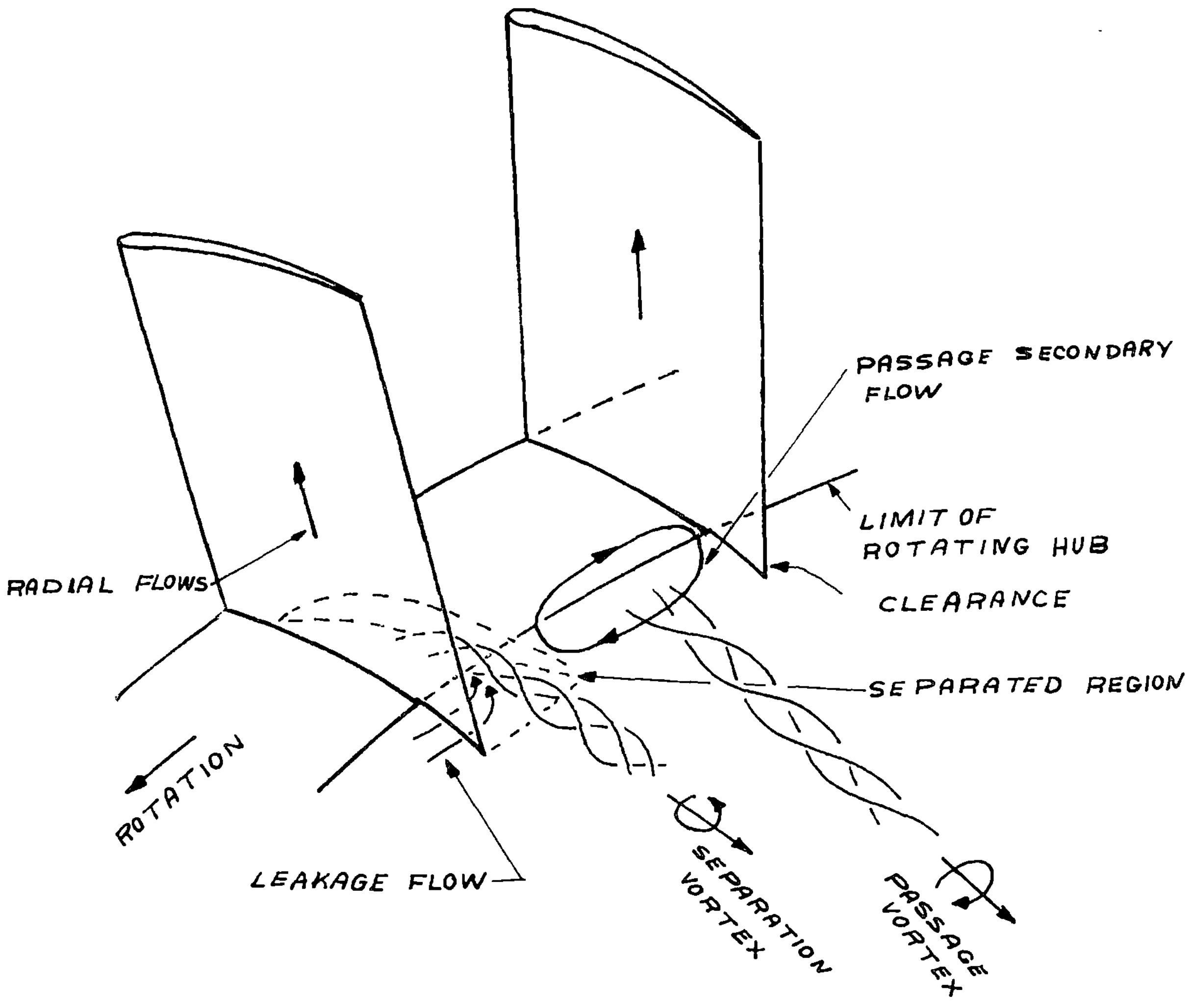
PASSAGE SECONDARY FLOW
LIMIT OF ROTATING HUB
CLEARANCE
RADIAL FLOWS
SEPARATED REGION
ROTATION
LEAKAGE FLOW
SEPARATION VORTEX
PASSAGE VORTEX

(a) SECONDARY FLOWS AND VORTICES IN ROTOR HUB REGION

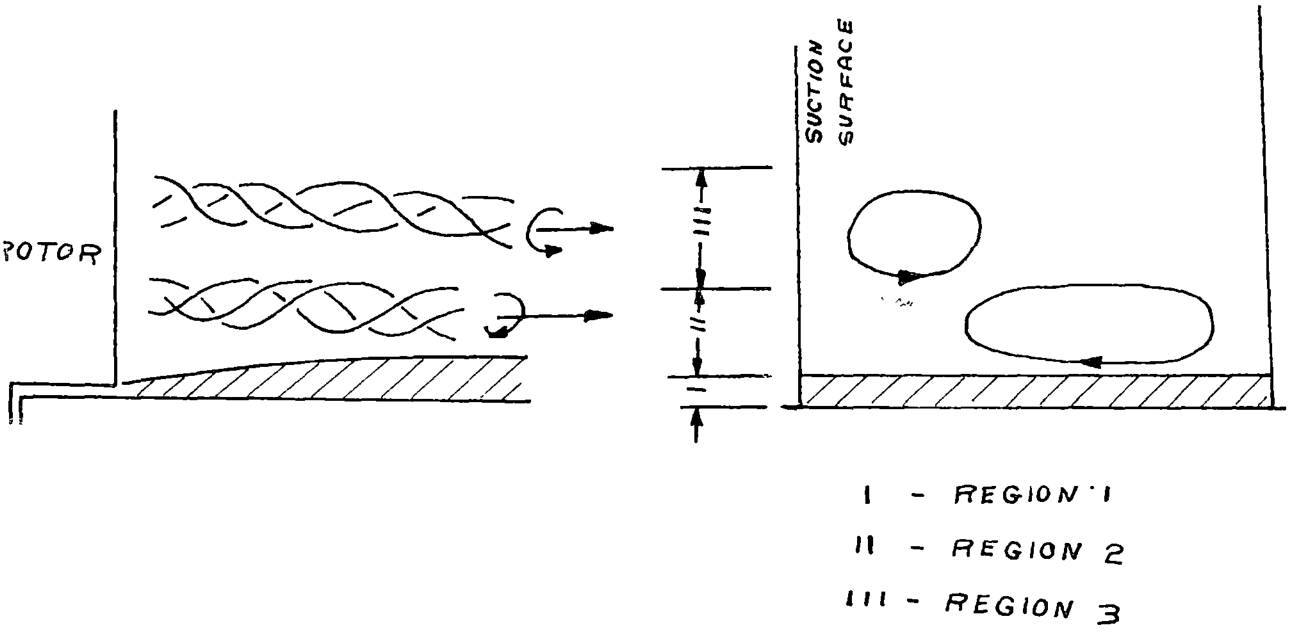
ROTOR
SUCTION SURFACE
III
II
I
I - REGION 1
II - REGION 2
III - REGION 3

(b) STRUCTURE OF BOUNDARY LAYER DOWNSTREAM OF ROTOR (RELATIVE TO ROTOR)

FIG. 51

HUB BOUNDARY LAYER DOWNSTREAM OF ROTOR

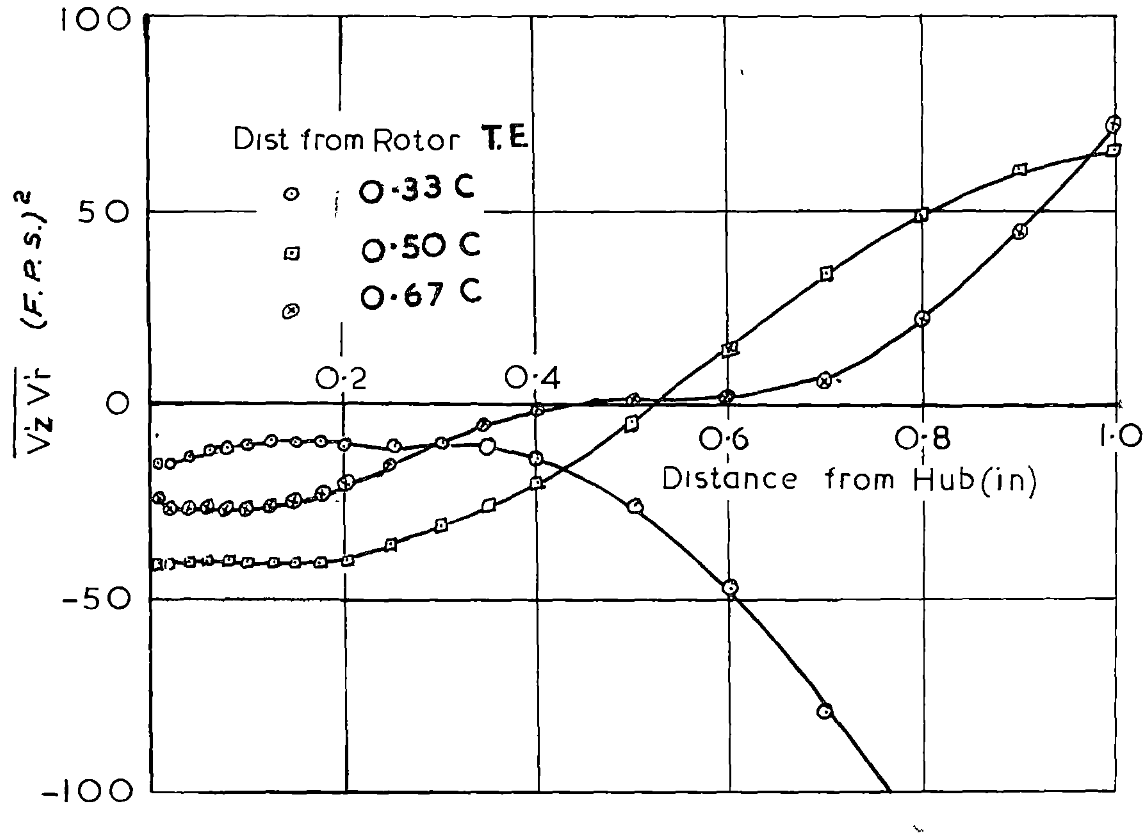

REYNOLDS SHEAR STRESS $\overline{V_r' V_z'}$

Fig. 52

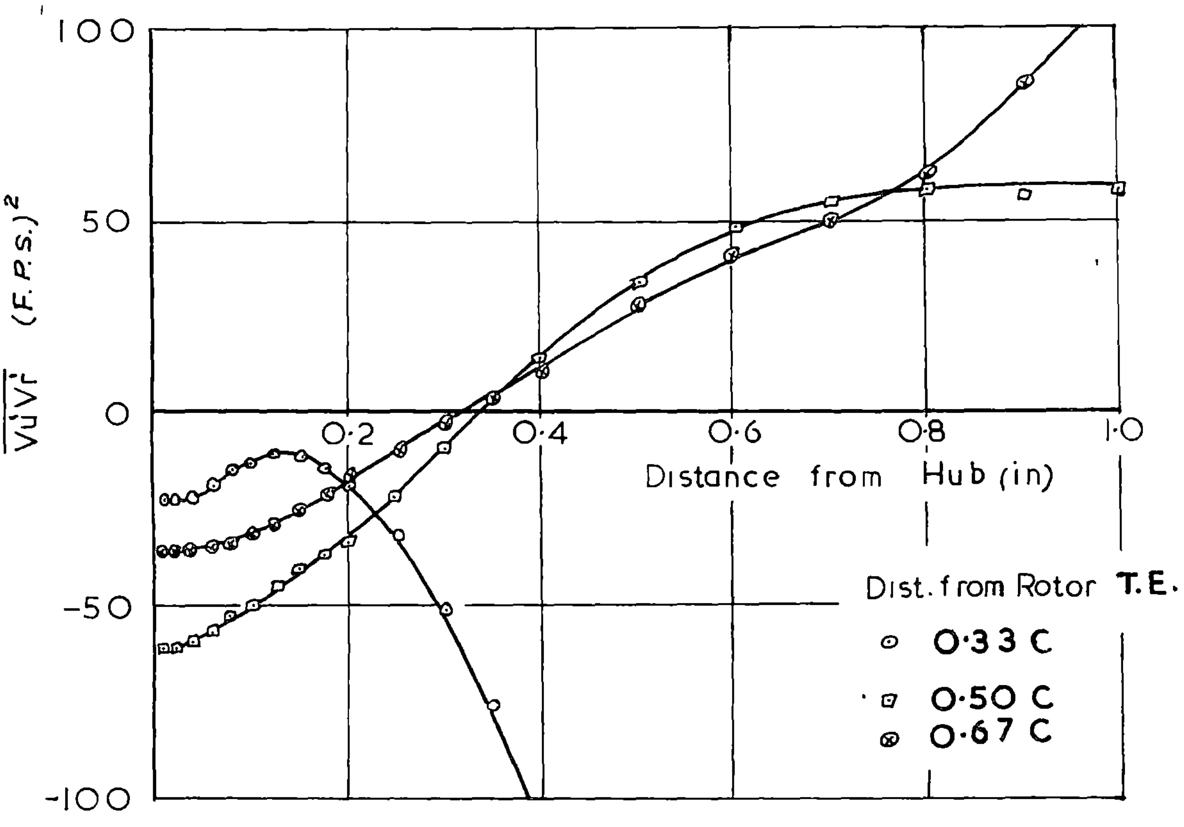

REYNOLDS SHEAR STRESS $\overline{V_u' V_r'}$

Fig. 53

C = 3 INS.

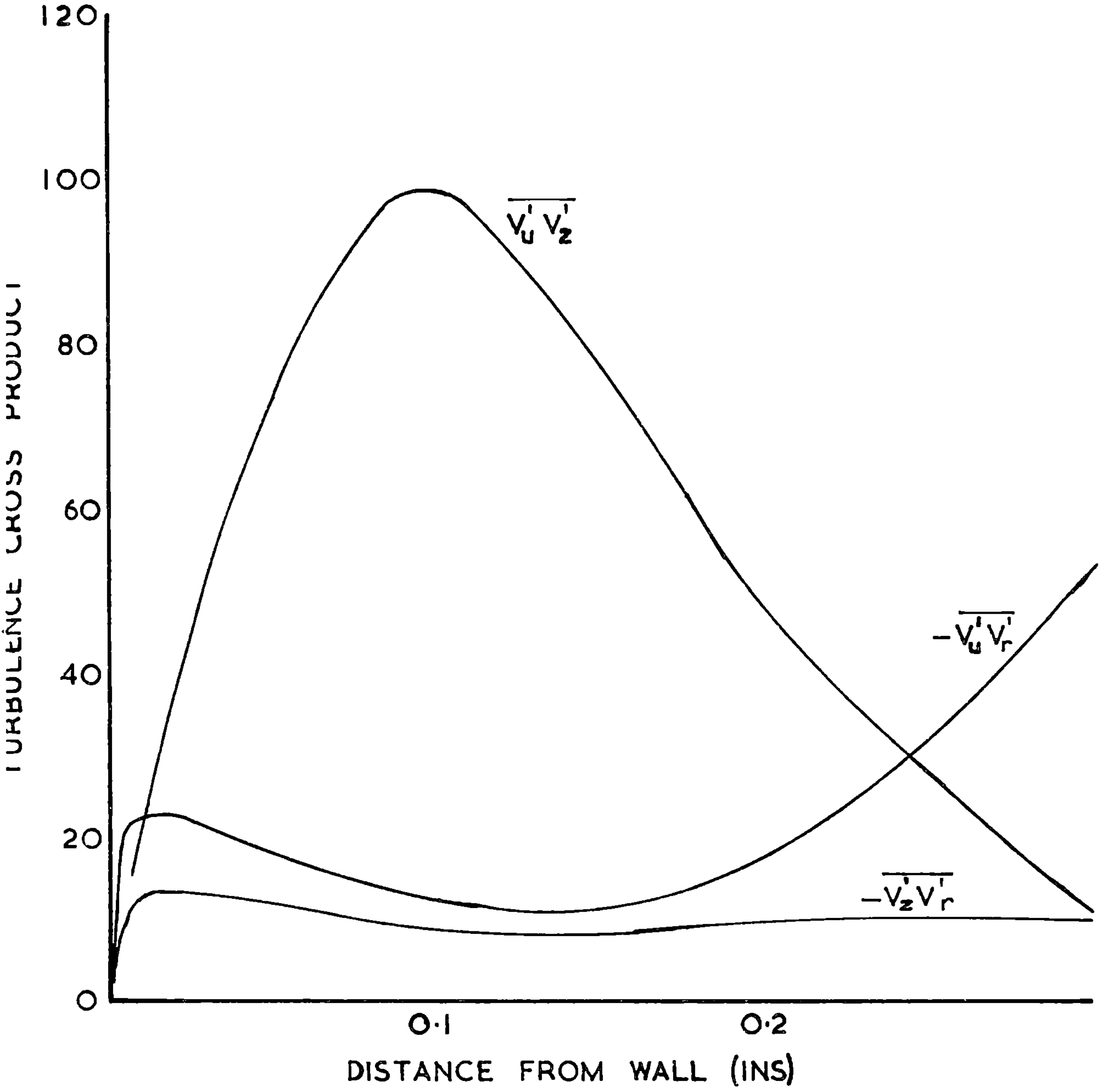

FIG. 54

TURBULENCE CROSS PRODUCTS IN HUB BOUNDARY LAYER 0·33 CHORD LENGTHS FROM ROTOR T.E.

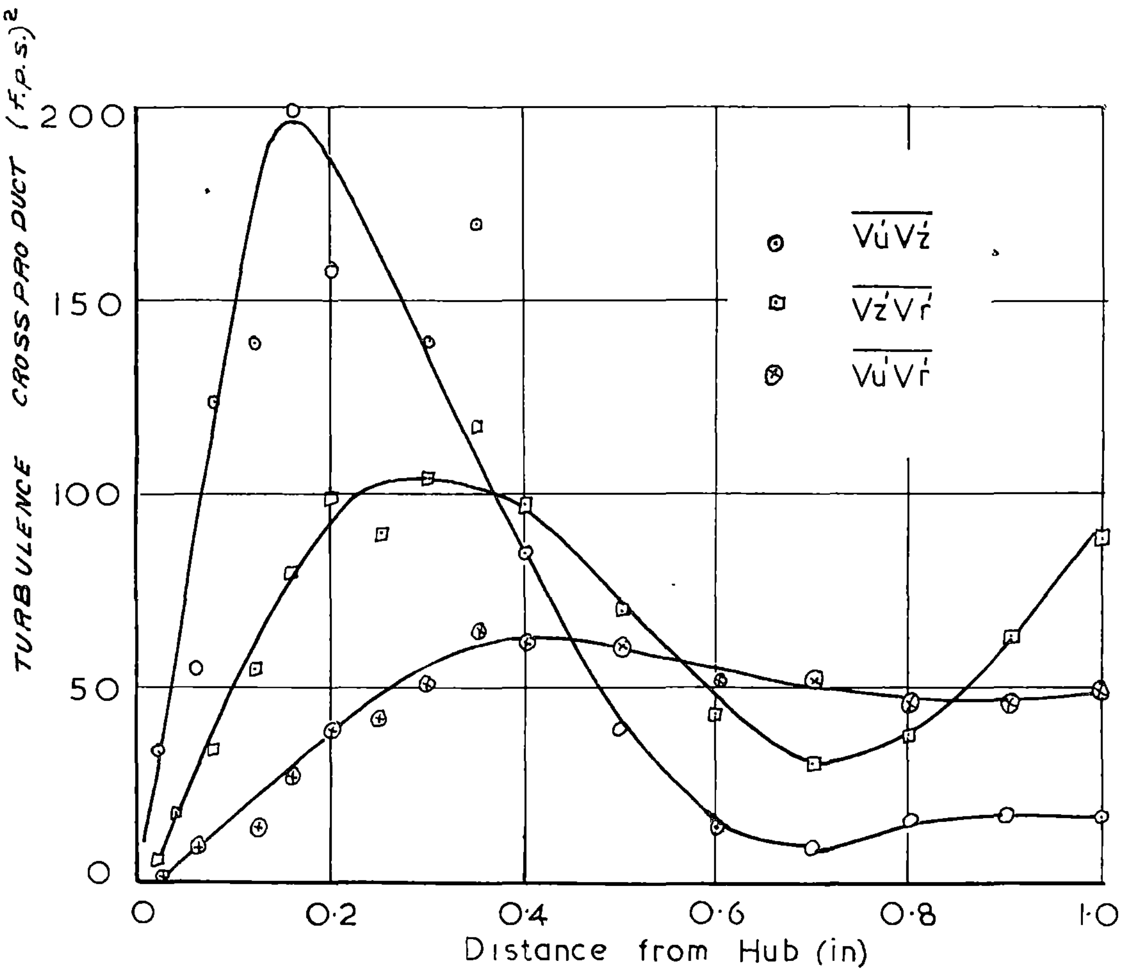

"TURBULENCE CROSS PRODUCTS"

0·17C D.S. OF STATOR T.E.

Fig. **55**

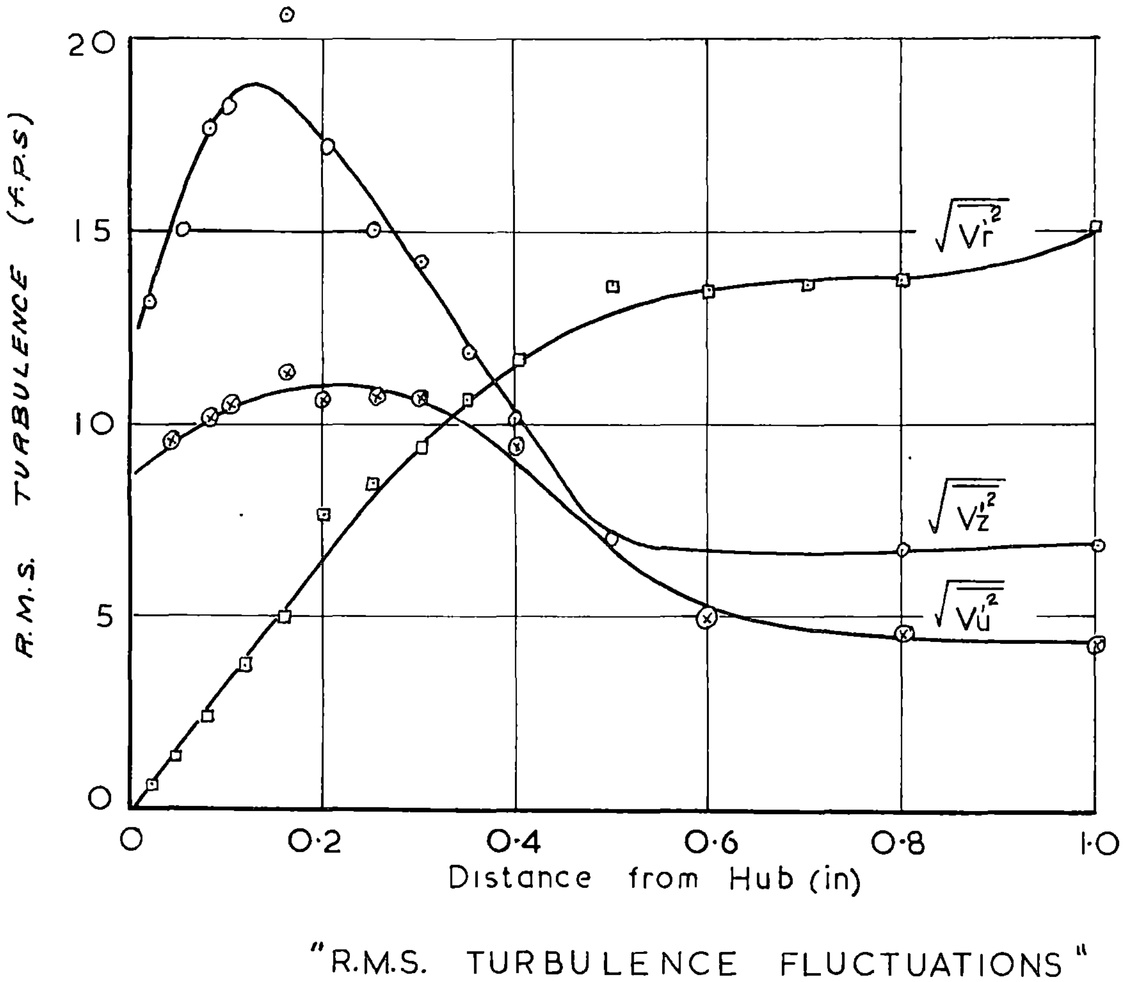

"R.M.S. TURBULENCE FLUCTUATIONS"

Fig. **56**

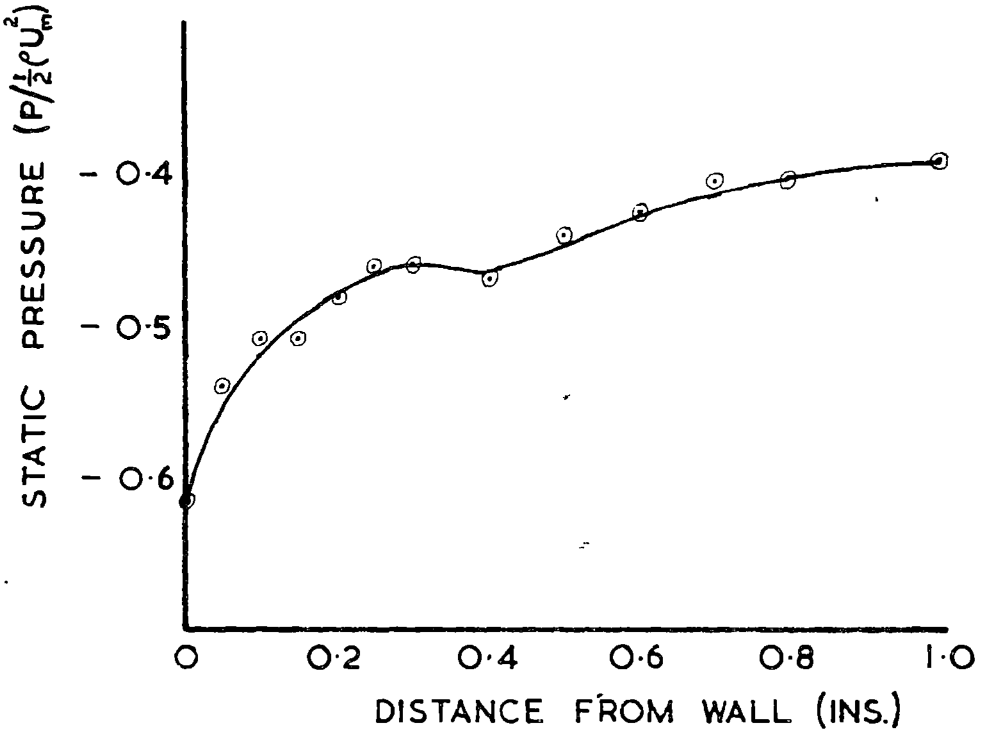

FIG. 57

STATIC PRESSURE THROUGH BOUNDARY LAYER 0·5 CHORD LENGTHS FROM ROTOR TRAILING EDGE (REF 41)